SINTERABLE POWDERS FROM LASER DRIVEN REACTIONS
SECOND ANNUAL REPORT

John S. Haggerty

W. Roger Cannon

Energy Laboratory

Massachusetts Institute of Technology
Cambridge, Massachusetts 02139

July, 1979

Prepared for:

The U. S. Department of Defense

ARPA order No:	3449
Program Code No:	NR039-153
Contract No:	N00014-77-C-0581
Contract Date:	1 July 1977
Contract Expiration Date:	30 June 1980
Contract Amount:	$416,580
Status Report Period:	1 July 1978-30 June 1979

unclassified

SECURITY CLASSIFICATION OF THIS PAGE *(When Data Entered)*

REPORT DOCUMENTATION PAGE		READ INSTRUCTIONS BEFORE COMPLETING FORM
1. REPORT NUMBER	2. GOVT ACCESSION NO.	3. RECIPIENT'S CATALOG NUMBER
4. TITLE *(and Subtitle)* Sinterable Powders from Laser Driven Reactions		5. TYPE OF REPORT & PERIOD COVERED 1 July 78 - 30 June 79 Second Annual Report 6. PERFORMING ORG. REPORT NUMBER MIT-EL 79-047
7. AUTHOR(s) John S. Haggerty, W. Roger Cannon		8. CONTRACT OR GRANT NUMBER(s) #N00014-77-C-0581
9. PERFORMING ORGANIZATION NAME AND ADDRESS Massachusetts Institute of Technology Cambridge, Massachusetts 02139		10. PROGRAM ELEMENT, PROJECT, TASK AREA & WORK UNIT NUMBERS (471) NR 039-153/7-20-79
11. CONTROLLING OFFICE NAME AND ADDRESS O. N. R. Department of The Navy 800 North Quincy Street, Arlington, VA 22217		12. REPORT DATE July 1979 13. NUMBER OF PAGES 115 pages
14. MONITORING AGENCY NAME & ADDRESS*(if different from Controlling Office)*		15. SECURITY CLASS. *(of this report)* unclassified 15a. DECLASSIFICATION/DOWNGRADING SCHEDULE

16. DISTRIBUTION STATEMENT *(of this Report)*

Unrestricted

17. DISTRIBUTION STATEMENT *(of the abstract entered in Block 20, if different from Report)*

Unrestricted

18. SUPPLEMENTARY NOTES

19. KEY WORDS *(Continue on reverse side if necessary and identify by block number)*

Laser synthesis of powders
Laser driven reactions
Gas phase synthesis of powders
Silicon powder
Silicon nitride powder
Laser heated gases
Silicon carbide powder
Ceramic powders

20. ABSTRACT *(Continue on reverse side if necessary and identify by block number)*

Extremely fine, uniform ceramic powders were synthesized from laser heated gas phase reactions. Resulting Si, Si_3N_4 and SiC powders have been characterized in terms of parameters which are important for densification processes. They are virtually ideal. The spherical particles typically have mean diameters from 120 to 1000 Å. The standard deviation is typically 25-45% and the diameter of the largest observed particle is typically less than twice that of the smallest particle. Purities are extremely high.

DD FORM 1 JAN 73 1473 EDITION OF 1 NOV 65 IS OBSOLETE
S/N 0102-LF-014-6601

unclassified

SECURITY CLASSIFICATION OF THIS PAGE *(When Data Entered)*

The laser heated process has been modeled in terms of fluid flow and heat transfer criteria. Many fundamental property measurements were made to provide data for these calculations. The process is extremely efficient; $\sim$ 95% of the SiH_4 is reacted in a single pass through the laser beam and approximately 2 kwhr. of energy are required per kilo of Si_3N_4.

TABLE OF CONTENTS

LIST OF FIGURES

LIST OF TABLES

Forward

This research program involved several groups within M.I.T., which represent different technical disciplines. The novelty of these processes for using lasers to produce ideal powders has intrinsically required an interdisciplinary approach. The principal investigators, Drs. J. S. Haggerty and W. R. Cannon, are materials scientists associated with both the Energy Laboratory and The Department of Materials Science and Engineering as is Dr. S. C. Danforth, who has worked on all aspects of this program. Mr. R. A. Marra, who has developed gas flow and gas heating rate models, is a Research Assistant in the Department of Materials Science and Engineering. Professor C. F. Dewey and Mr. J. H. Flint, who conducted the absorptivity and threshold experiments, are members of the Mechanical Engineering Department staff. Mr. C. Reiser, who investigated the feasibility of inducing unimolecular reactions, is a Research Assistant in the Chemistry Department.

I. Introduction

Coble (1960) established twenty years ago that ceramic materials could be densified by diffusional sintering processes to theoretical density provided important criteria were satisfied. The paradigms for this process have been established for oxides. The covalent materials such as silicon carbide and silicon nitride are less well defined and since they are being considered for high temperature structural applications, the requirements of theoretical density, uniform grain size, and elimination of flaws are fundamental to their eventual incorporation in power machinery. Without enumerating all of the justifications, an ideal sinterable powder (Si_3N_4) can be defined as one having the following characteristics: (1) fine grain size, less than 0.5 microns; (2) nonagglomerated particles, i.e., individual crystallites; (3) a narrow distribution in the sizes of the particles; (4) the morphology equiaxed, tending towards spherical; (5) phase purity, i.e., no mix of alpha and beta crystal structures; (6) compositional purity (less than 0.1%, except oxygen, less than 2%). A powder with these ideal characteristics can presumably be sintered to theoretical density without pressure or additives, and the grain morphology could be controlled to give useful high temperature properties. If not, it will serve as an ideal research vehicle to learn how to achieve the desired sintering characteristics. Although there have been significant improvements in the characteristics of fine silicon nitride and silicon carbide powders in recent years, they still have many deficiencies. In this program, a laser heat source has been studied as a means for synthesizing and modifying Si_3N_4 powders.

Most of the Si_3N_4 process techniques involve DC arcs, conventional vapor phase reactions in heated tube furnaces or nitriding or carbiding of silicon metal. The nitriding of silicon metal typically leaves a silicon core within the silicon nitride particle. Furthermore, because the process is done in the solid state, grinding and separating of particles is necessary, but this does not result in narrow size distribution, nonagglomerated, phase pure powders. The

vapor phase method (furnace heated vapor and arc plasma techniques) yield a finer and more uniform powder than the nitriding of solid silicon; but from the point of view of studying the ultimate properties of materials formed from ideal powders, these techniques have less than ideal thermal profiles and reaction zones which allow for a distribution in nucleation and growth times and the formation of agglomerates. Despite these specific process deficiencies, direct synthesis of powders from dilute gas phase reactants is the most promising route of producing ideal powders.

The processing technique of using laser driven gas phase reactions, emphasized in the second year, offers many advantages. It is a clean process which permits cold, nonreactive chamber walls. The reaction volume is very well defined and consists only of that volume traversed by reaction gases and particles, i.e., the laser beam area. The ability to maintain steep temperature gradients in the effective thermal environment, and thus a well defined reaction zone, should allow precise control of the nucleation rate, the growth rate and exposure times, permitting the nucleation and growth of very fine particles. The available power with a CO_2 laser, the stability of the delivered power, its cost, reliability and efficiency, allow this to be a viable process which will yield improvements in fabrication of powders for these high performance materials. The use of this technique as an experimental tool has tremendous potential, and its eventual use as a production tool should also be considered.

Three specific laser means for synthesizing and modifying powders were proposed. The first technique, a homogeneous gas phase reaction, involves the absorption of laser radiation by gas phase molecules and their subsequent reaction to form particles. The advantages are a clean system, cold walls, and a controlled hot zone. The second primary technique is pyrolysis of a silicon reactant to form composite particles of silicon on silicon nitride. In this case, a silicon nitride particle would be heated, and provide a heterogeneous surface

for a film of silicon deposition. The subsequent nitriding during reaction sintering would go to completion because the core would be silicon nitride. The third area involves comminution of particles and is related to both of the other primary research areas. The fundamental principle is that 10.6 μm wavelength CO_2 laser radiation couples with particles whose diameters are a micron or larger, but not with much smaller particles. In this way, vaporization of agglomerates or large particles causes the refinement in the particle size and size distribution. This also tends towards more equiaxed particles, as well as nonaqqlomerated ones. The first and third approaches were studied during the first year of this program.

The character of this research program has changed considerably in two years. At the beginning, the concept of forming powders by laser induced reactions had not been demonstrated. The program was viewed as having a high risk of not functioning as anticipated and most of the experiments were empirical. Since then it has been shown that the process works extremely well and produces powders with most of the desired ideal characteristics. With this evolution, the program has progressively focused more on analysis and modeling to describe how the process works and to determine how to make it work better. Making the detailed absorptivity measurements required for estimating the transfer of energy to the reactant gases is a typical example of the more recent emphasis. To date and in the future, the program will emphasize both direct observation (empirical) and analytical modeling.

Our ultimate objective is to develop an understanding of the interrelationships between process variables and powder characteristics, producing agreement between observations and models. To reach this goal, we must be able to describe heating rates, nucleation and growth rates, the distribution of temperature, and mass flow throughout the "reaction zone."

We have studied the effect of several process variables on powder characteristics, including beam intensity, gas composition (stoichiometry and dilution), gas pressure, and gas velocity. The effect of these process parameters has been correlated with both powder characteristics and process characteristics, e.g., emitted spectra, temperature, and percent conversion.

Two fundamentally different reaction types have been investigated. Most of our work has been carried out under laser intensity and gas pressure conditions where many collisions occur between molecules during the period that the gas molecules are heated. These reactions probably proceed as normal thermal reactions. In this case, the principal attributes of the laser heat source are process control and possibly unique reaction paths because of high heating rates and resonance effects between the coherent light and the molecules. The second type of reaction, involving multiphoton unimolecular or biomolecular reactions, is uniquely possible with laser heating. In this case, the molecules absorb sufficient energy to dissociate before colliding with the other molecules. We have investigated both types of processes.

The use of this synthesis technique as an experimental tool has tremendous potential, and its eventual use as a production tool appears increasingly probable. It is now apparent that it can be applied to elements, oxides, carbides, and nitrides. With slightly different process conditions, it can be used to deposit thin films rather than for powders.

II. Description of Previous Year's Work

Research in this program is now in its third year. The purpose of this report is to summarize the work carried out in the past year. Since there are obvious overlaps in the discussion of our work on laser synthesis with the previous annual report, and since we did not continue experiments on the laser comminution process, we have only briefly summarized the work done in the first year.

During the first year, we investigated two laser heated processes for producing powders with characteristics which make them superior for subsequent consolidation into finished parts. In the first process, powders were produced directly from laser heated gas phase reactants. In the second process, the size and shape of oversized or elongated particles were selectively reduced to acceptable dimensions by a laser heated vaporization process. Because of its importance for high temperature engine components, we concentrated on powders for silicon nitride ceramics, Si_3N_4 and Si powders. Silicon is used for reaction bonding processes. These tasks involved processing experiments, material characterization and analytical modeling. The two processes are sufficiently distinct that they are summarized separately.

- Powder Synthesis

Both Si_3N_4 and Si powders were synthesized from SiH_4 or NH_3/SiH_4 mixture gas phase reactants which were heated by direct absorption of the nominally 10.6 μm light by the reactants. Both static and flowing-gas synthesis processes were investigated. Flowing-gas processes were developed in configurations where the reactant stream and the laser beam intersected orthogonally as well as in opposite, coaxial directions (counter flow). The exposure time and beam intensities which were investigated ranged from those required for unimolecular, multiphoton reactions to those of a normal thermal reaction. A wide range of process variables was systematically investigated and many of the process characteristics are understood to a first order.

The most important result was that both SiH_4 and NH_3 couple effectively to the highest gain emissions from a CO_2 laser. Consequently, it was feasible to induce the desired chemical reactions. Powders were formed with time-intensity conditions ranging from 10^{-9} seconds, 10^9 watt/cm^2 pulses to cw exposures at intensities as low as 8 watts/cm^2.

It appears that the powders which resulted from the short pulse, high intensity conditions did not form by unimolecular, multiphoton processes. Rather, it appears that a plasma was induced by the high electromagnetic fields and that the reaction was brought about by the localized plasma heating. Absorptivities measurements of other laser emission lines were planned to determine whether there are more favorable wavelengths to attempt unimolecular reactions.

The thermal reaction domain was studied and analyzed. A first order model of the heating and subsequent reaction was one of a spontaneous reaction at a critical temperature. This model correlated well with observed time-intensity effects. At high laser intensities, the process is controlled by sensible heat. At lower intensities, conductive heat losses become increasingly important.

Both Si and Si_3N_4 powders were produced and characterized. Powders were characterized by x-ray diffraction, electron diffraction, TEM, STEM, IR spectroscopy, BET, and wet chemical techniques. Particle diameters range from a minimum of 25-50 Å to approximately 1000 Å. The smallest particles were produced at the shortest, highest intensity pulses and became larger as the intensity was decreased. The Si_3N_4 particles had a narrower range of diameters than the Si particles. Gram sized quantities of Si_3N_4 powders were produced with particles whose diameters were entirely within the range of 100-200 Å. The best Si powders generally ranged from 200-600 Å, with a few particles in the range of 600-1000 Å. Characterizations indicated that these equiaxed Si_3N_4 particles were either amorphous or were of extremely small grain size, highly distorted crystals.

Preliminary results indicated that the latter may be the case. Detailed characterization with direct lattice imaging and dark field electron microscopy techniques was to continue to clarify this point. Knowledge of the crystal structure is important for defining the driving forces which are operative during sintering. The particles appear to have smooth surfaces and no open cell porosity.

The Si and Si_3N_4 powders produced during these nonoptimized processing experiments exhibited better diameter uniformity than had been achieved previously by other processing techniques. Also, the process was highly efficient energetically. The entire laser beam can be absorbed within an optical path length of a few centimeters. If all the thermal energy is provided by a CO_2 laser, the electrical energy investment in powder synthesis will be less than approximately 20 kw hr/kg of Si_3N_4 (from $10NH_3/SiH_4$). It can be reduced further by using preheating methods which are more efficient than the CO_2 laser ($\sim$13%) or exchanging heat between entering and exiting gases.

Based on the significant technological advantages of powders produced by this process and the probable low manufacturing cost, it appeared that this technique would ultimately emerge as an important synthesis process. Consequently, the second twelve month period concentrated on laser synthesis.

• Particle Size and Shape Modification

In this phase of the first year's work, controlled modification of particle size and shape by subjecting powders to high intensity laser illumination was successfully demonstrated.

The feasibility of selectively interacting with oversize or high aspect ratio particles by means of high intensity light from a CO_2 laser source was investigated. Selective heating causes particle

size reduction by vaporization until decoupling occurs when the oversize particles reach a specific dimension. This approach was based on the diameter dependence of the absorption efficiency (Q_{abs}) which small particles exhibit to electromagnetic radiation. The Mie theory (Vande Hulst, 1957) shows that above a specific diameter, the particles absorb heat with a high efficiency that is independent of diameter. Below a specific diameter, the absorption efficiency decreases with diameter so the particles effectively decouple from the radiation. The calculated absorption efficiency is shown in Figure 1.

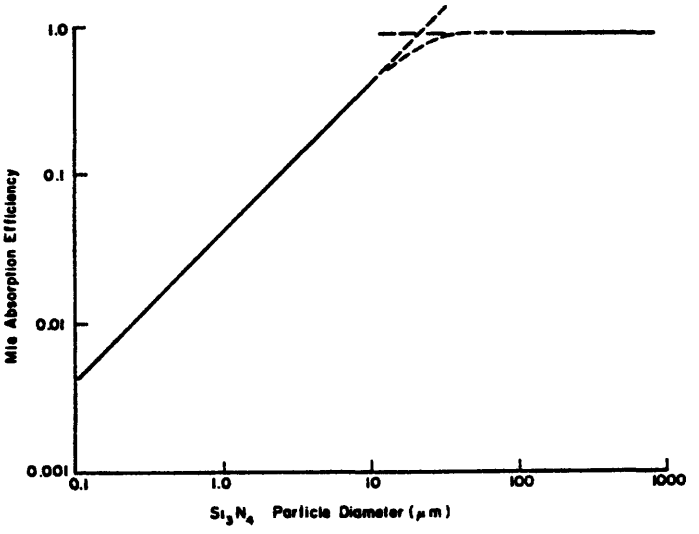

Figure 1. Mie absorption efficiency of Si_3N_4 particles to 10.6 μm light as a function of particle size.

This characteristic permits selective interaction with oversize particles. If they are heated long enough to cause considerable vaporization, their size can be reduced. Oversized particles can be eliminated from the powder avoiding subsequent problems with discontinuous grain growth and strength limiting flaws associated with oversize grains. Once the particles begin to decouple and cool down, the vaporization rate will effectively stop.

We developed process models which gave reasonably good agreement between analytical and observed experimental results which indicated that two vaporization processes probably occur. At the highest

intensities, Si_3N_4 particles vaporize as Si(g) and N_2(g). At lower intensities, they apparently decompose by losing N_2(g) leaving molten Si.

The intensity-time exposures required to cause particle size reduction were substantially more severe than predicted in our original analyses of the process. Achieving the process with a 150 watt laser was only marginal. So most of the mapping of conditions which caused comminution was done with supported particles in a pulsed laser mode. In this manner, longer, higher intensity exposures were realized than could be achieved with cw, gas entrained experiments.

These experiments demonstrated particle size reduction, leaving equiaxed particles. They did not unequivocally demonstrate the decoupling which will cause the predicted termination of the comminution process at a specific particle size. Some of the results suggested that all of the experiments were carried out in the domain where coupling efficiency was dependent on particle size. These experiments could not be completed because of the power limits imposed by existing laser equipment. The pulsed experiments showed that the process should operate as a cw, gas entrained process with approximately a 1.5 kw laser, power levels readily available with commercial equipment.

Both approaches for producing superior powders for Si_3N_4 ceramic bodies were successfully demonstrated. The direct synthesis of high purity uniform particle size powders appeared more important than the comminution process. Also, this phase could be explored with existing laser equipment, without imposing any serious limitations on the quality of the experiments. Therefore, we focused on direct synthesis of Si and Si_3N_4 powders during the second year of this program. We also explored the synthesis of SiC powders.

III. Laser Heated Powder Synthesis Process

A. Process Description

1. General

This powder synthesis process employs an optical energy source to transfer the energy required to initiate and sustain a chemical reaction in the gas phase. In this process, the gas molecules are "self-heated" throughout the gas volume, a process which is distinct from conventional ones where heat is transmitted from a source to the gas molecules by a combination of conduction, convection and radiative processes. The advantages of this means of heating, freedom from contamination, absence of surfaces which act as heterogeneous nucleation sites, and unusually uniform and precise process control, are discussed in length, elsewhere. These attributes should permit the synthesis of powders with characteristics which are ideal for making ceramic bodies.

A laser, rather than other possible optical heat sources, has been used in this program because of the narrow spectral width of emitted light and the brightness of this type of light source. The coherency of the light was not considered an important feature for this process. Coupling between the source and absorber requires virtual coincidence between the emitted and the absorption lines. If this matching occurs, the optical-to-thermal efficiency can be extremely high and the overall process efficiency is essentially that of the laser. Overall, this efficiency is much higher than is possible with broad band light sources because only small fractions of their light are absorbed by the gases. With CO_2 lasers, as have been used on this program, the overall process efficiency matches or exceeds that of other conventional heat sources: e.g., various types of plasmas, torches or heated tubes. In addition to the high efficiency, the use of laser energy sources makes possible unique reaction paths which may produce powders with unusual characteristics.

Two basic ranges of laser intensity and exposure time have been investigated. The equipment and experimental procedures used for reactions carried out in the normal or thermal domain and those used for the multiphoton, unimolecular reaction domain are so different that we have discussed them separately in this chapter of the report. The first part discusses the experimental procedures and equipment used to investigate the thermal domain. The majority of the remainder of the report discusses the various characterizations and analyses which apply to the thermal domain. The second part discusses our experiments under conditions anticipated to cause multiphoton, unimolecular reactions. This part includes the discussion of experimental results as well as equipment and procedures because the level of effort in this area was relatively limited.

2. Normal, Thermal Domain Experiments

a. Experimental Geometry

There are several choices of laser and gas stream geometry which can be applied to the thermal domain synthesis process. The laser and gas can intersect from opposite directions (counter flow) or orthogonally (cross flow). The effect gravity exerts on the heated gases and entrained particles can be varied by operating in horizontal or vertical directions. In varying degrees, all of these configurations have been investigated experimentally. Each has features which suggest different choices for experimental and production scale processes.

The majority of the experiments were carried out in the cross flow configuration where the laser beam and reactant gas stream intersect orthogonally. This experimental configuration produces a very stable reaction and the reaction zone where the laser beam and gas stream intersect can be analyzed. In addition, there is very little interaction between the reaction and the cold walls of the cell.

Unfortunately, this reaction geometry has several disadvantages. Both the gas stream and the laser beam have nonuniformities which are ideally axisymetric. Because of these nonuniformities, different volume elements within the gas stream are subjected to different laser intensity and velocity histories. In addition, the laser beam is progressively absorbed as it passes through the thickness of the gas stream further increasing the range of exposure histories between the entering and the exiting sides of the gas stream. The second source of variable history was effectively eliminated by designing the experiment so the gas stream is optically thin. Under "reference" operating conditions, approximately 2% of the incident power is absorbed by the reactant gas stream. While this configuration is suitable for experimental purposes, it is evident that a commercial process could not permit 98% of the laser light to be wasted. With a single laser beam, single gas stream configuration, increasing optical density of the gas stream results in an improved efficiency but causes an increasingly unacceptable variance in the local beam intensity. Multiple pass or multiple beam optical configurations can give acceptable uniformity and efficiency.

A counter flow geometry used for some of the absorptivity and threshold experiments has certain advantages over the crossflow configuration described above. In principle, each gas element can be subjected to an identical time-intensity history as it flows into the laser beam. Also, the gas column can be made long enough so all the light is absorbed, giving maximum optical efficiency.

In practice, however, there are also disadvantages. The gas velocity profile is parabolic and the laser beam is Gaussian, so both are nonuniform. These nonuniformities can be reduced to arbitrarily low levels by manipulating the laser beam and various coaxial gas flow velocities. By properly adjusting the laser and gas stream, it should be possible to achieve identical time-temperature histories for all gas elements which would then result in the desired uniform particles.

Both approaches are complex, which makes experimentation difficult and requires that they be thoroughly understood before they are used to produce quantities of powder. We are nearly at a point where we can design such a system.

b. Horizontal Gas Stream Configuration

The details of the horizontal flowing gas cell configuration used in these experiments have been described earlier, and will only be highlighted in this report(Haggerty and Cannon, 1978). The apparatus is shown in Figure 2. Under the reference conditions, an unfocused CO_2 laser beam enters the reaction cell through a KCl laser window. The reactant gases, SiH_4 and NH_3, enter orthogonally to the laser beam through a nozzle into the cell at controlled pressure. The reaction produces a visible reaction flame and the powder is carried to a microfiber filter between the cell and the vacuum pump.

A set of process conditions were defined which produced a stable reaction. These were established as a bench mark or reference conditions from which variations systematically were made. The reference conditions for Si_3N_4 synthesis (Table I) are a pressure of 0.2 atm, SiH_4 and NH_3 flows of 11 cc/min and 110 cc/min respectively, and a laser power intensity of 760 watts/cm^2. Approximately 2-5 watts are absorbed by the optically thin gas stream. These reference conditions yield approximately 1 g/hour of light brown to whitish-tan Si_3N_4 powder. Up to 5 grams of powder have been produced in one experiment.

TABLE 1

Reference Processing Conditions for Synthesis of Si_3N_4 Powders

Laser Power Density	760 watts/cm^2
Cell Pressure	0.2 atm.
SiH_4 Flow Rate	11 cc/min
NH_3 Flow Rate	110 cc/min
Argon Flow Rate (to window)	600 cc/min
Argon Flow Rate (to annulus)	400 cc/min

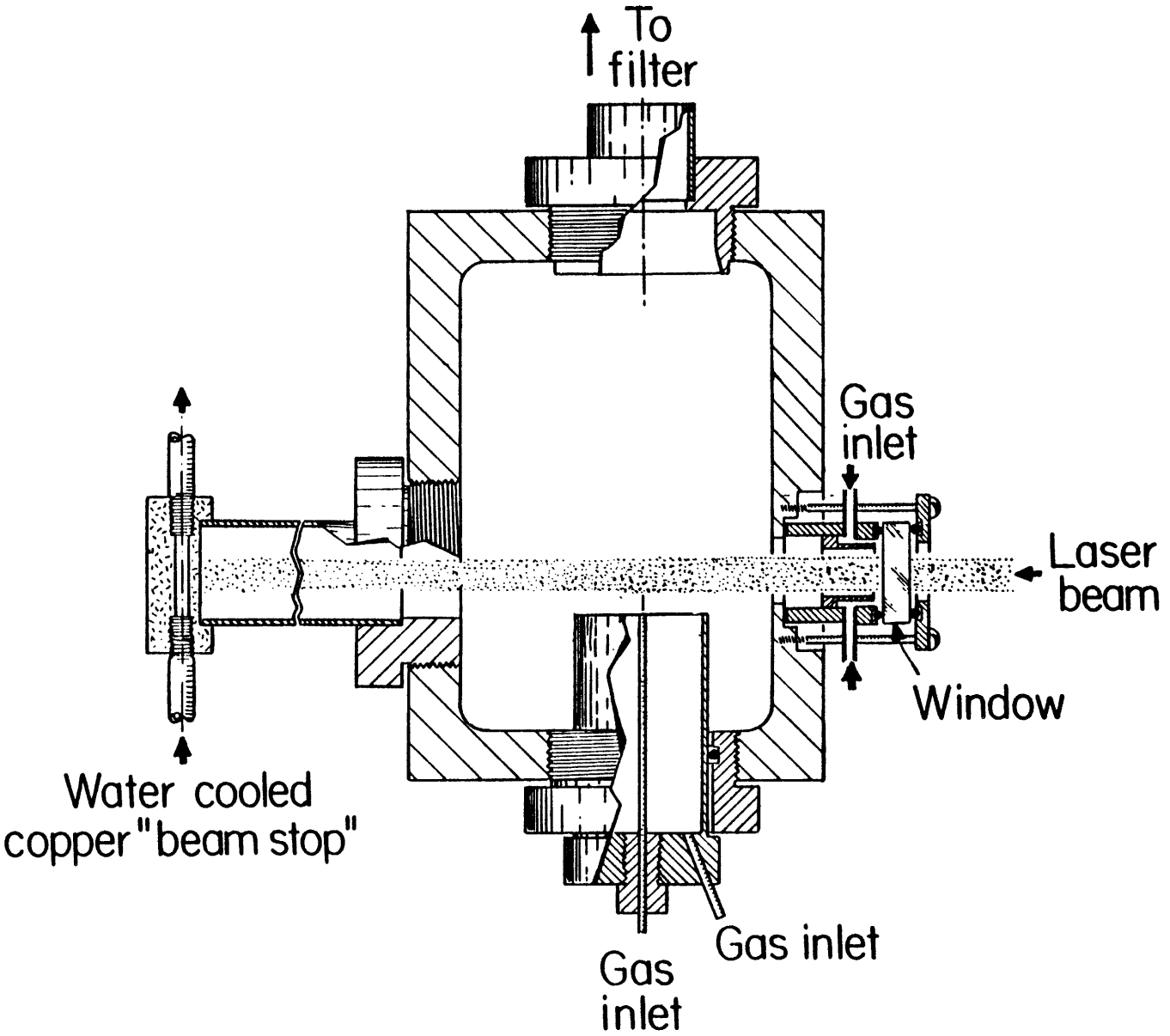

Figure 2. Schematic of Powder Synthesis Cell

The majority of the first powder synthesis experiments had a horizontal gas stream. This configuration has several difficulties associated with it. The buoyant forces carry the heated gas and particle streams toward the KCl window and the roof of the reaction cell. This causes window breakage and also powder build-up on the cell roof, leading to possible contamination. Although 600 cc/min of argon across the KCl window alleviates the breakage problem, we are concerned that it will compromise our ability to analyze the laser gas interactions and is a source of inefficiency.

It was anticipated that if suitable changes were made to allow the reactant gas stream to flow vertically with a horizontal laser beam, these problems could be greatly reduced or entirely eliminated.

c. Vertical Gas Stream Configuration

The apparatus was modified so that gases flow in the upward, vertical direction. Bouyant forces on the heated gas and powder act with, not against, the flowing reactant gases. This keeps the powders from depositing on the laser entry window and the cell walls for hours compared to only a few minutes with a horizontal cell, enabling prolonged powder synthesis experiments and increased powder production. Powder collection processing and purity maintenance are all easier.

There is no indication that the powders synthesized in the vertical configuration differ from those synthesized horizontally, except in uniformity of color. Powder color varied within the cell when in the horizontal position, but was more uniform in the vertical orientation. Further experiments will be performed to verify these preliminary conclusions.

With the cell in the vertical orientation, we have been able to reduce the argon flow rates across the KCl window and through the annular sleeve by a factor of 4 without undesirable powder build-up

inside the cell and on the KCl window. This, and perhaps further reductions in buffer gas flow rates, results in a cleaner, more efficient and more idealized reaction zone.

The increased protection to the KCl window offered by vertical operation has also allowed higher pressure reactions (0.75 atm NH_3/ SiH_4) to be investigated. The increased space above the reaction zone and improved reaction stability resulting from vertical operation have allowed thermocouple measurements of reaction zone temperature. The advantages of vertical operation are sufficient that the majority of current and future experiments will be performed in this position.

d. Atmosphere Control

The reactant gases employed are electronic grade NH_3 and SiH_4. Prepurified argon is used as a buffer gas. The gas train includes a Cu oxygen getter, a molecular sieve, a dry train, and an oxygen analyzer. There are currently 10-15 ppm O_2 in the argon gas. A Ti getter will be in place shortly in an effort to further reduce the O_2 content of the buffer gas.

e. Particle Collection

The powders are collected in a cylindrical microporous filter. Up to 5 grams of powder can be collected at one time. Beyond this, the filter clogs rapidly and we are no longer able to maintain a constant cell pressure. Additional efforts are underway to use a longer filter system (about 15 gram capacity) and attempt electrophoretic means of powder collection.

f. Powder Handling

All post production handling of these laser synthesis powders is performed in an argon inert atmosphere glove box (Vacuum Atmospheres)

with < 10 ppm O_2 and < 10 ppm H_2O. The glove box includes an evacuable antichamber and a regeneratable H_2O and O_2 gettering train. The glove box will soon be fitted with an extension which will incorporate a press and a sintering-nitriding furnace to allow all processing to be done without exposing the powders to the atmosphere. These future efforts will allow production and processing of larger amounts of powders with total atmosphere control.

3. Multiphoton Unimolecular Reaction Domain Experiments

A series of experiments were undertaken to determine the feasibility of inducing unimolecular, multiphoton reactions. In this type of reaction, individual gas molecules absorb sufficient energy to cause dissociation prior to colliding with other gas molecules, thus precluding a normal distribution of energies and a "thermal" reaction. The unimolecular reaction conditions were investigated to determine whether the resulting powders would exhibit unusual, advantageous characteristics.

Unimolecular reactions have only recently been studied since the advent of powerful infrared lasers. A sample calculation illustrates why they are only possible at low pressures and require extremely high intensity laser radiation. A 10.6 μm photon has approximately 0.1 eV energy and the average dissociation energy for an H atom from silane is 3.4 eV. (JANAF Thermochemical Tables, 1971) Thus the energy of at least approximately 34 photons must be absorbed and retained to cause dissociation. The energy transfer per collision is approximately 0.2 eV, (Jensen, et al., 1978) so the molecule cannot suffer more than a few collisions while absorbing the exciting photons. At 10 Torr pressure, the reaction must occur in less than 10^{-7} sec, since the collision frequency is approximately 10^{8} sec^{-1}. With an absorption cross-section of 10^{-20} cm^2, an intensity of approximately 10^{8} $watts/cm^2$ is required to transmit the necessary dissociation energy/molecule in a 10^{-7} sec pulse. Higher intensities may not produce unimolecular reactions since the gas may break down into a plasma. In fact, only highly absorbing molecules are candidates for unimolecular reactions because of the breakdown phe-

nomenon. With laser intensities on the order of 10^3 to 10^4 watts/cm^2 and pressures near one atmosphere as described above, the reactions can be expected to be well into the thermal region from the formal criteria of having a normal energy distribution.

These experiments used a tunable, pulsed TEA CO_2 laser. The conditions which caused a reaction were determined by varying fluence and reactant pressure in the closed reaction cell. The occurence of a reaction was determined by an irreversible pressure change, the IR spectra of the gases after irradiation and the appearance of powder within the cell. The apparatus is shown schematically in Figure 3.

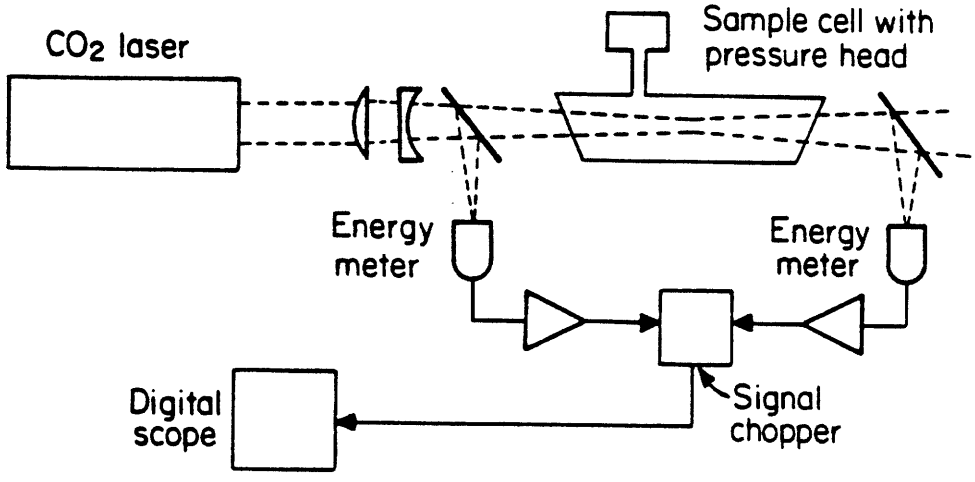

Figure 3. Schematic of laser, diagnostics and reaction cell used to investigate the feasibility of unimolecular reactions

A Tachisto Model 215 G TEA CO_2 laser was used. Pulses contain 0.3-0.5 J with a FWHM of about 50 ns. Three different focal length lenses were employed to vary the beam fluences at their diffraction limited wastes. Peak fluences were 20, 29, and 185 J/cm^2 for 80, 67, and 28 cm focal lengths respectively. These fluences correspond to peak inten-

sities in the range of 4×10^8, to 4×10^9 watts/cm^2.

Mixtures of reactant gases were established by successively freezing known quantities of SiH_4 and NH_3 into a liquid N_2 cooled cold finger. Experiments were undertaken after the cell had warmed to room temperature. Cell pressures were monitored with a MKS 2000 A pressure transducer before and after irradiation and both with and without condensible gases frozen into the cold finger. After irradiation, the products were characterized by their infrared spectrum with a Perkin-Elmer 567 IR spectrometer.

Table II contains a summary of results for the TEA laser experiments. No reaction was noted for conditions which did not produce dielectric breakdown inside the cell, which is evidenced by a blue-white spark. The breakdown threshold is sensitive to sample pressure and peak intensity. Breakdown always occurred with fluences of 185 J/cm^2 for pure silane at pressures above 2 Torr. For fluences below 185 J/cm^2, however, breakdown did not occur for pressures up to approximately 5 Torr. For conditions where no breakdown occured, no incondensible gas (i.e., H_2) was observed in the cell after irradiation and no change in the reagent IR spectrum occurred. In one case, Cl_2 was added to the gas mixture to "getter" any hydrogen produced and thus prevent the back reaction. However, for this case breakdown was experienced at pressures of approximately one torr using the 28 mm focal length optics. Several attempts were also made to induce reactions in mixtures of silane and ammonia. These experiments produced the same results as the silane-only experiments. For a given pressure of gas, a long focal length produced no reaction, and a short focal length caused breakdown. Lower reactant pressures might have avoided breakdown, but the quantities of products have been too small to detect with our apparatus, so this experiment was abandoned.

Although reactions were induced with both P(20) and P(24) emissions, they do not appear to have resulted from multiple-photon absorption. Reactions occurred only when a white spark was evident near the focus

of the beam, an indication that dielectric breakdown occurred at these high fluences. The reactions were probably induced by plasma or arc heating rather than multiple-photon absorption.

Recently evidence has been cited (Ronn, 1979) which suggests that the reaction products and intermediates formed during multiple photon and breakdown induced reactions are identical to one another. The evidence is admittedly tenuous; but it suggests that it would be worthwhile to continue these series of experiments to determine whether unique powders are produced by this type of reaction.

TABLE II. TEA laser Experiments Performed on Silane

Line	p(torr)	Lens f.l. (cm)	# of shots	Results
SILANE ONLY:				
P(20)	4.6	80	2000	no change in pressure or spectrum; no powder
	1.21	28	2200	slight brown powder
	5.4	28	400	heavy powder; pressure increase; breakdown
	2.2	28	500	light powder; pressure increase
	2.4	67	1000	no changes
	2.4	28	1500	breakdown on first pulses
P(24)	2.0	28	2200	slight powder; pressure increase; breakdown
	3.57	28	700	powder, breakdown
	0.54	28	2000	no change
	1+1 torr Cl_2	28	1500	breakdown on first 250 shots
SILANE/AMMONIA:				
P(24)	0.6/1.2	67	2300	no changes
	0.6/1.2	28	1000	no changes
	1.4/3.7	67	1000	no changes
	1.4/3.7	28	1000	breakdown; slight powder; pressure increase

B. Analyses and Characterizations

Our efforts on this program have been approximately equally divided between developing a description of the process and the resulting powders. The process itself is completely new and consequently has required many fundamental property measurements and new analyses to develop the most rudimentary description. Powder characterizations have followed normal practice for these types of materials. Extremely small particle size has required special handling procedures to avoid contamination. Our ultimate objective is to understand the interrelationships between process variables and powder characteristics.

1. Process

a. Optical Absorptivities

The CO_2 laser emissions and the reported absorption peaks for SiH_4 and NH_3 are summarized in Fig. 4. Despite the profusion of absorption peaks, which are extremely close to the emitted lines, this data cannot be used to estimate absorptivities. Unless the emission and absorption lines lie within a few doppler widths of one another (1 doppler width $\simeq 2\text{-}4 \times 10^{-5}$ μm), there will be virtually no coupling at low pressures. The resolution with which the absorption spectra were determined does not permit the location of the peaks to be stated with this precision. At higher temperatures and pressures, the actual peak widths are determined by subtle thermal and pressure broadening effects. The spectra appearing in the literature were not measured with sufficient precision to allow us to calculate absorptivities. Therefore, the actual absorptivities must be measured with laser sources and with gas conditions which are very close to those of interest for the reaction. No data of this type existed for SiH_4 and only one measurement was located for ammonia. For very dilute ammonia in one atmosphere of air, the absorptivities (Patty, et. al., 1974) were 0.14 and 0.12 cm^{-1} atm^{-1} for the P(18) and P(20) emissions respectively of the (00°-10°0) band which as noted below are of particular interest. Absorptivity measurements

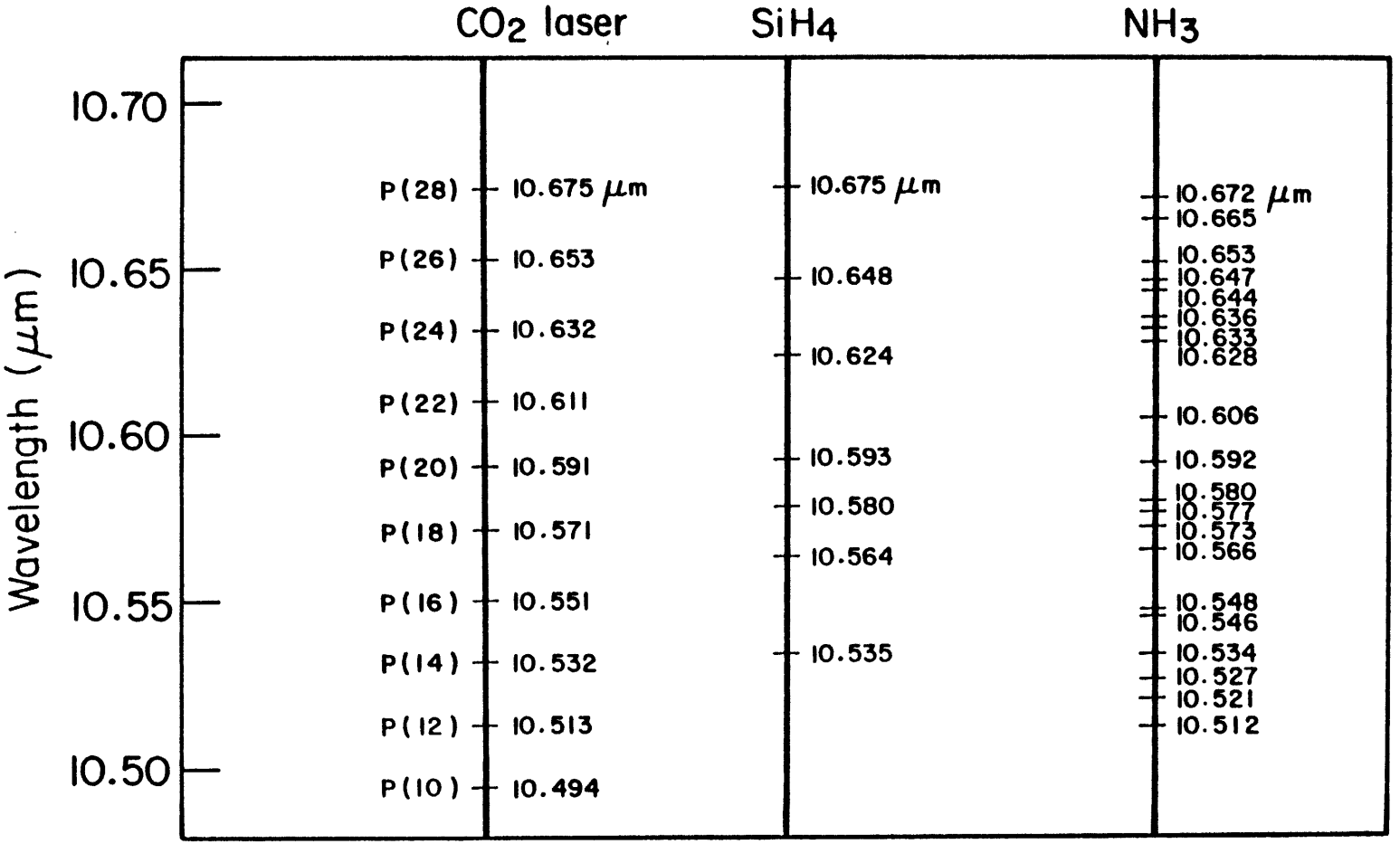

Figure 4. A comparison between the spectral absorption lines in SiH_4 (Tindal, et. al., 1942) and NH_3 (Garing, et. al., 1959) near 10.6 μm, and the emission lines of a CO_2 laser.

were an essential part of the experimental program because their values are needed for modeling the energy absorbing processes.

i. Absorption Measurements

The absorptivity measurements were made in a manner which permitted the results to be interpreted directly in terms of the Beer-Lambert equation,

$$I = I_o e^{-\alpha p x}$$

where, I and I_o are the transmitted and initial laser intensities passing through a column of absorbing gas of depth x and at a pressure p. The pressure and temperature dependent absorptivity (α) is calculated directly from the experimental conditions and the observed I/I_o. The value of α is extremely sensitive to several factors which include the exact wavelength of the emitted light, and both the temperature and pressure broadening effects that accompany absorption of light. While the theory is qualitatively useful, the quantitative measurements and their results must be viewed as largely empirical at this time. Therefore, experiments must be made very carefully over a range of conditions which approach, but do not exceed, the reaction thresholds.

We have conducted two series of absorbtivity measurements. The first used an untuned Coherent Radiation Model 150 CO_2 laser. This laser was used for the majority of synthesis experiments, thus all analyses and modeling had to be based on the specific lines emitted by this laser in either pulsed or cw modes. Furthermore, the line widths emitted from individual laser cavities vary enough from one another to cause different effective absorptivities. The second measurement series used a line tunable CO_2 laser built at M.I.T.(Burak, et. al., 1969). This laser was used to survey the absorptivity levels for most lines emitted by a CO_2 laser in the vicinity of 10.6 μm.

ii. Measurements made with non-tunable laser

a. Laser Emission

The Coherent Radiation Model 150 CO_2 laser mirrors were aligned in the cw mode to emit a nominally gaussian energy distribution, which approximately coincides with the maximum emitted power. The laser's spectrum was analyzed in cw and pulsed modes with an Optical Engineering Spectrum Analyzer.

In a cw mode or in long duty cycle pulsed modes (pulse length > 50% pulse period), this laser emits entirely at the P(20) line of the 00°1 - 10°0 band (10.591 μm). In a low duty cycle pulsed mode (pulse length $\leq$ 10% pulse period), the laser emits alternately on either the P(20), or the P(18) (10.571 μm) lines. The energy in individual pulses (measured with a Gen Teck joule meter coupled to a storage oscilloscope) was essentially constant (within $\pm$ 10%) whether the laser emitted on the P(20) or P(18) lines.

b. Absorption

The apparatus used for the absorption measurements is shown schematically in Fig. 5. The optical path length is 10.2 cm with the O-ring sealed KCl windows in place. The cell has ports which are used for gas inlet, evacuation and pressure monitoring purposes. Pressure is monitored during absorptivity measurements to determine whether a reaction was induced since all of the reactions investigated produced a net increase in the number of gas molecules. Measurements were made under fixed volume conditions at predetermined initial gas pressures by alternatively measuring the pulse energy at the "transmission detector" either with or without partially absorbing gases in the cell. The ratio of these intensities yields the absorptivity directly since the effect of the absorptivities and reflections of the beam splitter and windows cancel out in the ratio. A KCl window was used as a beam splitter to reduce the pulse energy below reaction thresholds. The laser was pulsed at 1 hz with pulse lengths of 0.1 and 1.0 msec and energies of approximately 25 or 100 mJ.

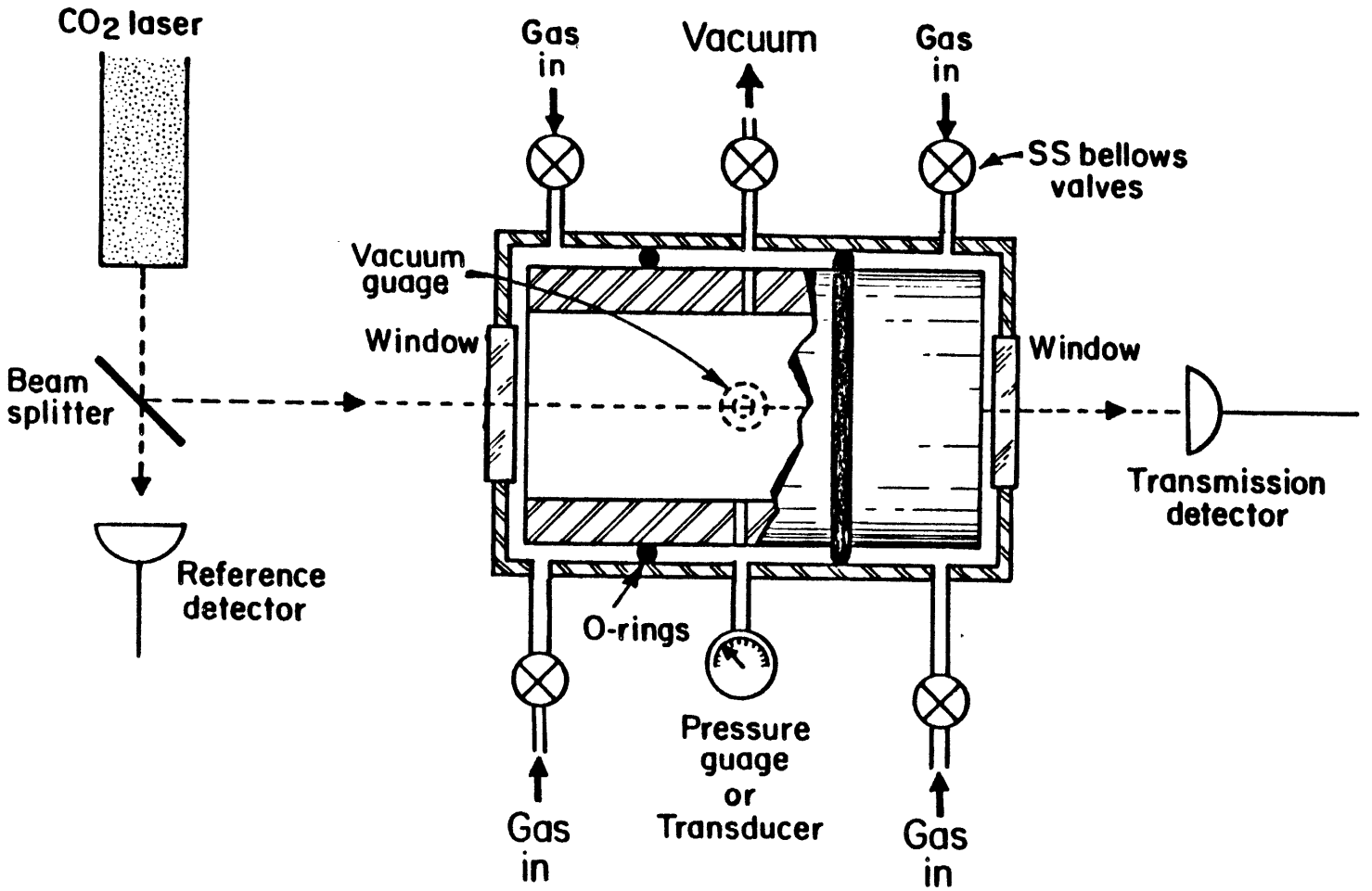

Figure 5. A schematic representation of the stainless steel cell used for absorption measurements and counterflow powder synthesis experiments. The inner sleeve and O-rings were removed for absorption measurements.

The calculated absorptivities based on results of these measurements are shown in Figs. 6 and 7. These energies as we will see later are on the order of 1/6 to 1/2 of that needed to raise the gas temperature to the reaction threshold. We must then conclude that during these absorption measurements, the gas is heated by the laser pulse. Silane exhibited two distinct absorptivities which are attributed to the laser emitting on either the P(18) or P(20) line. The assignment of the lower absorptivity to the P(18) line was based on information from the literature (Tindal, et. al., 1942) rather than direct correlation with spectrographic data. Ammonia exhibited equal absorptivities to the two CO_2 lines which are approximately 20 to 50 times lower than SiH_4 absorptivities.

The variation in silane's absorptivity with pressure is probably due to pressure broadening effects with closely spaced, strongly absorbing lines. With gas absorbers and laser emission sources, the apparent absorptivity is a much more sensitive function of the overlap between an absorption line and an emission line than is apparent with conventional spectroscopy. At low pressures ($P \leq 1$ torr), the widths of the absorption lines and the laser emission lines are only approximately one doppler width ($\Delta\lambda \simeq 2\text{-}4 \times 10^{-5}$ μm). Unless the laser emission and gas absorption lines lie within a few doppler widths of each other, the absorptivity will be extremely low. The absorption lines broaden progressively with increasing pressure for pressure levels above a few torr. Since the total area under the absorption peak remains constant with increasing pressure, the maximum absorption intensity decreases as the peak broadens. The variation in apparent absorptivity with pressure will depend on both the relative locations of the emission and (possibly many active) absorption lines as well as the details of the broadening characteristics of each active absorption line. For a single absorption line, increasing pressures will cause an increased absorptivity as long as the peak broadening effects dominate and then may cause a decrease if the shrinking peak height effect dominates. A continuous increase in absorptivity is expected if the emission and absorption lines are widely separated.

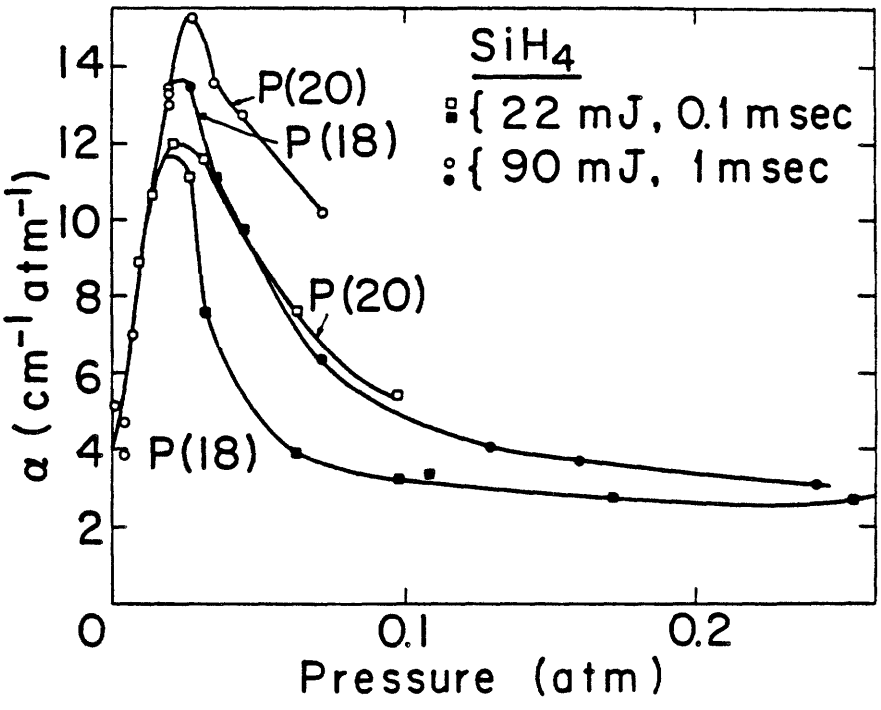

Figure 6. The absorption coefficients of SiH_4 as a function of pressure for the P(18) and P(20) CO_2 laser lines.

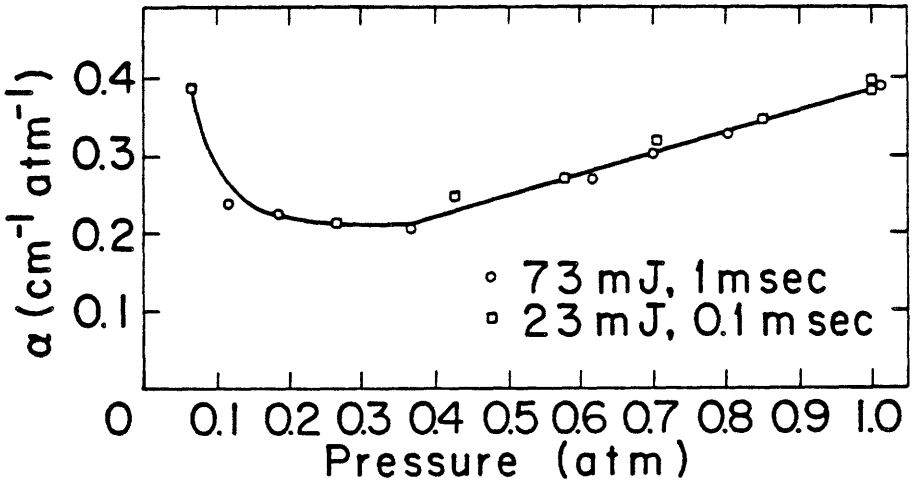

Figure 7. The absorption coefficients of NH_3 as a function of pressure for the P(18) and P(20) laser lines.

Ascending, then descending behavior is expected when they are closely spaced but are not coincident.

Silane's absorptivity, shown in Fig. 6, follows the ascending and descending pattern. We conclude by this behavior and the high absorptivities, that the active absorption line(s) is closely spaced to both the P(18) and the P(20) lines. It is likely that the P(20) line is absorbed by the SiH_4 line at 10.593 μm, but it is difficult to determine whether the P(18) line is primarily absorbed by the SiH_4 line at 10.580 or at 10.564 μm (see Fig. 4). Ammonia's absorptivity probably results from the combined effects of many weak absorption lines which are in the vicinity of the emission lines. Thus, the absorptivities to the P(18) and P(20) lines are equally low and weakly dependent on pressure and are of the same order of magnitude reported previously for NH_3 (Patty, et. al., 1974).

The high absorption coefficient of the silane is very important since it allows efficient absorption of laser energy for powder synthesis. For instance, about 70% of the laser energy would be absorbed in the first cm of a one atmosphere 10/1 NH_3/SiH_4 mixture. Since all of the energy is absorbed directly in the reaction zone, the efficiency of the powder synthesis process is dependent only on the efficiency of the CO_2 laser. A 10-15% wall-plug to light efficiency is typical for a CO_2 laser.

Additional absorption measurements were made with a tunable CO_2 laser to determine if the reactant gases had higher absorption coefficients in bands other than the P(18) and P(20) lines of the Coherent 150 laser.

iii. Measurements made with a tunable laser

Absorption measurements performed in this series differed from the others in two major ways:

(1) line selection was obtained through a tunable CO_2 laser which allowed the absorption coefficient of a large number of lines to be measured;

(2) laser intensity was sufficiently low to preclude virtually any heating of the silane or ammonia.

Two methods were used to obtain the absorption coefficients of SiH_4 and NH_3, differing slightly in technique as dictated by the availability of equipment. The apparatus in Fig. 8 was employed for all but a few data points; it employs two choppers to modulate the sample and reference beams at different frequencies, allowing two lock-ins to detect the sample and reference intensities independently while using the same detector. When only one chopper was available, it was positioned to modulate the two beams at a relative phase of 90°, again allowing independent measurement with one detector (see Fig. 8).

The laser itself consists of a 1 m gain cell with rotatable grating and a 5 m radius mirror forming the cavity; the beam emerges via a small hole in the mirror, which is mounted on a piezolectric crystal. The stabilization network depicted in Fig. 9 minimizes output intensity drift caused by thermal expansion of the aluminum girder supporting the optical elements. By modulating the mirror position by $\pm$ 0.5 μm, the frequency of the cavity resonance is modulated under the CO_2 gain curve. A lock-in detects the slope of the gain curve at the cavity mode frequency by demodulating the very slight ripple in the laser output and applies an error voltage to the pzt to bring the cavity mode to the gain profile.

Two cells were employed with 1.73 cm and 9.97 cm optical path lengths, fitted with perpendicular NaCl windows. When possible, sample pressures of about 130 torr were used; for very strongly attenuated lines, lower pressures were needed. Gas pressures were read from an MKS 2000 A pressure transducer with a 0.1 - 1000 torr stated range, although the head was found to be sensitive to 10^{-2} torr. The response

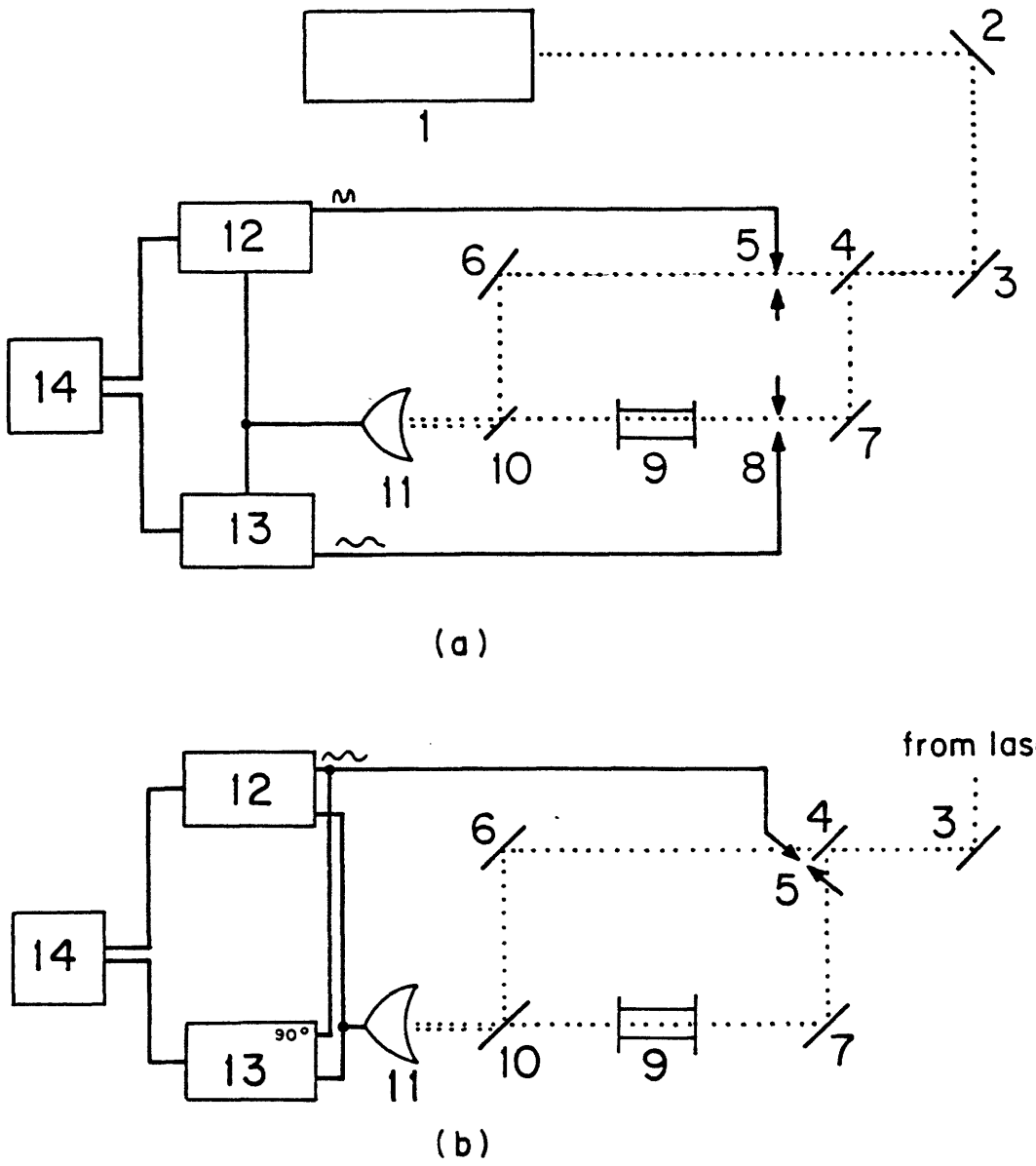

Fig. 8. Apparatus for absorption measurements. a) two chopper method. 1 - laser; 2,3,6,7, - mirrors; 4,10 - ZnSe beamsplitters; 5,8 - choppers; 9 - sample cell; 11 - pyroelectric detector; 12 - reference channel lock-in; 14 - PDP 8/L computer. b) single chopper method; lock in 13 is set to 90° relative phase.

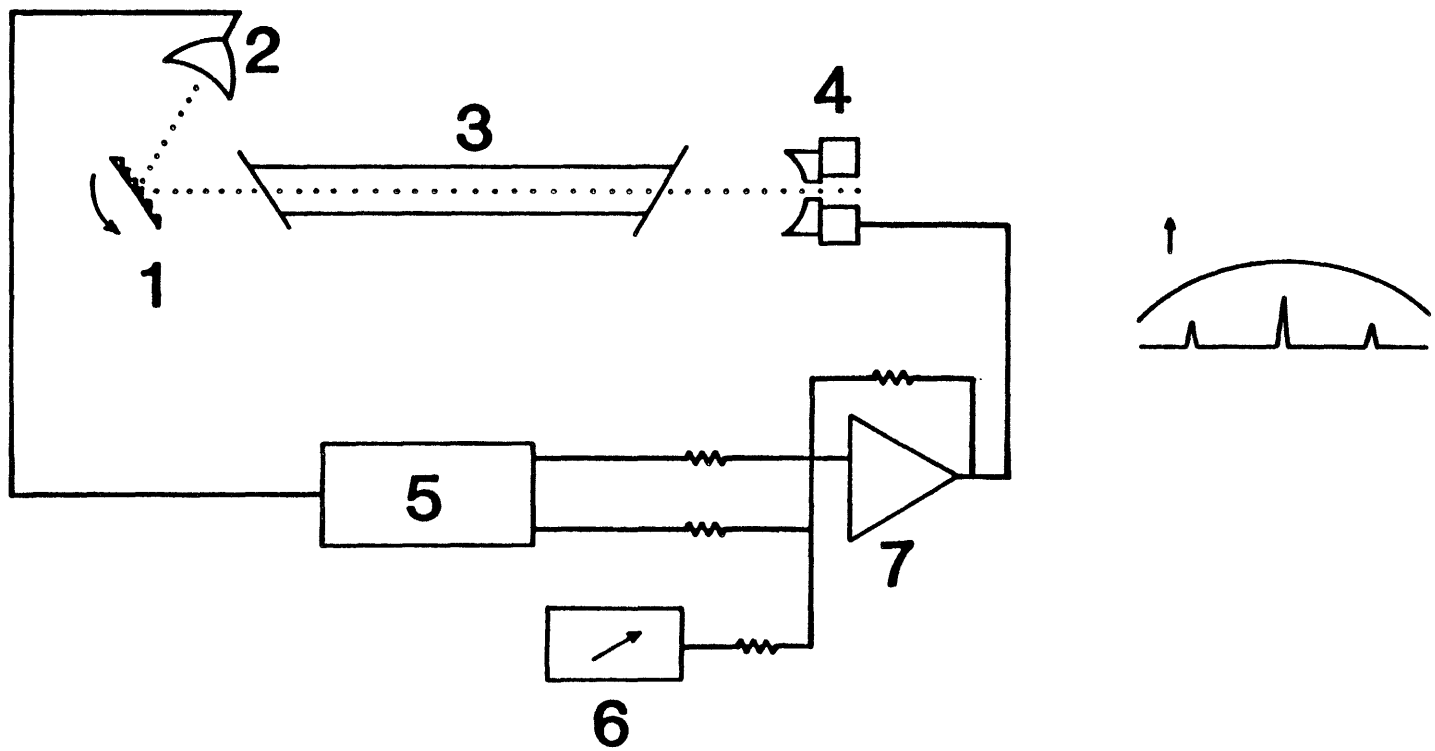

Fig. 9. Stablized CO_2 laser used in absorption measurements. 1 - rotatable grating; 2 - detector; 3 - 1m gain tube; 4 - pzt mounted mirror; 5 - lock-in; 6 - manual dc offset; 7 - high voltage op amp. Depiction of cavity resonances under a Doppler-broadened gain profile is shown at right.

of the transducer was checked against a dibutylphthalate manometer. Electronic grade (Airco) silane was used from the tank after many freeze-pump-thaw cycles; anhydrous (Airco) NH_3 was treated similarly.

The procedure for measuring the attenuation of a sample is similar to the previously discussed experiments. The laser is tuned to the desired line, and the stabilization network activated. With the sample frozen into a cold finger in the cell, the ratio of the sample and reference lock-ins' signals was averaged for approximately one minute (about 400 samples) by a PDP 8/L computer. The sample was then thawed and the ratio again averaged for one minute. The laser is then tuned to the next line, etc. The transmittance, T, is given by

$$T = \frac{I/I_o \text{ (sample unfrozen)}}{I/I_{io} \text{ (sample frozen)}}$$

where I and I_o are actually the voltages from the sample and reference lock-ins, respectively. Typically the 67% confidence limits of T were $\pm$ 3%. The absorption coefficient α is calculated from T and the known sample pressure p, and cell length ℓ, via

$$\alpha = \frac{-1}{p\ell} \ln T$$

All measurements were taken at room temperature.

Table III gives the absorption coefficients, α, for NH_3 and SiH_4 for laser lines in the 10.6 micrometer CO_2 laser band. For very strong attenuations, it was necessary to decrease the sample pressure; values for α are noted in parentheses where the uncertainty in I/I_o (with sample) exceeded 25%, due to the capacity of the gas at the particular laser line.

P(18) and P(20) silane and ammonia absorption coefficients measured with the untuned laser (Figs. 6 and 7) agree quite well with those in

TABLE III. Absorption coefficients $(atm - cm)^{-1}$ for the 10.6 μm (00°1 - 10°0) band of the CO_2 laser.

Spectral Line	Wave Length (μm)	Absorption Coefficients $(atm^{-1} cm^{-1})$ NH_3	SiH_4	Spectral Line	Wave Length (μm)	Absorption Coefficients $(atm^{-1} cm^{-1})$ NH_3	SiH_4
R(38)	10.137	.044 A	1.68 C	P (8)	10.476	.35 A	2.70 C
R(36)	10.148	not measured	.27 C	P(10)	10.494	.16 A	.50 C
R(34)	10.159	.0072A	(small) C	P(12)	10.513	.65 A	3.95 C
R(32)	10.171	.0065A	.19 C	P(14)	10.532	.83 A	1.94 C
R(30)	10.182	.047 A	.96 C	P(16)	10.551	.41 A	.96 C
R(28)	10.195	.057 A	2.68 C	P(18)	10.571	.18 A	11.8 C
R(26)	10.207	.059 A	.70 C	P(20)	10.591	.30 A	(43.0) C
R(24)	10.220	.056 A	.31 C				12.9 D
R(22)	10.233	.071 A	1.36 C	P(22)	10.611	.13 A	(28.9) C
R(20)	10.247	.12 A	1.61 C				8.17 D
		.22 B		P(24)	10.632	.16 A	(34.5) C
R(18)	10.260	7.25 B	.87 C				10.7 D
R(16)	10.275	.24 A	1.14 C	P(26)	10.653	.42 A	7.42 C
R(14)	10.289	.47 E	.79 C	P(28)	10.675	.35 A	(29.4) C
		.50 A					8.94 D
R(12)	10.304	21.5 E	.23 C	P(30)	10.696	.87 A	6.46 C
R(10)	10.319		.34 C	P(32)	10.719	13.6 E	3.79 C
R (8)	10.333		.007C	P(34)	10.741	3.5 A	5.01 C
				P(36)	10.765	1.8 E	18.1 C
				P(38)	10.788	1.02 E	1.05 C
				P(40)	10.812	1.0 A	

Conditions:
A: 136 ± 2 torr 10 cm cell
B: 130 ± 2 torr 1.7 cm cell
C: 53 ± 1 torr 1.7 cm cell
D: 11 ± 1 torr 1.7 cm cell
E: 25 ± 1 torr 1.7 cm cell
( ) denote uncertainty in precision of results

Table III. The values determined with the untuned laser were measured at comparable pressures, but using higher laser fluences per pulse. Results taken at comparable pressures are given in Table IV. The differences between the two sets of data likely result from the different conditions and the different lasers with which the measurements were performed. A temperature change in the gas due to higher laser fluences would probably affect the values. Also the emitted line widths are probably different for the two lasers.

Table IV. Comparison of Optical Absorptivities Measured with Tuned and Untuned CO_2 Lasers.

Gas	Pressure (torr)	Line	Absorptivity ($cm^{-1}atm^{-1}$) untuned	tuned
SiH_4	53	P(18)	3.7-6.4	11.8
SiH_4	53	P(20)	7.0-10.5	43
SiH_4	11	P(18)	11.0	-
SiH_4	11	P(20)	11.0	12.9
NH_3	130	P(18)	0.24	0.18
NH_3	130	P(20)	0.24	0.30

There is also agreement with the results of Patty, et. al. (1974). They prepared ammonia samples with parts-per-million concentrations in one atmosphere of air. One would expect a somewhat larger pressure broadening effect for their experiments than for the conditions used in ours. This pressure broadening causes NH_3 absorption features to overlap the spectral band width of the CO_2 laser employed. Greater pressure or laser band width will generally cause greater absorption, so their values are usually slightly higher than ours. Note that for neither Patty's nor these measurements, is the laser line width accurately known, although the lasers are of similar construction.

The absorptivities reported in Table III have two important consequences. The first is that the highest absorptivity level is exhibited

by SiH_4 for the P(20) emission from the CO_2 laser. Fortuitously, the highest gain, most efficient emission from the laser is most strongly absorbed by the reactant gas we selected based on other criteria. Also, there are other emission lines where SiH_4 and NH_3 have approximately equal absorptivities (e.g., P(34) and P(38) lines) or where NH_3 has a higher absorptivity than SiH_4 (e.g., R(18) and P(32) lines). Changing the gas species which preferentially absorb the laser radiation may influence the chemical reaction and kinetics even though the process is usually carried out in the thermal domain where a normal distribution of energies is assumed.

Although the absorptivity measurements have been extended substantially this year, we have still not measured some data which is important for modeling the process reaction thresholds and propagation velocities, etc. Absorptivity measurements must be made at elevated temperatures as a function of pressure for unreacted, partially reacted and fully reacted gases and entrained solids. We plan to make these rather difficult experiments next year.

b. Gas Flow Modeling

For characterizing the reaction zone, it is essential to understand the reactant gas flow characteristics. The Reynold's number for the "reference" conditions is approximately 140. This Reynold's number and those calculated for other experimental conditions are well below the laminar to turbular transition. A computer model has been employed to characterize this laminar, streamlined gas flow behavior (Patanker and Spalding, 1970). The results of this modeling have been qualitatively useful but have not been quantitatively consistent with observations of the reaction flame shape. A more sophisticated computer model (Spalding, 1977) has been obtained recently. We hope it will provide more accurate calculations.

Both models treat the gas flow as an axi-symmetrical emerging jet

from a circular orifice which enters into a coaxial stream having the behavior of a two dimensional boundary layer. The values of the dependent variables, i.e., fluid velocity in the direction of flow, stagnation enthalpy, mass fraction of a particular chemical species in the fluid mixture, etc., are calculated by a finite difference numerical integration of differential equations having the form:

$$\frac{\partial \phi}{\partial x} + (a + b\omega) \frac{\partial \phi}{\partial \omega} = \frac{\partial}{\partial \omega} c \left\{\frac{\partial \phi}{\partial \omega}\right\} + d$$

where: x and ω are the coordinates in the direction of the flow and the radial coordinate respectively;

a and b are arbitrary functions of the coordinate x which are related to the mass flow rates of fluid across the internal and external fluid boundaries (The internal boundary is coincident with the symmetric axis and has zero mass flow across it.);

c is a measure of the transport property which is appropriate to the variable ϕ (fluid velocity, stagnation enthalpy, mass fraction of a particular chemical species) i.e., for fluid velocity. c may have term related to the fluid viscosity and density;

d represents the source of the entity ϕ within the fluid. If ϕ represents the mass fraction of a chemical species, d will be a measure of the rate of reaction or depletion of the species within the fluid by way of a chemical reaction. If ϕ stands for longitudinal velocity, the d-term will contain an element which is proportional to the rate of diminution of pressure with distance x. If ϕ stands for stagnation enthalpy, d may contain a term expressing the influence of kinetic heating on the redistribution of temperature within the flow.

In the present form, the computer model is only concerned with the velocity distribution and the mass within the gas jet. It treats the

fluid within the jet as a single phase containing only one chemical species with constant density and viscosity. The outer jet is assumed to have the same fluid properties as those of the inner jet. Gradients in temperature and pressure as well as the effect of an exothermic reaction are ignored.

Figures 10, 11, and 12 show typical computer-calculated results describing: (1) the change in average velocity with distance from the inlet nozzle, (2) the boundary between the inner stream of reacting gas, and the outer flow of argon, (3) a typical velocity profile at a particular distance from the nozzle. The figures shown use reference conditions for orthogonal reactor geometry. An ammonia-silane gas mixture of ratio 10 to 1 and a volumetric flow rate of 121 cc/min at room temperature and 0.2 atmosphere were used for the calculations.

Comparison of the calculated gas flow behavior with the observed flame shape as shown in Figure 19, shows that at the base of the flame the diameter of the flame is almost five times larger than the calculated gas stream diameter. The diameter of the flame corresponding to the distance between the lower cusps, which may be indicative of the boundary between the inner and outer gas streams, is about 2.5 times larger than predicted by the computer model. Since the computer model does not consider the volumetric increase in the gas due to heating and reaction products, these effects should be added to the calculated stream width. A temperature increase from 300 to 1100°K will produce a volume increase of 3.6x while the increase due to the reactions, 3 $SiH_4(g)$ 30 $NH_3(g) \rightarrow Si_3N_4(s)$ + 26 $NH_3(g)$ + 12 $H_2(g)$, gives a volume increase of less than 2x. This corresponds to a total radial increase of about 1.6 x if Δr is proportional to $(\Delta V)^{1/3}$ or 2.1x if Δr is proportional to $(\Delta V)^{1/2}$, which assumes only radial expansion. The combination of these two effects substantially resolves the difference between the observed and calculated stream diameters. A more precise analysis will be possible with the new computer program.

This new computer model will permit consideration of gradients in temperature, density, viscosity and pressure of both the reacting gas

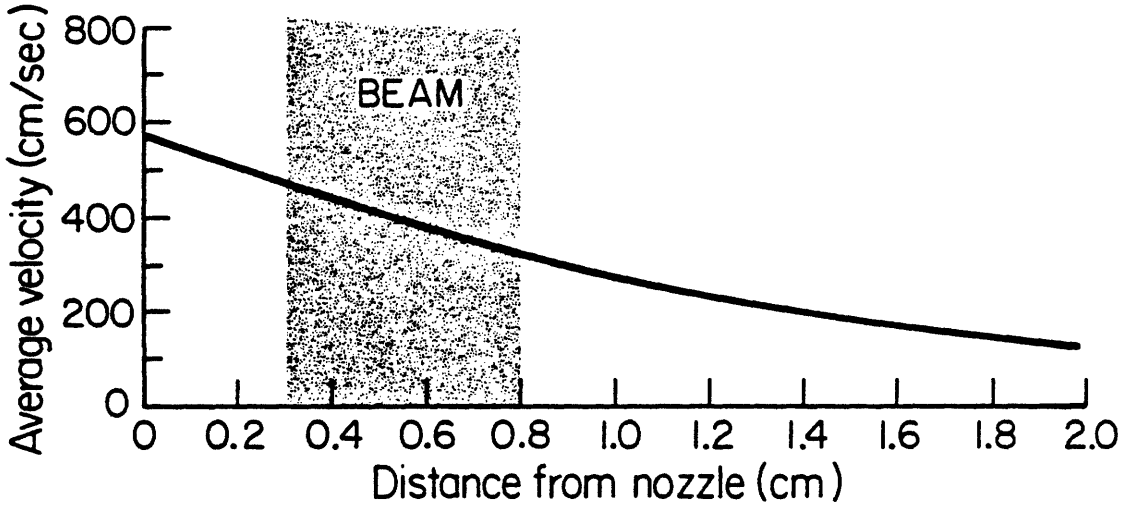

Figure 10. Average velocity of gas stream calculated for reference conditions.

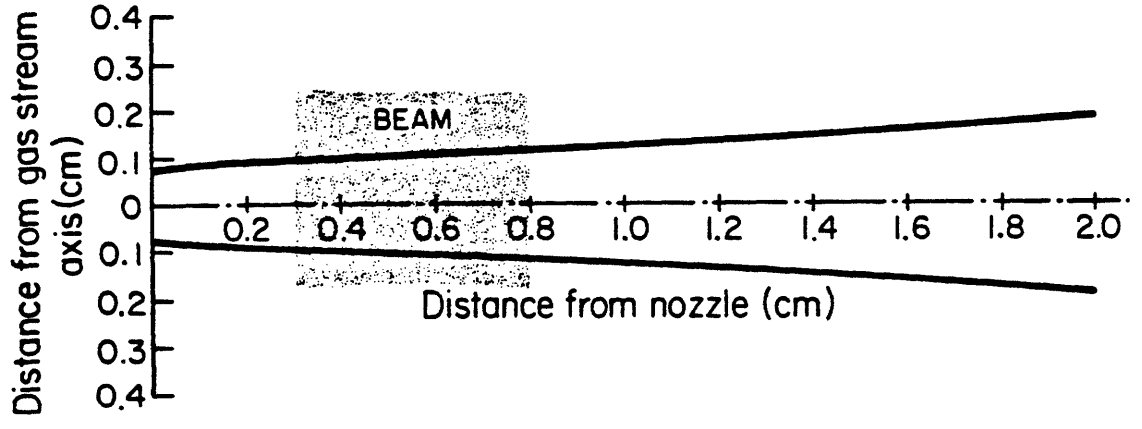

Figure 11. The computed width of the gas stream under reference conditions.

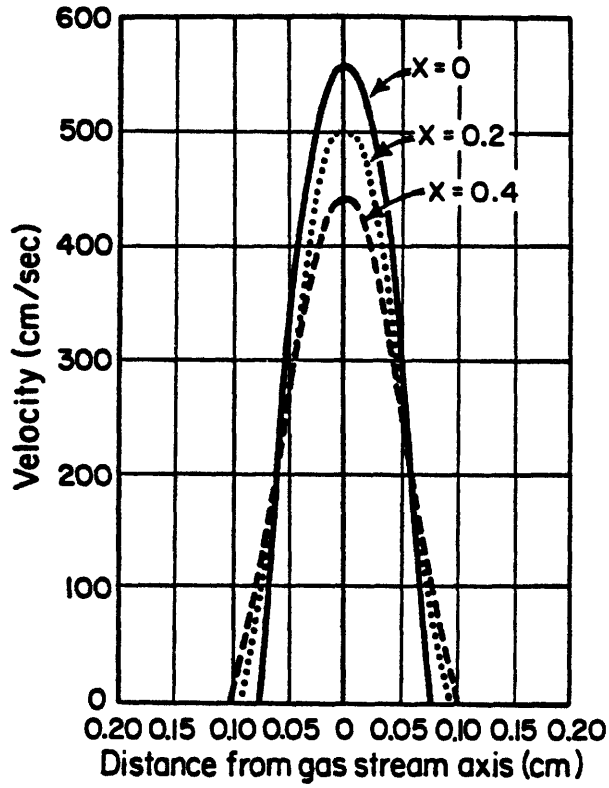

Figure 12. The computed velocity profiles of reactant gases at several distances (x) from the nozzle.

and annular flow. A single or multiple step chemical reaction can be employed and the mass fractions of the chemical species involved can be determined at various points of interest. It also has the versatility of being able to handle radiative transfer by black body emission and change in the size of particles carried by the gas stream due to condensation, vaporization, combustion or other processes.

This more sophisticated analytical tool is presently being made operational. We are also installing experimental equipment to map the stream diameter directly by holographic as well as Schlieren techniques.

c. Reaction Thresholds and Reaction Propagation Velocity

Static- and flowing-gas experiments have been carried out to map laser-intensity pulse-length thresholds required to induce chemical reactions in SiH_4 and NH_3 + SiH_4 mixtures. These threshold determina-

tions provided data for modeling studies and served as an empirical basis for designing a continuous synthesis process.

Threshold pulse lengths were determined for various static reactant gas mixtures and pressures with fixed pulse intensities. Reaction threshold experiments were undertaken in the cell shown in Fig. 5. A reaction was detected by a permanent pressure change in the closed volume cell. Typically, the transient pressure rise, which occurs with heating the gas, disappears within 30 msec unless a reaction occurred. Multiple pulses above threshold conditions caused visible concentrations of powder to form on the entrance window. The persistent formation of this powder caused us to abandon these static threshold determinations in favor of the flowing-gas experiments.

It was anticipated that the powder deposit on the input window would cause two serious problems. Whether formed from SiH_4 or NH_3/SiH_4 mixtures, the powders would attenuate the laser beam resulting in erroneous, higher than actual threshold determinations. In addition, the KCl windows might be broken with high energy pulses and large quantities of powder. The only beneficial effect of powder forming on the KCl window was that the window could be used as a support for IR spectrographic analyses.

Static threshold and synthesis experiments were successfully completed. They proved too time-consuming to use for detailed mapping of the threshold conditions and were abandoned once it was verified that static and flowing experiments gave identical thresholds.

Counter flow synthesis experiments were also carried out in the cell shown in Fig. 5. Slight modification was required from the configuration used in both the absorption measurements and the static synthesis experiments.

The stainless steel insert was put in place to direct the flow paths of the gas streams. Gases are pumped from the cell in a radial

direction at approximately the midpoint along the cell's axis. An inert, transparent gas is introduced at the laser entrance window which flows axially along the beam's propagation direction. The absorbing reactant gases are introduced at the laser exit window. They flow axially, opposite to the beam's propagation direction. They meet the inert gas at approximately midpoint in the cell where they are subjected to the full intensity of the laser beam. They are then drawn out of the cell.

The principal advantage of this cell configuration is that the reaction occurs far away from the laser windows and reaction products do not reach the windows because of the gas flow directions. The inert gas protects the entrance window area and the beam is fully attenuated by the time it reaches the exit window, so there is no problem with heating in that region. The exit window can be used safely for direct observation or other optical characterizations of the reaction zone. For short laser pulse lengths, this experimental configuration is indistinguishable from a static synthesis experiment except for the important feature of preventing reaction products from forming on the windows. These features, combined with the good visibility of the reaction zone, proved to be a superior experiment for determining reaction thresholds than the static experiments.

Reactions were visibly evident in several ways. With long, high intensity pulses, a weak, blood-red emission was evident near the center of the cell. Weaker or shorter pulses resulted in a momentary increase in the optical density of the gas within the cell; when sighting through the cell against a light background, laser intensity pulse-length combinations above certain threshold levels caused a darkening effect. Under some light combinations, wisps of white smoke-like powder were also visible. Threshold combinations were taken to be the minimum conditions which produced any visible effect. Thresholds determined in this manner agreed closely with the static thresholds identified by an irreversible pressure change.

The purpose of these experiments was to map the laser intensity

pulse-length thresholds which cause a reaction as a function of gas pressure and composition. The small quantities of powders which formed in pulsed experiments were not captured by any means. The results of the reaction threshold experiments with SiH_4 and NH_3/SiH_4 mixtures are shown in Figs. 13 and 14.

These experimental results are reported separately on Figs. 13 and 14, because the laser pulse characteristics change for pulse lengths shorter than approximately 10 msec. For pulse lengths longer than approximately 10 msec and laser beam plasma current in the range of 20-50 ma, the intensity of the laser beam is independent of pulse length. Thus, the energy emitted in a pulse is directly proportional to pulse length. For pulse lengths shorter than 10 msec, the average beam intensity in this particular laser becomes dependent on pulse length. Fig. 14 indicates the average pulse intensity as a function of pulse length. The longer pulse length experiments employed a KCl beam splitter to reduce the intensity of the beam at the cell to approximately 10% of the emitted beam.

The equation which describes the absorption of laser energy and the resulting temperature rise and heat losses is straightforward to write, but has not been solved in a general manner. The solution is difficult because optical characteristics of the materials are not well known and mass/heat transfer processes are intrinsically difficult. Limiting solutions have been developed.

The heat power balance in any volume element of partially absorbing gas exposed to light is given by the following equation:

$$I_o \Delta A \exp(-\Sigma \alpha_i p_i x)[1 - \exp(-\Sigma \alpha_i p_i \Delta x)] = C_p \frac{n}{V} \Delta V \frac{dT}{dt} + \Delta H \Delta V \frac{dn}{dt} + \text{heat transfer losses}$$

where: I_o is input intensity in watts/cm^2

ΔV is the element of volume in question

ΔA is the cross section of the element ΔV

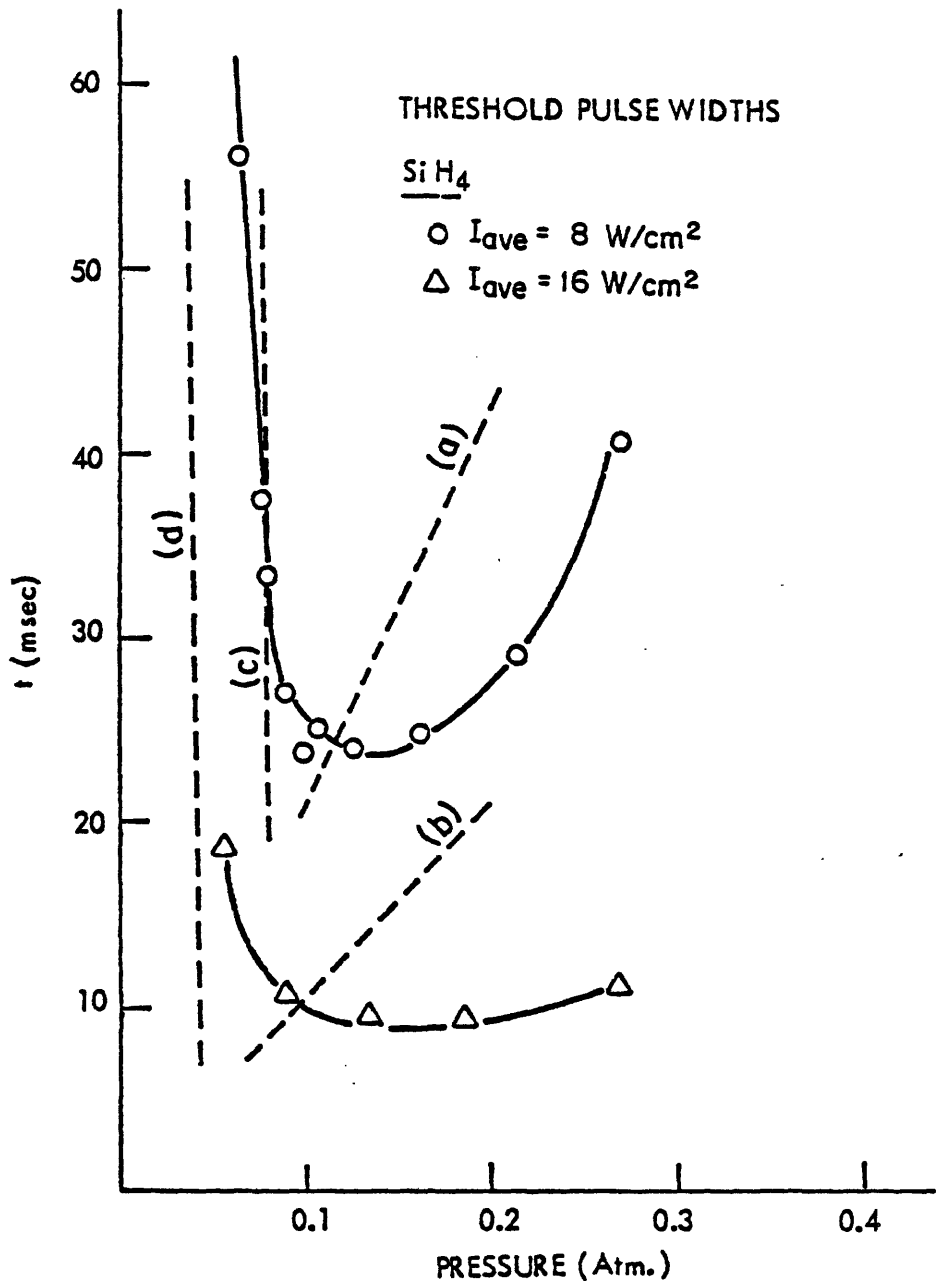

Figure 13. Threshold pulse-lengths which result in the formation of Si powder from SiH_4 as a function of pressure. Dotted lines a, b, c, and d are calculated thresholds equating the absorbed power to the sensible heat (a,c) and to the conductive losses (b,d). Lines a and c correspond to 8 W/cm^2 and b and d correspond to 16 w/cm^2.

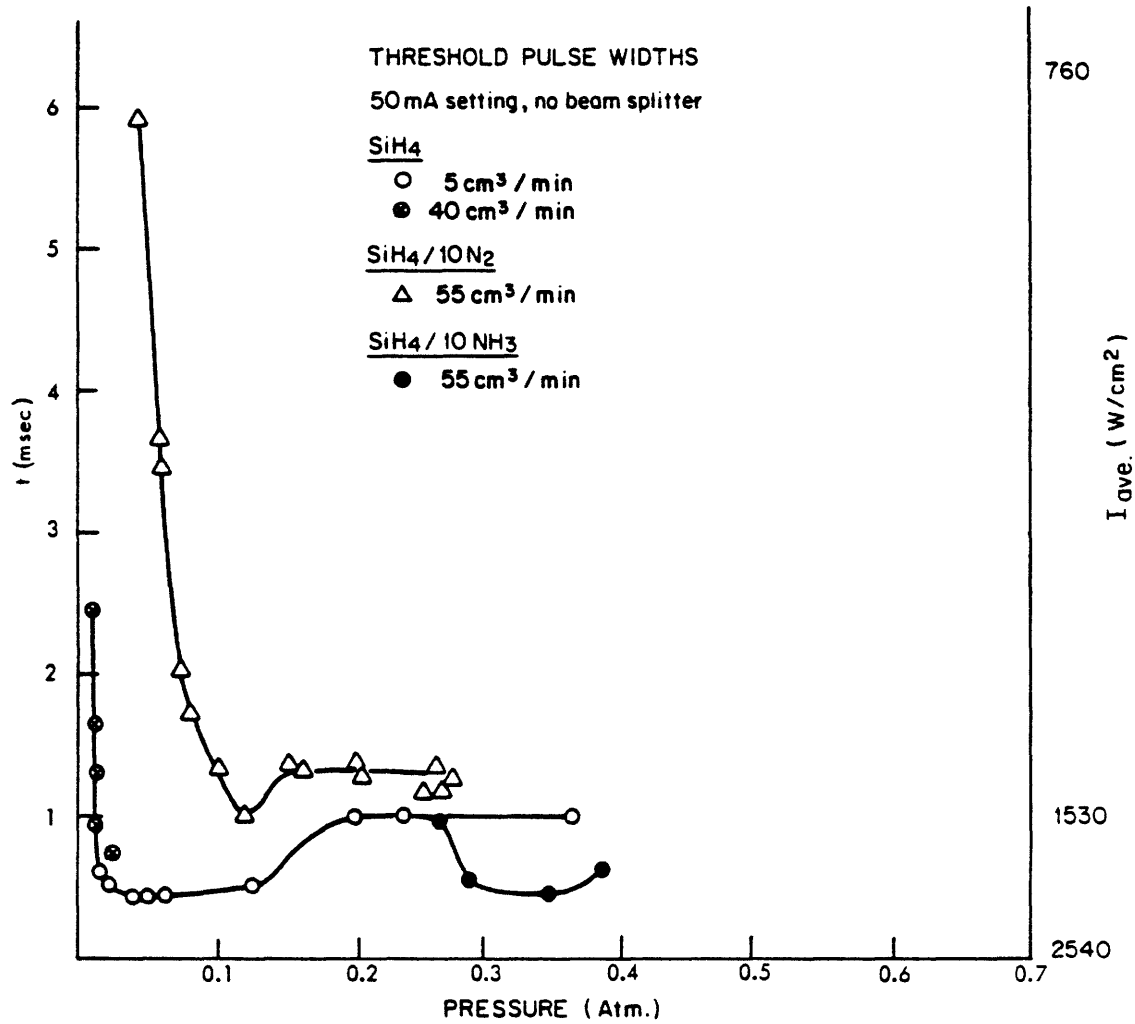

Figure 14. Threshold pulse-lengths which result in the formation of powders from several gas mixtures as a function of pressure. Pulse length dependent pulse intensities are indicated. For pulse lengths greater than 10 msec, I_{ave} equals 760 watt/cm^2.

α_i is the absorption coefficient of the i^{th} species

p_i is the partial pressure of the i^{th} species

x is the distance of the element ΔV from the window

Δx is the thickness of the element ΔV

C_p is the heat capacity of the gas

$\frac{n}{v}$ is the molar density in the volume element ΔV

$\frac{dT}{dt}$ is the rate of change of temperature

ΔH is the heat of reaction in joules/mole

$\frac{dn}{dt}$ is the moles of gas reacting per unit of time per unit volume.

The geometrical relationships are shown in Fig. 15. The expression on the left of the equation indicates the heat absorbed within a volume element ΔV after a beam, having an initial intensity I_o, has traveled a distance x through a partially absorbing medium. The terms on the right represent the means by which the absorbed heat can be dissipated. These are the sensible heat, the latent heat, and heat losses by conductive, convective and radiative processes.

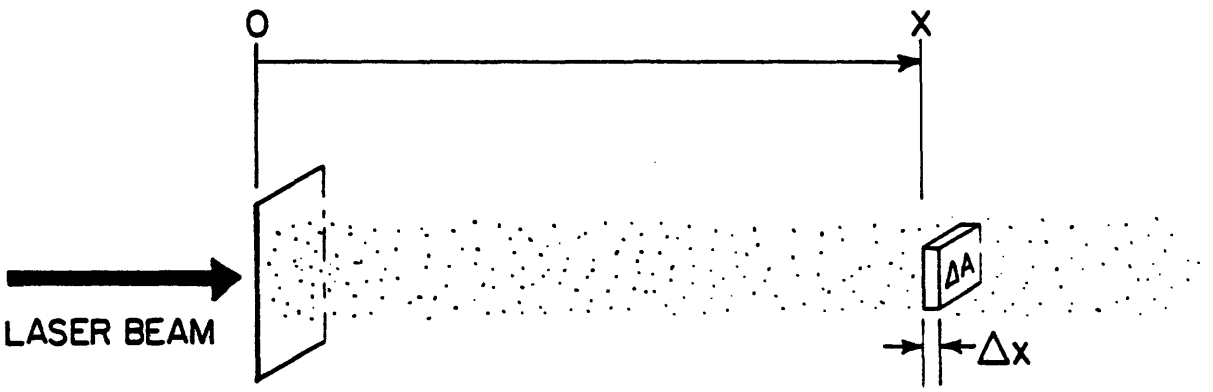

Figure 15. Schematic representation of the volume element (ΔV) within a column of gas which is absorbing the laser beam. At $x \leq 0$, there is no absorption of the laser beam.

The details of the absorption expressions become uncertain once sufficient power has been absorbed to cause heating along the path of the beam. Sudden temperature rises cause both the α_i and the p_i values to change. The experimental results shown previously in Figs. 6 and 7 show how α_i varies with moderate pressure changes under essentially constant temperature conditions. It can be anticipated that the α_i's will vary with temperature, but no experimental measurements have been made yet. Also, no quantitative α_i measurements have been made through partially or completely reacted gases. These factors, combined with uncertainties about the temperature, pressure, and density along the path of the laser beam preclude meaningful calculations for locations which are remote from the first interaction volume. To evaluate the terms on the right, it is necessary to develop a model for mass transfer which accompanies the intense localized heating from the laser as well as that from the exothermic reactions. We are presently developing models and evaluating the solutions. To date, only simplified solutions have been examined to explain the high and low pressure regimes of the threshold experiments shown in Figs. 13 and 14.

One set of solutions considers the volume element which is first exposed to the laser beam. In the counter flow geometry, this is at the plane where the two axially flowing gas streams intersect. This point is subjected to the most intense illumination within the cell, it is the first to reach threshold conditions. Also, the illumination intensity is not complicated by a complex "upstream" history. For this set of solutions, we have assumed that the reaction proceeds spontaneously to completion when the premixed reactant gases reach a critical temperature. The exothermic heat, therefore, does not affect the threshold. Convective and radiative heat losses were assumed to be negligible. The assumption about convective heat losses is valid since the pulse lengths are short compared to the gas residence time in the cell. Below threshold temperatures, the radiative power of the gas is very low. Conductive heat loses are considered below.

The first solution assumes that all of the absorbed heat is con-

verted to sensible heat. Using the substitutions $\exp(-\alpha p \Delta x) \simeq 1 - \alpha p \Delta x$ and $\frac{n}{V} = \frac{P}{RT}$, and a correction for the effect of temperature on absorption ($\alpha p(T) = \alpha_o p_o \frac{T_o}{T}$) for a freely expanding gas gives

$$\Delta t = \frac{C_\rho (T_R - T_o)}{\alpha_o R I_o T_o}$$

where Δt is the threshold pulse length to raise the reactants to the reaction temperature (T_R).

The calculated threshold pulse lengths in SiH_4 for initial laser intensities equal to 8 and 16 watts/cm^2 are shown in Fig. 13 as lines "a" and "b." The absorptivity as a function of pressure was taken as the P(20) value shown on Fig. 6. T_R is taken to be 700°C for decomposition of silane. This value was estimated for temperature ranges found in the literature (Braker and Mossman, 1971). The calculated Δt values have approximately the correct value and correct pressure dependence for pressures greater than 0.075 atm. A better fit to experimental results is obtained by choosing T_R = 300-400°C. Below a pressure of 0.05 atm, it is apparent that this simplified model does not approximate the observed behavior; threshold pulse lengths increase sharply with decreasing pressure rather than continuing to decrease.

A constant mass flow was used in all these experiments and thus the gas velocity varied inversely with cell pressure. Even at the lowest pressure, the time required for a volume element to transit the full length of the heated gas column exceeds the longest investigated pulse length by a factor of 20. Since this ratio was generally substantially larger than 20, all of the experiments fulfilled pseudo-static conditions from the criteria of pulse length and residence time. The heat flux due to the gas flow rate at the reaction temperature is also negligible with respect to the laser beam power. Only 0.7 watts is required to produce an exit temperature of 600°C at a volumetric flow rate of 25 cm^3/min.

Therefore, the rapidly increasing threshold pulse lengths with decreasing pressure do not result from either of these two dynamic effects.

The second solution to the heat flux equation treats the steady state case where absorbed heat is lost to the cold cell walls by conduction. For this case, the heat transfer rate per unit length ($\dot{Q}/L$) between the inner cylindrical column of heated gas and the cell wall is

$$\dot{Q}/L = 2\pi k \frac{T_i - T_o}{\ell n(r_o/r_i)}$$

where k is the thermal conductivity of the gas medium which is approximately independent of pressure, T_i and r_i are the inner gas column temperature and radius, and T_o and r_o are the outer wall temperature and radius.

The heat generated per unit length of the absorbing gas column is

$$\dot{Q}/\Delta x = I_o \pi r_i^2 \alpha p \exp(-\alpha p x)$$

where the terms are the same as previously defined. Equating these two expressions and solving for pressure (p) with x = 0, gives the critical pressure where conduction heat losses with a gas temperature T_i just equal absorbed power in the first exposed volume element. For T_i equal to the reaction temperature (T_R), this procedure indicates the critical minimum pressure at which a reaction can be induced,

$$P_{crit} = \frac{2k}{\alpha I_o r_i^2} \frac{(T_R - T_o)}{\ell n(r_o/r_i)}$$

With k (SiH_4) = 0.65 x 10^{-3} watts/cm°C, the critical pressures are 0.09 and 0.05 atm for I_o equal to 8 and 16 watts/cm^2, respectively and are indicated as lines "c" and "d" in Fig. 13. These critical pressures, at which the threshold pulse lengths should go to infinity, are in

sufficient agreement with the behavior exhibited by the threshold experiments to conclude that conductive losses to the cold walls caused the departure from the assumed domination by sensible heat as used in the first solution. The time required to establish fully developed steady state conduction in 0.1 atm SiH_4 is estimated to be approximately $40 - 50 \times 10^{-3}$ sec, by the equation

$$t = \frac{x^2}{4\kappa}$$

where κ is the thermal diffusivity.

Although highly simplified, these solutions to the heat balance equation give a useful description of the conditions required to initiate the chemical reaction. Once initiated at a critical temperature, it appears to proceed to completion in the heated volume element.

A second set of calculations was made to estimate the propagation of a reaction through a partially absorbing reactant gas. Generally, the conditions for initiating and propagating a reaction are the same as assumed in the threshold analyses. In addition, it was assumed that the gas becomes completely transparent to the laser light once the reaction occurs and also that the reaction exotherm does not affect the reaction. Computer calculations give the power absorbed in each volume element along the beam axis as a function of time and calculates the instantaneous local temperature in the same manner used for the threshold estimates in the first volume element. Reaction is assumed to occur when the local temperature reaches the reaction temperature (T_R). The extent of the reaction is followed by calculating the location of T_R for various time increments.

Representative results of these calculations are shown in Fig. 16. The curves marked 1-5 correspond to the times indicated in the caption. Curve "1" corresponds to the condition where the threshold has just been exceeded in the first volume element. Curves"2-5" track the propagation of the reaction (at the intersection of T(x) with the 973°K isotherm)

through the partially absorbing reactant gas column. The velocity with which the reaction propagates through the reactants is derived directly from the penetration of the reaction as a function of time. Figure 16 was calculated for the SiH_4 partial pressure and the total pressure, both equal to 0.2 atm. Figure 17 summarizes the results of similar calculations for pressures ranging from 0.04 to 0.2 atm. The time intercept (at distance = 0) is the threshold time required to induce the initial reaction. A plot of these intercept times as a function of pressure will give the equivalent of curve "a" in Fig. 13, except, in this case, a constant αp product was assumed rather than using experimentally measured values for $\alpha(p)$, as used in Figure 13. The reciprocal of the slopes of the time-distance curves are equal to the penetration velocities (V_p). The calculated values of V_p are indicated for each pressure. Similar calculations have been made for a wide range of laser intensities, gas mixtures and ambient pressures.

Results such as these are extremely important for designing process experiments. In the orthogonal synthesis configuration, the gas must reside in the laser beam long enough for the reaction to penetrate through the entire gas stream. With a thin reactant gas stream in this experimental configuration, the residence time needs to be only slightly greater than the threshold time, since the entire stream is subjected to an approximately uniform laser intensity. Achieving a stable reaction position in the cw counter flow configuration requires that the reactant gas velocity and the reaction penetration velocity be equal and opposite to each other. If the gas velocity is too low, the reaction will penetrate to the back of the cell; if it is too high, it will prevent the reaction. In pulsed, counter flow experiments, the pulse-length reaction-velocity product cannot exceed the length of the reaction chamber.

Although these analyses have not been verified quantitatively by experiment, observations have qualitatively agreed with predicted behavior. In the orthogonal synthesis experiments, residence times were generally made long enough to insure full penetration of gas stream. In specific experiments the reaction was disrupted by raising the reactant

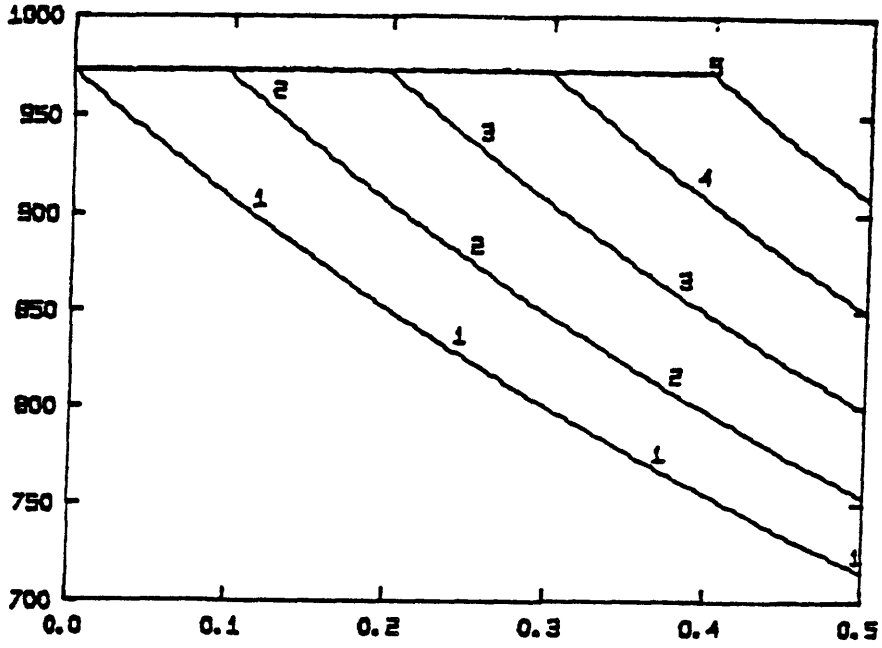

Figure 16. The temperature profile within 0.2 atm SiH_4 at various times after exposure to the laser beam. The times are: (1) 41 msec, (2) 43.2 msec, (3) 45.7 msec, (4) 48.1 msec, (5) 50.6 msec, after the laser beam is switched on. The beam intensity is 8 w/cm^2 and the product αp is assumed to be constant and equal to 0.6 cm^{-1}.

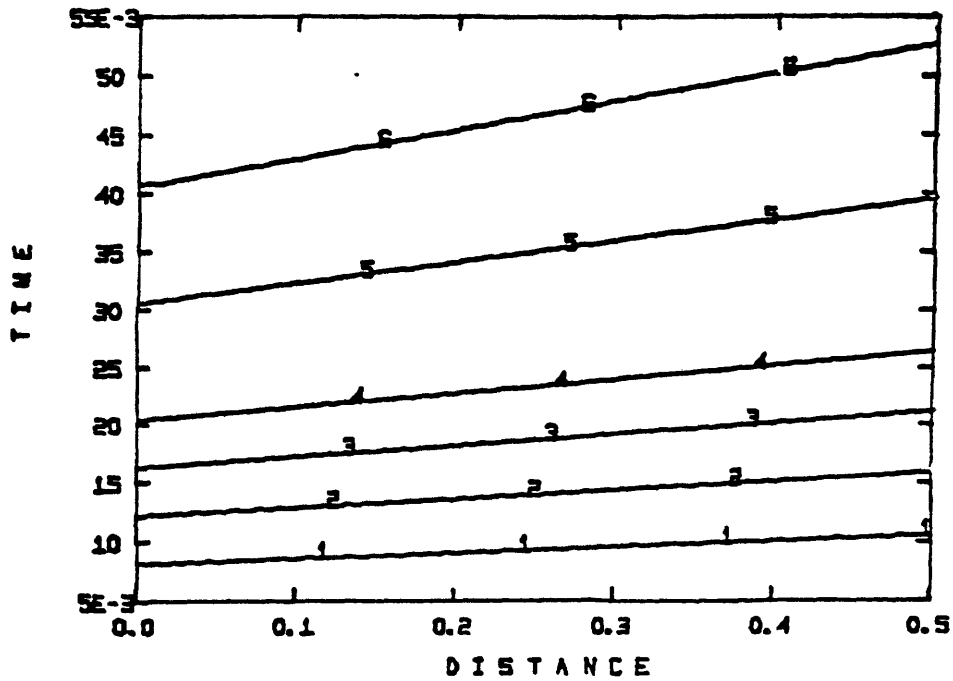

Figure 17. The time necessary to propagate the reaction zone to a specific distance for several SiH_4 pressures. The pressures are: (1) 0.04 atm, (2) 0.06 atm, (3) 0.08 atm, (4) 0.10 atm, (5) 0.15 atm, (6) 0.20 atm. The calculated propagation velocities are (1) 233 cm/sec, (2) 135 cm/sec, (3) 104 cm/sec, (4) 86.2 cm/sec, (5) 56.8 cm/sec, (6) 42.5 cm/sec.

gas velocity to a level where the residence time approximately equaled the calculated threshold time. In pulsed, counter flow experiments, pulse lengths were shorter than times calculated for the reaction to penetrate to the end of the cell. No evidence of reaction was found at the end of the cell.

Other more detailed analyses of the orthogonal configurations are recounted later in this report. Even though they are fairly complete, they require additional experimental data to permit an accurate description of the process. The least understood optical property is the effect of temperature on the absorptivities of the reactants of the gas from the time a reaction has been initiated until it is completed. The detailed gas flow paths and rates which result from laser heating and exothermic reactions require further understanding. With this base, it should be possible to develop a fundamental description of the nucleation and growth kinetics. Besides satisfying the obvious scientific interest, this knowledge is required to optimize the process variables and cell geometry.

d. Reaction Zone Mapping

An accurate empirical description of the physical boundaries and regions of the reaction zone is useful and important, by providing a reference against which the accuracy of analytical models, such as gas heat transfer, chemistry, kinetics, and fluid flow, can be evaluated. It can also be used to provide good direct estimates of many experimental parameters such as heating rates and optical absorptivities of reacted and unreacted regions of the stream. This section will describe the physical and thermal characteristics of the laser heated reaction zone.

Description and analysis of the spectral features emitted from the reaction zone as well as our analysis of various parameters such as gas velocities, gas mixtures, laser intensities, etc. are discussed in later sections.

Many features of the laser heated process are visible to the eye and can be recorded on conventional films. Figure 18 shows a photograph of the reaction flame taken under reference process conditions and in a cross flow configuration. Figure 19 is a graphic, scaled representation of the reaction. It locates the flame and particulate products with respect to the inlet gas tip, the calculated gas stream boundary and the CO_2 laser beam. The calculation of the gas stream boundary was discussed previously. The locations of various features were recorded photographically, by cathetometer and by siting directly against graph paper positioned behind the flame. The latter proved simplest and provided adequate precision. The time variance of the flame position negated any advantage in precision gained by using the cathetometer. The flame positions are generally reproducible to within approximately 0.5 mm for any set of process conditions.

The distribution of laser intensity observed in the CO_2 beam is shown in Figure 19. It was recorded by burning into a PMMA block where the depth of penetration is proportional to intensity. For comparison, the gaussian distribution of an ideal $T_{M_{oo}}$ mode is also shown. The actual intensity is sensitive to the alignment or "tuning" of the optical cavity and is found to vary slightly with the power level and time for any specific alignment. Although a difference between ideal and actual intensity distributions is evident, these results show that the total exposure to which a volume of gas is subjected as it passes through the laser beam is reasonably represented by the gaussian function.

The position, size, shape, and distribution of colors are easily reproduced for this reaction flame. There are distinct zones within the flame with the reference process conditions used for synthesizing Si_3N_4. There is a lower highly luminous zone and an upper transparent zone which terminates with a "feathery," nondistinct boundary. All other boundaries are sharp and have constant positions. Altering the input laser intensity, the reactant gas velocity, stoichiometry or ambient pressure causes the flame to change character. The effect of gas velocity, stoichiometry, and dilution are treated analytically in a later section.

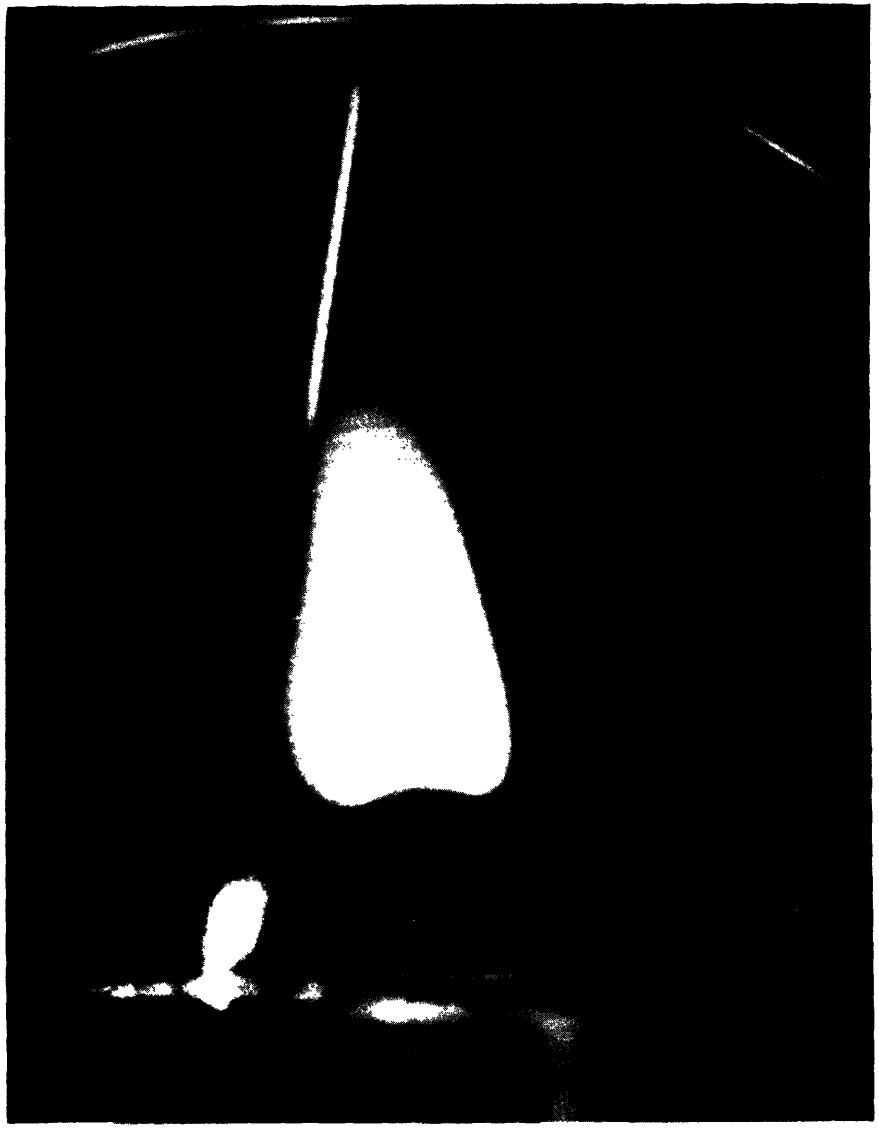

Figure 18. Photograph of reaction flame under reference conditions. The bar of light above the flame results from light (He-Ne laser source) scattered from the particulate reaction product.

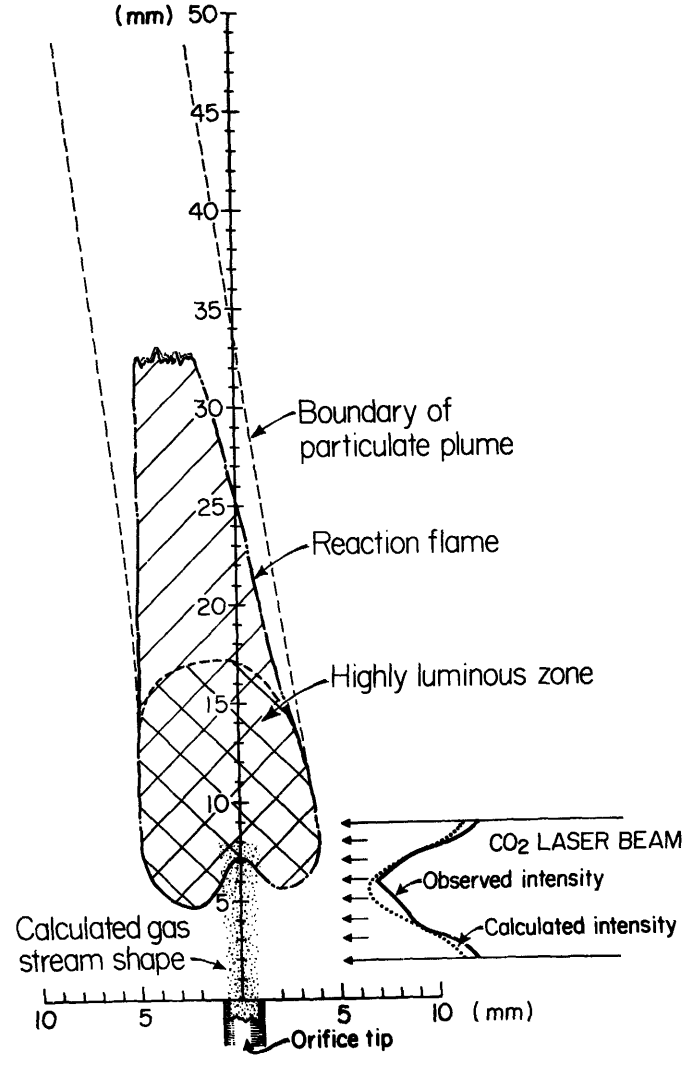

Figure 19. Schematic presentation of reaction photographed in Figure 18. Particulate plume boundary was mapped with He-Ne laser. Scattering from particles was evident to lowest point in luminous zone.

Two apparently anamalous features exhibited by the reaction flame are explained by the process conditions. The deflection of the flame and plume to the left of the vertical axis is caused by the Ar flow from the laser entrance window at the right side. The deflection angle is influenced by the reactant gas and/or argon flow rates. As will be shown analytically, the bottom contour of the flame (one upper and two lower cusps) is determined by the parabolic velocity profile in the premixed reactants, rather than mass transport effects which cause similar shapes in diffusional flames (Gaydon and Wolfhard, 1970). The two lower cusps should be at the same level; but the relative positions of the right and left lower cusps is caused by dilution of the energy absorbing gas by Ar from the right side.

It has been possible to determine the existence of a particulate reaction product at any point by light scattering, using a He-Ne laser source (λ = 6328 Å). In this manner we have been able to identify where a reaction proceeded to any extent within SiH_4 and NH_3 + SiH_4 flames as well as where and how the reaction products leave the reaction zone. As the photograph in Figure 18 shows, the scattered light is readily visible either above the flame or within the transparent upper region of the flame. Within the luminous zone, it was necessary to make observations through a narrow bandpass filter to suppress the background light.

Scattering from particulate reaction products was evident throughout the flame. At the bottom side, scattering was first evident at a point coincident with the lower boundary of the luminous zone. Above that point, the intensity of scattered light appeared constant within the sensitivity limits of the eye. Particles travel upward in a cylindrical plume as denoted by dotted lines in Figure 19. Within the accuracy of the measurements, the plume diameter is equal to the maximum diameter of the luminous zone. We could not observe any distortion from a circular cross section in the plume.

The abrupt emergence and essentially constant intensity of scattered light supports our previous assumption that the reaction occurs spontaneously and goes to completion when a threshold temperature is reached. Obviously, the terms "spontaneously" and "to completion" are meant to be referenced against our ability to make faster or higher resolution observations since the reaction requires a finite time to go to completion and occurs while traversing over a corresponding distance in the flame.

Measurements of CO_2 laser power transmitted through the reaction zone support another assumption regarding the transparency of the reacted gases and particulate product to the 10.6 μm light. Burn patterns have been made to map the laser intensity distribution both with and without reactant gases in its path. These results indicated that the reaction products were no more absorbing than the reactant gases. More precise statements cannot be made because of the long optical pathlength in the cell ($\ell \simeq 22$ cm) which tends to accumulate unreacted NH_3 during a run. With the long path length, the absorption caused by the ammonia became the same order of magnitude as that absorbed by the reactant stream. It was evident, however, that there was neither a sharp boundary nor any systematic difference across the beam corresponding to the reaction which occurs at approximately the center of the beam (Figure 19).

e. Emissions from the Reaction Zone

The relatively bright and stable visible emission of light from the reaction flame suggested that this type of nonintrusive analyses could be used to characterize the laser induced reactions as has been done with other types of more conventional flames (Gaydon and Wolfhard, 1970). In principle, the emitted spectra should provide a spacial description of chemical species and temperature in the reaction zone. This type of characterization should complete the description of the reaction which occurs within the flame boundaries discussed in the previous section.

Synthesis of Si by pyrolysis of SiH_4 and synthesis of Si_3N_4 from various reactants have been studied by many scientists (Purnell and

Walsh, 1966; Haas and Ring, 1975; Galasso, et al., 1978; Billy, et al., 1975; Cochet, et al., 1975; Greskovich, et al., 1976; Lin, 1977), yet no definitive model for these reactions has emerged for conventional process conditions. Most authors suggest that the pyrolysis reaction occurs by a step-by-step polymerization reaction (Purnell and Walsh, 1966; Galasso, et al., 1978) involving a Si_2H_6 radical. High molecular weight hydrides ultimately condense to pure silicon, simultaneously giving off H_2. It is also suggested (Cochet, et al., 1975) that Si_3N_4 is formed by Si and N bearing polymers condensing to form the nitride.

The reaction path for this specific process must be studied further. There are several reasons to believe that the descriptions in the existing literature do not apply directly to this reaction. The most obvious reason is the lack of an accepted description of even, slow, highly controlled reactions. In hydrocarbon flames, it has been found that reaction schemes deduced from measurements on slow reaction (combustion) processes cannot be applied to propagating flames with any sense of certainty. The slow reactions are usually dominated by catalytic and other surface effects. Also, the reaction temperature in the flame is usually much higher than those measured in slow or spontaneous ignition experiments (Gaydon and Wolfhard, 1970). The laser heat source itself might also be suspected of affecting the reaction by various resonance effects in the molecules. For these reasons, the prior work on the chemistry of the reaction is useful background, but it is not directly applicable to the laser heated synthesis process. The temperature distribution is obviously unique to this process.

Two sources of emissions can be expected. Banded or line emissions can be expected from reaction intermediates and reaction products. Of the possibilities, SiH_2 (Dubois, 1968), SiH_1 (Pease and Gaydon, 1976), NH_2 (Gaydon and Wolfhard, 1970; Dressler and Ramsey, 1959), and H_2 (Pease and Gaydon, 1976) have transitions which emit in the visible and ultra violet. The optical characteristics of the intermediate SiH_3 have not been studied because it is apparently too reactive. Continuous thermal emission can also be expected from hot Si and Si_3N_4 particles,

whose wavelength dependence is determined by the high temperature real and imaginary indices of the particles, as well as size effects. The determination of local chemistry and temperature requires the identification, characterization and modeling of each source of emitted light.

Three spectrometers have been employed to characterize the emission from the reaction flame for wavelengths between 4000 and 8500 Å. Moderately high resolution (5 Å) spectra were measured with a 1/4 m Jarrell-Ash monochrometer coupled to a RCA C53050 photomultiplier. This apparatus was calibrated against a tungsten lamp to permit absolute intensities to be measured over the wavelength range. Higher resolution measurements (0.5 Å) were made with a 1 m SPEX double monochrometer. Both instruments employed a PAR lock-in amplifier which yields a dynamic range of 10^4. Lower resolution (30 Å) measurements were also made with an optical multichannel analyzer (OMA) instrument which analyzes the entire spectrum simultaneously. The time-variant intensities of the flame make it extremely tedious to characterize the spectra using either of the monochrometer instruments with a confidence level which is superior to that of the lower resolution multichannel analyzer. The high resolution instrument was used to determine whether the broad spectrographic features consisted of a "forest" of lines that were spaced closer than resolution limits of the other instruments.

Figure 20 illustrates spectra emitted from CO_2 laser heated SiH_4, NH_3, and NH_3/SiH_4 gases under process conditions which are close to the reference conditions. These specific results were obtained with the 1/4 m Jarrell-Ash monochrometer at the denoted wavelengths. Equivalent results were also obtained with the multichannel analyzer instrument. At pressure levels of approximately 0.2 atmospheres or greater, the spectra emitted no spectral features. Overall, the intensity of the $NH_3 + SiH_4$ flame is approximately 1000 times higher than the NH_3 flame and 20-50 times higher than the SiH_4 flame. The NH_3 flame is fundamentally different from the other two since the latter produce hot particulate reaction products which contribute to the emission. Products from the

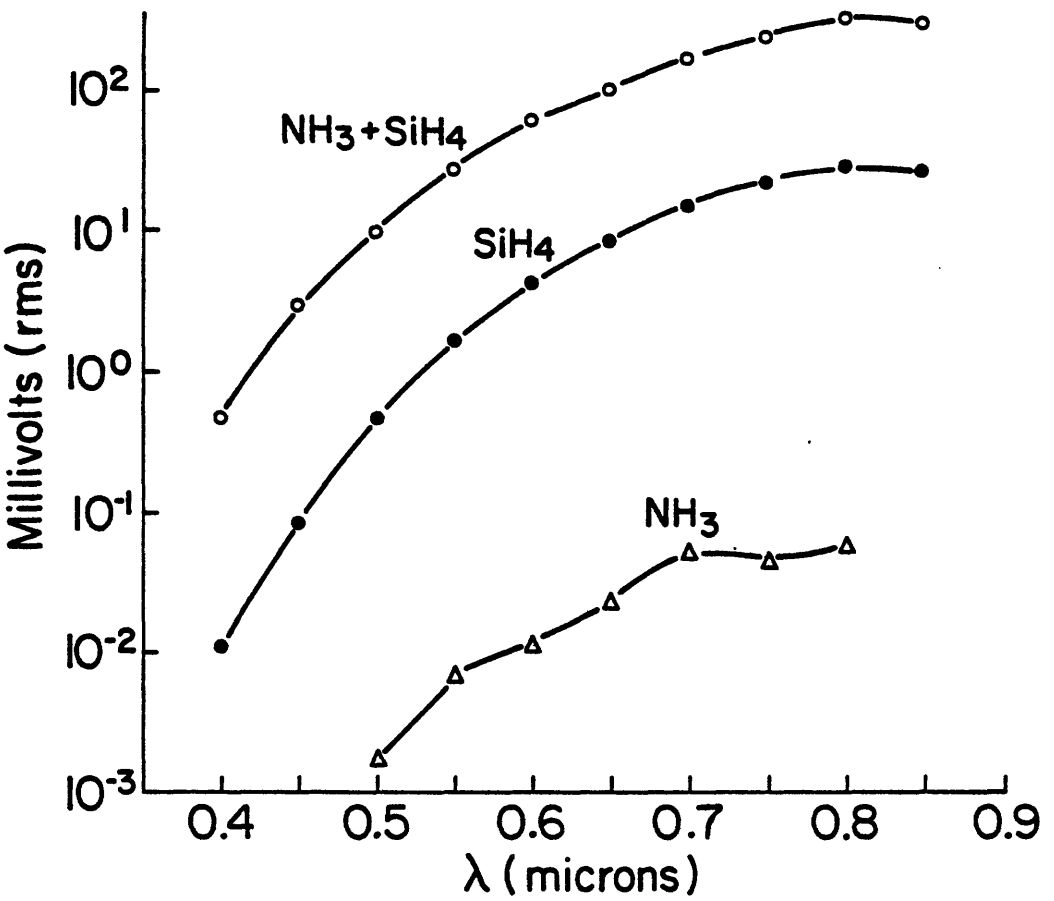

Figure 20. Emission spectra from reaction flame measured with a 1/4 meter Jarrell-Ash monochrometer. Cell pressure was 0.2 atm and gas flow rates for SiH_4 were 11 cm^3/min and NH_3 were 110 cm^3/min. Measurements were made only at the discrete wavelengths indicated in the figure. Millivolt output from PM tube amplifier was corrected for sensitivity of PM tube at a particular wavelength. Thus values are proportional to intensity.

NH_3 flame result only from gaseous reactant, intermediate and product species.

At low pressure, ($P \leq 0.07$ atm) band emissions were evident in SiH_4 and $NH_3 + SiH_4$ flames with the multichannel instrument for wavelengths between 0.4 and 0.5 μm. Typical flame emissions are shown in Figures 21 and 22. These peaks disappear completely into the continuous thermal emission by a pressure level of 80 torr (0.1 atm). Broad bands are also evident in the NH_3 flame at these low pressures. They persist to the higher pressures with progressive broadening and diminishing

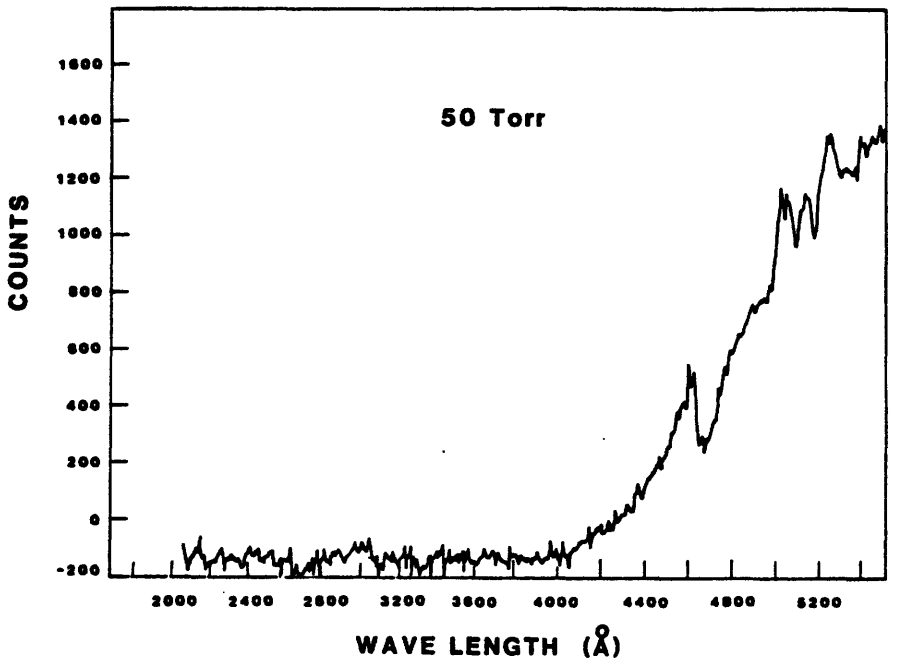

Figure 21.

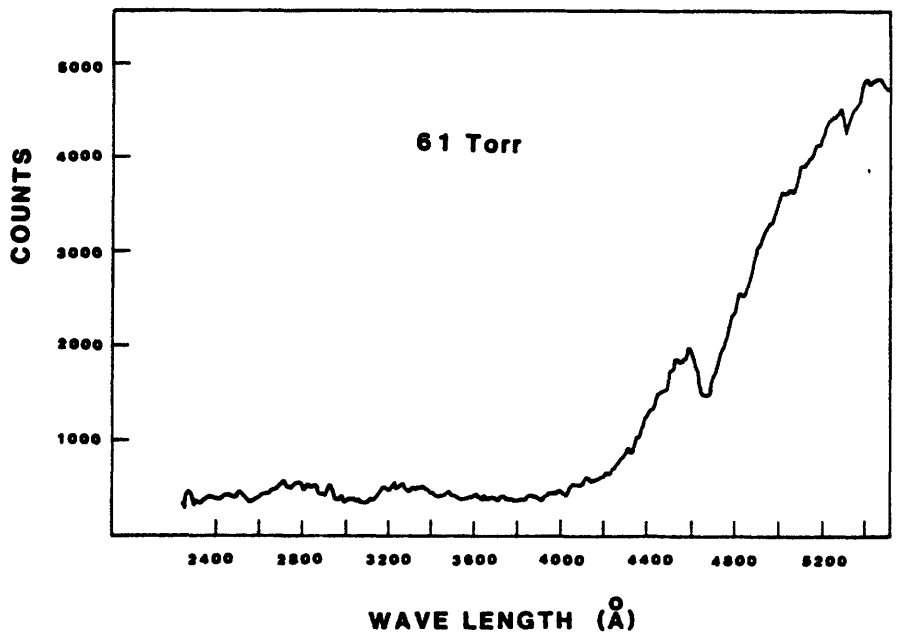

Figure 22.

Figures 21 and 22. The spectra from the SiH_4 reaction flame. The spectra was measured with a PAR OMA II multichannel analyzer. The abscissa is given as the difference in counts between a scan of a flame and a background scan.

height relative to the background, to the point where the emission appears effectively continuous.

The weak peaks observed with the SiH_4 and $SiH_4 + NH_3$ flames have not been identified with any certainty. The high resolution spectrometer has shown that, within a resolution of 0.5 Å, these peaks do not consist of a multitude of closely spaced lines. The band structure observed with the NH_3 flame is probably the ammonia α bands reported for NH_3-O_2 and CH_4-NO_2 flames (Braker and Mossman, 1971). No NH emission was detected although the multichannel analyzer is less sensitive in this region (λ = 3360 Å) and a strong thermally emitted background may have obscured it.

These results indicated that it will be very difficult to extract information about the chemical species in the flame near the reference conditions because of the dominance of the emissions by the hot particles. Pressure and temperature broadening effects also contribute to the masking of this information. Low pressure reactions will be studied to identify species which are present under those conditions and we will attempt to verify their existence at the higher pressures by appropriate modeling and analyses.

f. Temperature Measurements

We made temperature measurements by analyzing the spectrum and by direct measurement techniques, including thermocouples and brightness pyrometer. When the thermal emission is used to determine particle temperatures, the analysis must be based on the optical properties of the hot particles which will change throughout the flame with progressive reaction, varying stoichiometry, size, and temperature. We have made initial calculations of particle temperature based on room temperature properties of the particles. Assuming Wien's approximation of Planck's law, and Kirchoff's law, it can be shown that the relative thermal intensity is

$$I_\lambda = \frac{C_1 \alpha_\lambda e^{-C_2/\lambda T}}{\lambda^5}$$

Using measured absorptivities (α_λ) for the particles, least square curve fitting techniques yield an optimum fit to the experimental data for a temperature of 1400°C. The agreement between observed and calculated results is very good at short wavelengths as shown in Figure 23.

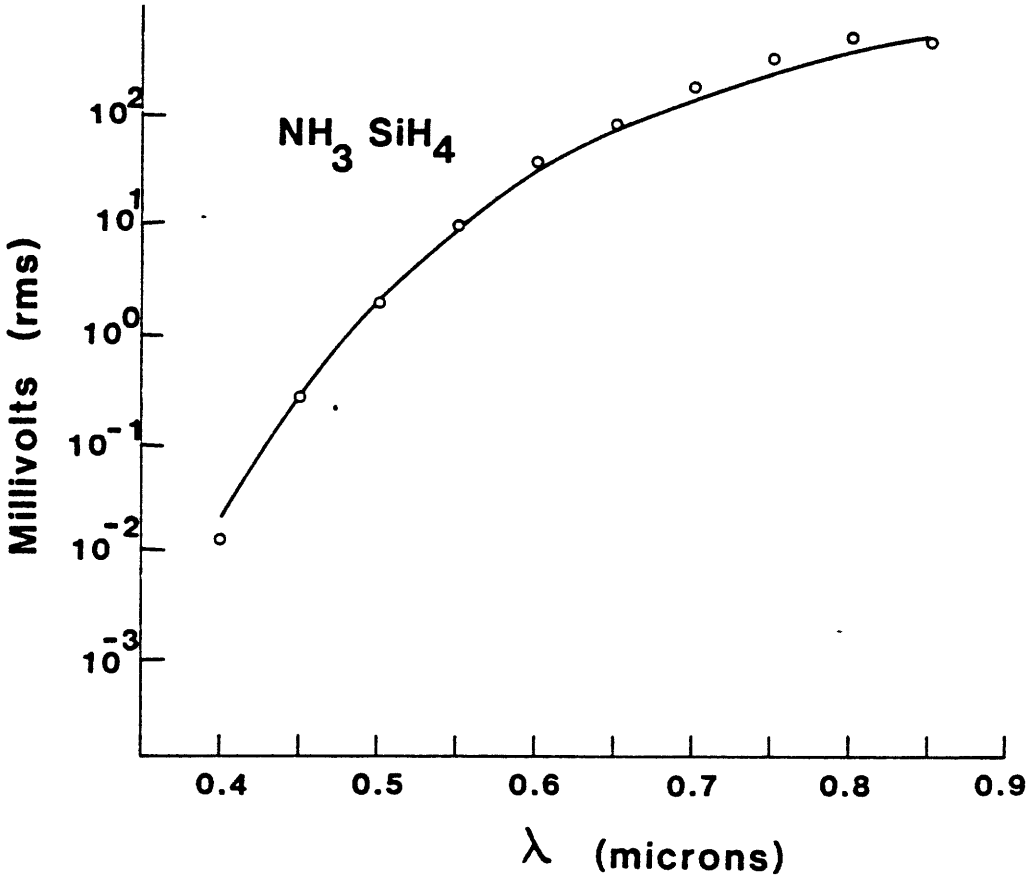

Figure 23. A least squares curve fit made by varying C_1 and T as referenced in the text, for data shown in Figure 20. The best fit temperature is 1400°C.

The value of the "optimum temperature" determined by this technique represents a more serious issue than the poor fit between observed and calculated values of long wavelengths. This temperature is higher than

those measured by two direct observation techniques and is also higher than accepted reaction temperatures. As indicated below, measurements of flame temperature with thermocouples indicated 709°C and optical pyrometry using a brightness pyrometer indicated 867°C (Appendix IB). The SiH_4 pyrolysis reaction (Braker and Mossman, 1971) and the reaction of SiH_4 with NH_3 (Greskovich, et al., 1977) are known to occur rapidly above 700°C. Thus, other indications show that the flame temperature is substantially lower than 1400°C.

In the first direct measurement technique, a chromel-alumel thermocouple was inserted in the cell at the expected flame position. First, only NH_3 was introduced into the cell, and the thermocouple measured the temperature directly above the short luminous area. The temperature varied from 331°C to 794°C as the pressure varied between 0.08 atm and 0.75°C. When the SiH_4 was introduced, the temperature immediately began to steadily decrease. Powder collecting on the thermocouple bead was thought to be responsible for the temperature drop.

The second technique, used more as a relative temperature measurement, was a brightness pyrometer sighted directly on the flame. The use of this technique rests on the flame radiation being a black body radiation from particles in the flame. The emissivity of such fine particles is expected to be much less than unity, so measured temperatures are expected to be low. A second effect which lowers the measured temperature is the low density of particles in the flame. If the area of radiation is not solid with particles, then its brightness cannot be compared with the brightness of a solid which is the basis of a brightness pyrometer.

Although, based on the above comments, the measured pyrometric temperature may be low, the relative temperatures from run to run may be correct, since the emissivity of the approximately constant sized particles is nearly constant. Rather large differences in emissivity are necessary to appreciably affect the temperature. Therefore, these

relative temperatures may also be nearly accurate. Throughout the remainder of this report, therefore, optical pyrometric measurements are reported.

To obtain the information we want, it will probably be necessary to work at lower pressures where spectral features are observable. We must also work to analytically model the thermal emission from the particles based on actual high temperature properties so the thermal and chemical luminescent emissions from the gases can be determined by difference. This spectral characterization will require a major effect to achieve our ultimate objective. Although the absolute temperature of the flames is still uncertain, it appears to be in the vicinity of 800°C.

g. Analysis of the Cross Flow Process

Throughout this program, process variables have been manipulated to determine their effect on both the process characteristics and the particle characteristics. This section discusses our analysis of the process. The following section considers their effects on powder characteristics.

Analyses have been developed which intend to explain empirical observations and infer what is occuring in the reaction zone. These analyses are becoming more complex and involve increasingly more thorough fluid flow and heat transfer considerations. The results are so sensitive to many extrapolated properties and assumptions that seemingly reasonable calculations produce results which range from being extremely plausible to clearly nonsensical. Simplified calculations can also be made which are so free of assumptions that they serve to test the accuracy of the more complex analyses. Examples of the latter are calculated heating rates, reaction times and depletion volumes.

i. Order of Magnitude Rate Estimates

We have made the following order of magnitude estimates for the reference process conditions used to synthesize Si_3N_4 powders. With a volumetric flow rate of 120 cm^3/min, the average gas stream velocity decreases from 570 cm/sec at the nozzle to approximately 400 cm/sec at the center line of the laser beam axis. Mapping the reaction zone showed that reaction products were evident within 3-5 mm penetration into the laser beam. Although the reaction temperature has not been determined precisely, we can state that it occurs at 800 $\pm$ 200°C. Combined, these parameters and observations indicate that the average heating rate is approximately 10^6°C/sec from the time the gas enters the beam to the point where reaction product is first evident. The exposure time required to initiate a reaction is approximately 10^{-3} seconds. The time required to complete the reaction is less than 7.5×10^{-3} seconds assuming that, at most, the reaction occurs throughout the highly luminous zone discussed in the mapping section (Figure 19).

ii. Depletion Volume

Once the reactant gases reach the reaction temperature, particles begin to nucleate and grow within the gas stream. As far as we can determine, this point coincides with the beginning of the visible flame. We have shown by mass balance measurements that the silane is almost completely depleted from the reactant gases, so particle growth is not limited by elapsed growth time, but by the depletion of silane between neighboring particles. This depletion volume is estimated by comparing the mass of silicon in a particle with the mass density of silicon atoms in the gas stream.

With the reference NH_3/SiH_4 conditions, the density of silicon in the gas stream is 5.6×10^{-6} g of Si/cm^3 and the mass of silicon in a 175 Å Si_3N_4 particle is 5.5×10^{-18}g. If the density of silicon in the gas stream is adjusted to account for the conversion efficiency, the

resulting depletion volume is 1.1×10^{-12} cm^3 which corresponds to a sphere of gas with a diameter 1.2×10^{-4} cm and an entrained particle density in the gas of 9.3×10^{11} particles/cm^3. If the gas volume increases by a factor of 1.15 due to the reaction $3\ SiH_4 + 30\ NH_3 \rightarrow Si_3N_4 + 26\ NH_3 + 12\ H_2$, the resulting particle density is 8.1×10^{11} particles/cm^3 after the reaction is completed.

Similar calculations have been made for Si_3N_4 powders synthesized at different pressures and laser intensities. These results are given in Table V. Within the precision of the calculation, the diameter of the depleted volume of gas is not affected significantly by these variables.

TABLE V

Diameters of Depletion Volumes for Various Si_3N_4 Synthesis Conditions

P (atm)	I (watts/cm^2)	Particle Diameter (cm)	Depletion Volume Diameter (cm)
0.2	760	1.75×10^{-6}	1.23×10^{-4}
0.5	760	2.05×10^{-6}	1.03×10^{-4}
0.75	1020	2.21×10^{-6}	0.99×10^{-4}

For the Si reference condition, the mass of silicon in the 435 Å particles is approximately 9.9×10^{-17} g of Si/particle and the density of silicon in the gas stream is 6.8×10^{-5} g of Si/cm^3. This corresponds to a depletion volume with a diameter of 1.38×10^{-4}cm. This approximately equals the diameter calculated for Si_3N_4.

The time required (t) to deplete a sphere of radius r by a diffusion rate limited process can be estimated by:

$$t \simeq \frac{r^2}{6D}$$

where D is the diffusivity in the gas. D is calculated from kinetic theory by:

$$D = 1/3\lambda\bar{c}$$

$$\lambda = \frac{1}{\sqrt{2}\pi d^2} \frac{kT}{P}$$

and $$\bar{c} = \left(\frac{N_o kT}{\pi M}\right)^{\frac{1}{2}}$$

where λ = mean free path

$\bar{c}$ = average molecular velocity

d = molecular diamter (4.2 Å)

k = Boltzmann gas constant

N_o = Avogadro's number

P = pressure (0.2 atm)

M = molecular weight (32 g/mole)

T = absolute temperature (1100°K)

The values of parameters given in parenthesis were used for sample calculations.

Substitution of these representative values into these expressions indicated that a 1.2×10^{-4} cm diameter sphere can be depleted in approximately 2.2×10^{-10} seconds if diffusion is rate controlling. This time is approximately 10^{7} shorter than the estimated residence time in the reaction zone. This large difference doesn't determine that the reaction does not occur throughout a major portion of the reaction flame, but, it clearly shows that if it does, the process is not rate controlled by gas phase diffusion. The extremely short times required to cause termination of the growth process by overlapping depletion volumes and the uniformity of the calculated depletion volumes, suggests that the observed particle size is controlled by the nucleation rate.

iii. Observed Effects of Process Variables on Reaction Zone Characteristics

Several process variables have been manipulated during development

of this synthesis process, and all had smooth, progressive effects on the reaction zone characteristics. Since no abrupt changes were observed, which would suggest that the process changed in any fundamental way, we can discuss the effects as trends. Investigated process variables include gas stream velocity, gas mixture, laser intensity, and chamber pressure. The techniques used to characterize the shape of the reaction flame and its position relative to the laser beam as well as some other general characteristics were discussed in the section on Reaction Zone Mapping. The observations cited in this discussion were made in this manner.

Under most processing conditions, the shape of the reaction flame was concave into the flame on the side facing the nozzle. The contour between the two cusps nearest the nozzle is defined by the parabolic velocity distribution in the gas stream. Increased gas velocity causes the concave shape to increase in its penetration into the body of the flame. This follows predicted behaviour because the outer boundaries of the stream move at the velocity of the argon carrier stream which flows through the annular orifice. The maximum velocity must therefore increase in proportion to the volumetric flow rate. A gas flow rate which is greater than two times the reference flow rate causes the central cusp to pass beyond the laser beam. Once this occurs, the reactant at the stream's center axis cannot be heated to the reaction temperature and the flame goes out with progressively increasing velocity. Lower than reference velocities cause the concave shape to disappear progressively. With a volumetric flow rate equal or less than half the reference conditions, the flame flattens out on this side. Qualitatively, this behavior follows that expected on the basis of velocity distributions in the gas stream.

With constant laser power, beam intensity, total pressure, and volumetric flow rate, any dilution of the silane gas with a lower absorptivity gas causes the reaction threshold boundary to penetrate further into the laser beam. The reason for the effect is obvious. These observations were made with both Ar and NH_3 dilutants in the vicinity of reference conditions. With extreme dilution by NH_3, the overall absorptivity should be dominated by the NH_3; so, the effect

should disappear progressively. This dilution effect also accounts for the relative position of the two cusps nearest the nozzle tip. The cusp nearest the laser entrance window penetrated further into the beam than the other despite the higher laser intensity at this side. Dilution by the Ar gas stream used to protect the window causes this shift.

With constant laser power, beam intensity, volumetric flow rate, and gas stream composition, increased pressure caused reduced penetration of the reaction threshold boundary into the laser beam. This is primarily a gas stream velocity effect because gas velocity decreases with increasing pressure under these conditions. To a first approximation, pressure should have no effect on the time required to heat the gas to the reaction threshold because the mass per unit volume and energy absorbed per unit volume both increase proportionally with pressure.

iv. Analysis of the Effects Process Variables have on Reaction Zone Characteristics

Since the laser beam intensity and gas flow velocity are both spacially variant, the analysis of the temperature-time history experienced by a volume element of reactive gas must reflect these variations. The analytical problem involving a gas stream having a parabolic velocity distribution which intersects a laser beam having a Gaussian-shaped intensity distribution is not easily solvable. The dimensionality of the problem cannot be reduced, since both the laser beam and gas stream have circular cross-sections. This problem can be simplified by considering a small gas volume element at some particular position in the gas stream, and performing a stepwise calculation to determine the temperature-time history of the volume element as it passes through the laser beam.

Before elaborating on this analysis, it is beneficial to examine the possible intensity-time profiles a volume element in various positions in the stream may experience. If the gas stream and and the laser beam are aligned so that their central axes intersect (see Figure 24),

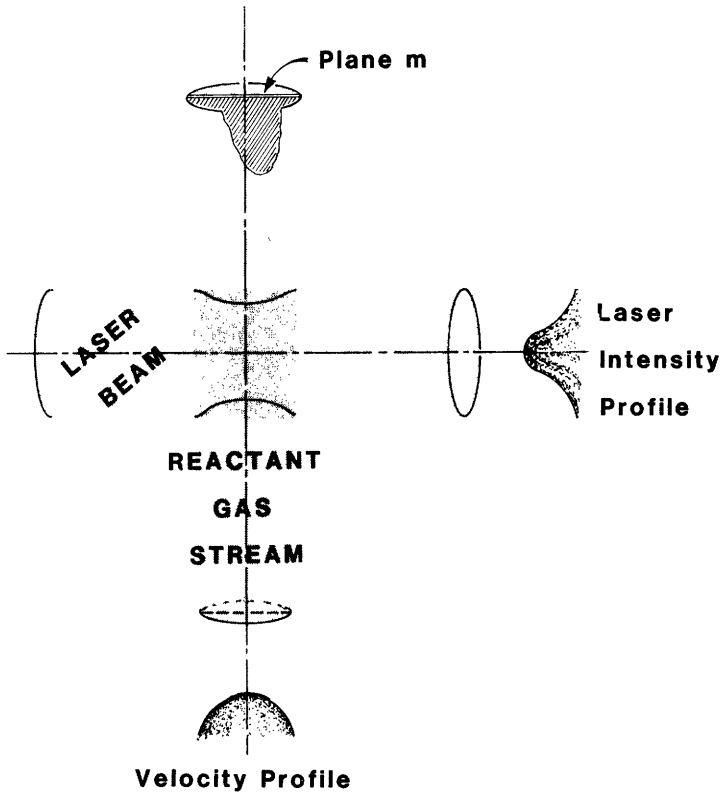

Figure 24. A schematic of the reactant gas stream intersecting the laser beam.

the gas volume element in the center of the gas stream, which will have a maximum velocity, will be subjected to the full diameter and the maximum power intensity of the laser beam. Any other gas element in the plane, m, shown in Figure 24 will also intersect the maximum beam intensity distribution, but will have a velocity related to its distance from the center line which is less than maximum. Volume elements within the plane m should reach reaction threshold temperatures in a shorter penetration distance than volume elements traveling at the same velocity in any other region of the gas stream. It is these gas volume elements that probably form the lower boundary of the flame, as exemplified in Figure 19, and this boundary should be indicative of the velocity profile within the beam. The following analytical procedure was employed to calculate the temperature-time history for any particular reactive gas volume element.

The path of a gas element through the laser beam is divided into a finite number of intervals. In each interval, the gas element is assumed to have a constant velocity and is subjected to a constant laser beam intensity. The laser beam intensity in each interval is calculated

from a Gaussian-shaped distribution. The gas velocity at any point is determined by the computer model previously described. The volume element is assumed to have a square cross-section of width Δx along the edge, and a length, ℓ, determined by the number of intervals in the path. It is assumed that there is no dilution of the gas stream by the annular Ar stream. Thus, the gas volume consists of only NH_3 and SiH_4 in proportions defined by the volumetric flow rate. After reaction occurs, it is assumed that the residual gas stream and particles produced by the reaction are transparent to the laser beam.

The power absorbed (ΔP) by a specific gas element in a particular spacial interval can be calculated from:

$$\Delta P = I(\Delta x \ell)[1 - \exp(-\Sigma \alpha_i p_i \Delta x)]$$

where: I is the average laser intensity in the interval
$(\Delta x \ell)$ is the cross-section of the element exposed to the beam
α_i is the absorption coefficient of the ith chemical species
p_i is the partial pressure of the ith species
Δx is the thickness of gas element exposed to the beam.

Using the substitutions $x_i p_{tot} = p_i$, $\Sigma x_i \alpha_i = \alpha_{ave}$ and $1 - \exp[-a] = a$, we obtain

$$\Delta P = I \Delta x^2 \ell \alpha_{ave} p_{tot}$$

Assuming all absorbed power is converted to sensible heat, the temperature increase, $T_2 - T_1$, in the spacial interval can be calculated from:

$$T_2 - T_1 = \frac{\Delta t \Delta P}{C_p \frac{n}{V} V}$$

Substitutions of $n/V = p_{tot}/RT_{ave} = 2p_{tot}/R(T_2 + T_1)$ and $\Delta t = \ell/\bar{v}$, where $\bar{v}$ is the computer calculated velocity within the interval, and simplification yields:

$$\frac{T_2 - T_1}{T_2 + T_1} = \frac{R\ell I\alpha_{ave}}{2\bar{v}C_p}$$

The gas element temperature when it leaves the interval T_2 can be calculated with the knowledge of T_1, the temperature of the element when it enters the interval. The heating rate within the interval as well as a temperature-time history for the entire path of this volume element through the laser beam can also be calculated.

Figure 25 shows the calculated time-temperature histories of gas volume elements traveling along the center line of the gas stream, and at distances 1/4 r_o and 1/2 r_o from the central axis; where, r_o is the radius of the reactant gas stream at a particular distance from the nozzle tip, corresponding to the calculated boundary between the reactive gas stream and annular stream of Ar. These three volume elements lie in a plane corresponding to the plane m shown in Figure 24 and are exposed to the maximum power intensity distribution. Also shown on Figure 25 are the reaction times calculated from the positions where the flame was first observed in the mapping exercise.

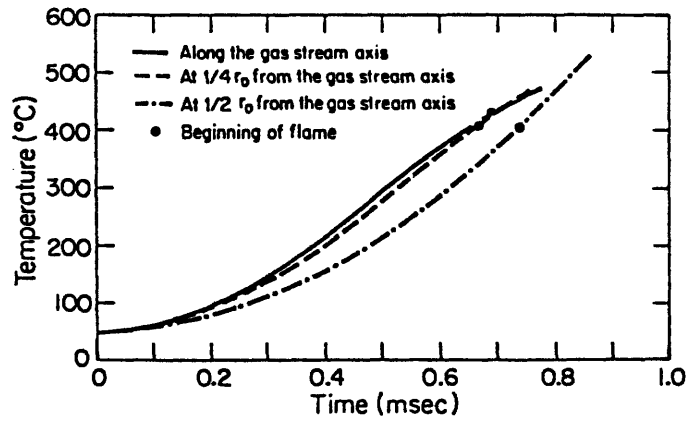

Figure 25. The calculated temperatures of volume elements of reactant gas after they enter the laser beam at time = 0. All volume elements lie in plane m of Figure 24 and r_o is the radius of the gas stream. The times corresponding to the points designated as the beginning of the flame were calculated from the measured distance to the flame as given in Figure 19 and the calculated velocity of the particular elements in the reactant gas stream. Reference flow conditions are assumed.

The calculated temperatures at the reaction times are relatively constant for the three gas elements. Also, the average heating rates between inlet temperature and reaction temperatures are essentially equal for all three gas elements. They range from 5.5×10^5 to 6.2×10^5 °C/sec. These are about a factor of two lower than we calculated as an order of magnitude estimate. In contrast, the instantaneous heating rates experienced at the observed reaction times and temperatures do show a wide range of variation. The instantaneous heating rate calculated for the central axis gas element is 3.8×10^5 °C/sec. The rates increase progressively in the outward direction to 6.9×10^5 °C/sec at 1/4 r_o and 9.6×10^5 °C/sec at 1/2 r_o. The instantaneous heating rate at the reaction threshold temperature is more important than the average heating rate since it influences nucleation rate, super-heat, stoichiometry, etc. It is probable that we will strive to achieve more uniform laser intensities and plug flow gas streams to produce more uniform particle size distributions.

It should be noted that the temperatures calculated by the preceding analysis do not agree either with measured estimates of the reaction temperature for this process nor spontaneous reaction temperatures reported in the literature for these gases (Braker and Mossman, 1971). It appears that the error is systematic because all of these and other calculated reaction temperatures are close to 400°C. Probably, the source of the error is the assumed constant optical absorptivity. High temperature absorptivity measurements, such as those presented for low temperatures, are required to resolve this discrepancy.

This analysis shows that the heating rate is not explicitly related to pressure. This follows the assumption that $\exp(-\alpha p \Delta x) \approx \alpha p \Delta x$ where $\alpha p \Delta x$ is small. Since Δx can be chosen arbitrarily small, the assumption always holds. At high pressures, it can no longer be assumed that the gas is optically thin. We anticipate a pressure effect which causes a systematic variation in heating rates across the gas stream resulting from progressive absorption of the laser beam. These analyses also assume that α_i is independent of p_i and p_{tot}. It should be reemphasized that the pressure dependence of the absorption coefficients of SiH_4 and

NH_3 are not known. The conclusion regarding a lack of pressure dependence is clearly an approximation. Its limits of validity require further definition.

Figure 26 shows the heating curves for gas elements traveling through the center of the gas stream into the maximum intensity distribution of laser beams with average power intensities of 765, 2×10^4, and 1×10^5 watts/cm^2. The NH_3/SiH_4 ratio is 10/1 and the flow characteristics at each intensity are the same. These calculated curves were extended to temperatures well above the reaction temperatures to qualitatively show the shape of the entire heating curve, and to indicate the extremely large effect the power intensity has on gas heating rates. The time equivalent of the beam diameters are indicated for the power intensities of 2×10^4 watts/cm^2 and 1×10^5 watts/cm^2. The figure shows that with average intensities of 2×10^4 watts/cm^2 and 1×10^5 watts/cm^2, the gases reach reaction temperatures so soon after entering the beam that the reaction is initiated before the maximum intensity and maximum heating rates are experienced. The average heating rates and instantaneous heating rates at the reaction threshold both increase with beam intensity. The average heating rates for intensities of 2×10^4 watts/cm^2 and 1×10^5 watts/cm^2 may be as high as 2×10^7 °C/sec and 1×10^8 °C/sec, respectively. Beam intensity should have a major effect on reaction kinetics and, consequently, particle characteristics.

Figure 27 shows the calculated effect of varied NH_3/SiH_4 ratio on the gas heating behavior for the central axis gas element which travels through the diameter of the laser beam. The NH_3/SiH_4 ratio was varied from 5/1 to 10/1 to 20/1. In each case, the average power intensity was 760 watts. The time equivalent of the position where the flame was first visible is indicated. The average heating rate increases with increasing silane content from 3.7×10^5 °C/sec for the 20/1 NH_3/SiH_4 ratio to 7.5×10^5 °C/sec for the 5/1 NH_3/SiH_4 ratio. The instantaneous heating rates at the observed reaction point increase more dramatically with increased silane content. They change from 1.5×10^5 °C/sec to 1.3×10^6 °C/sec as the NH_3/SiH_4 ratio changes from 20/1 to 5/1. The calculations suggest that

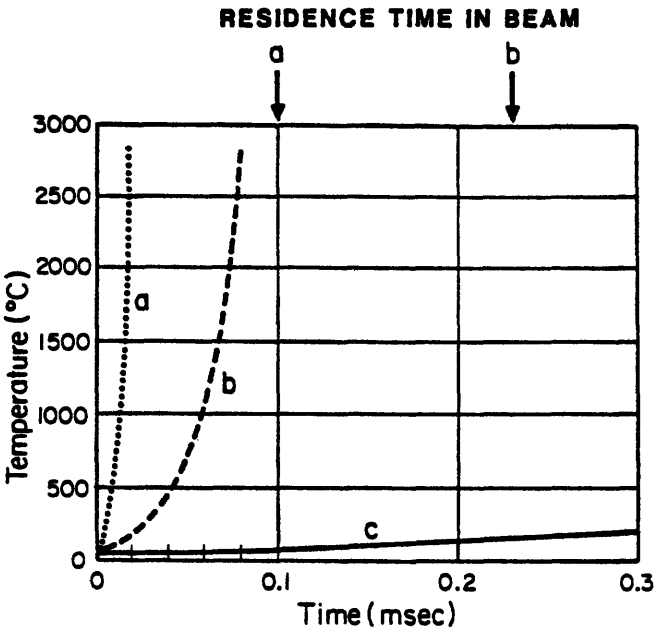

Figure 26. The calculated temperatures of the axial volume elements of reactant gases after they enter the laser beam at time = 0. Curve a and b refer to focused beams with intensities of 1 x 10^5 W/cm^2 and 2 x 10^4 W/cm^2, respectively. Residence times a and b were calculated from the diameter of the focused laser beam at two different intensities, and from the calculated velocities of the reactant gas stream. Curve c refers to the volume element of gas at the reference condition using an unfocused laser beam (760 W/cm^2).

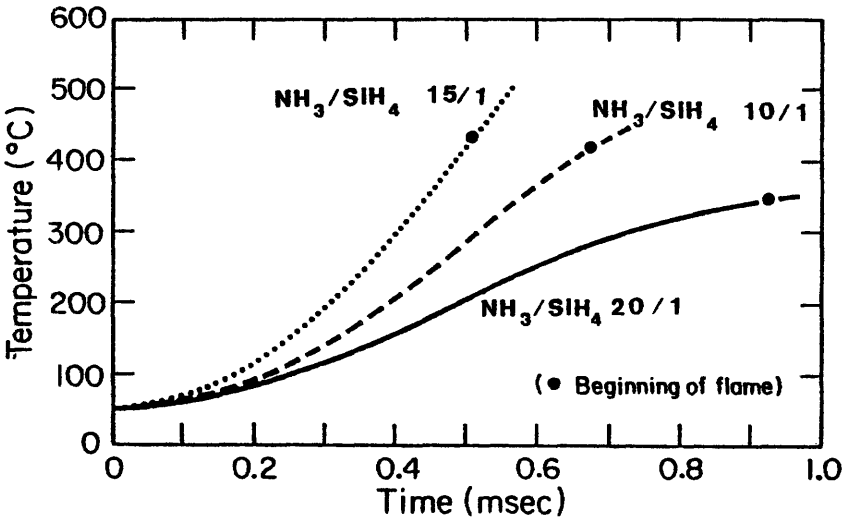

Figure 27. The calculated temperatures of the axial volume elements of reactant gas after entering the laser beam at time = 0. The times corresponding to the points designated as the beginning of the flame were calculated from the measured distance to the beginning of the flame and the calculated velocities of the axial volume elements.

the temperature at the reaction point increases slightly with increasing silane content in the reactant gas stream. Because of uncertainty in the values of observed and calculated reaction temperatures, we have less confidence in this conclusion than those regarding heating rates at the reaction threshold.

The effect of the gas stream velocity through the laser beam is shown in Figure 28. The velocities of the gas elements as they entered the beam were 375, 500 and 625 cm/sec. These velocities do not correspond to specific run conditions, but were selected to exemplify their effect on heating rate at the reaction temperature. A cell pressure of 0.2 atmospheres and an average Gaussian distribution laser beam intensity of 760 watts/cm^2 were assumed. The calculated average heating rates to reach an assumed reaction temperature of 440°C were essentially constant, i.e., 1.0×10^6, 1.1×10^6 and 9.4×10^5 °C/sec for velocities of 375, 500, and 625 cm/sec respectively. The instantaneous heating rates at the temperature exhibit a stronger dependence on velocity. They decrease with increasing gas velocity, e.g., from 1.3×10^6 °C/sec at a velocity of 375 cm/sec to 2.9×10^5 °C/sec at a velocity of 625 cm/sec. While this conclusion is similar to that made regarding lower velocity elements within a gas stream, this calculation illustrates the effect of a gas element passing beyond the maximum laser intensity prior to reaching the reaction threshold temperature. At the point where the flame is nearly "blown out," the instantaneous heating rates are very low when the reaction is finally initiated.

These results illustrate that achieving an understanding of the effects of process variables on rate kinetics and powder characteristics will require precise control of these variables. It is also probable that more uniform powder characteristics will be achieved only with either very uniform conditions or carefully manipulated laser intensity and gas flow conditions which are not intuitively evident. Clearly, because the reaction happens quickly in a very small region, it is not necessarily uniform in character.

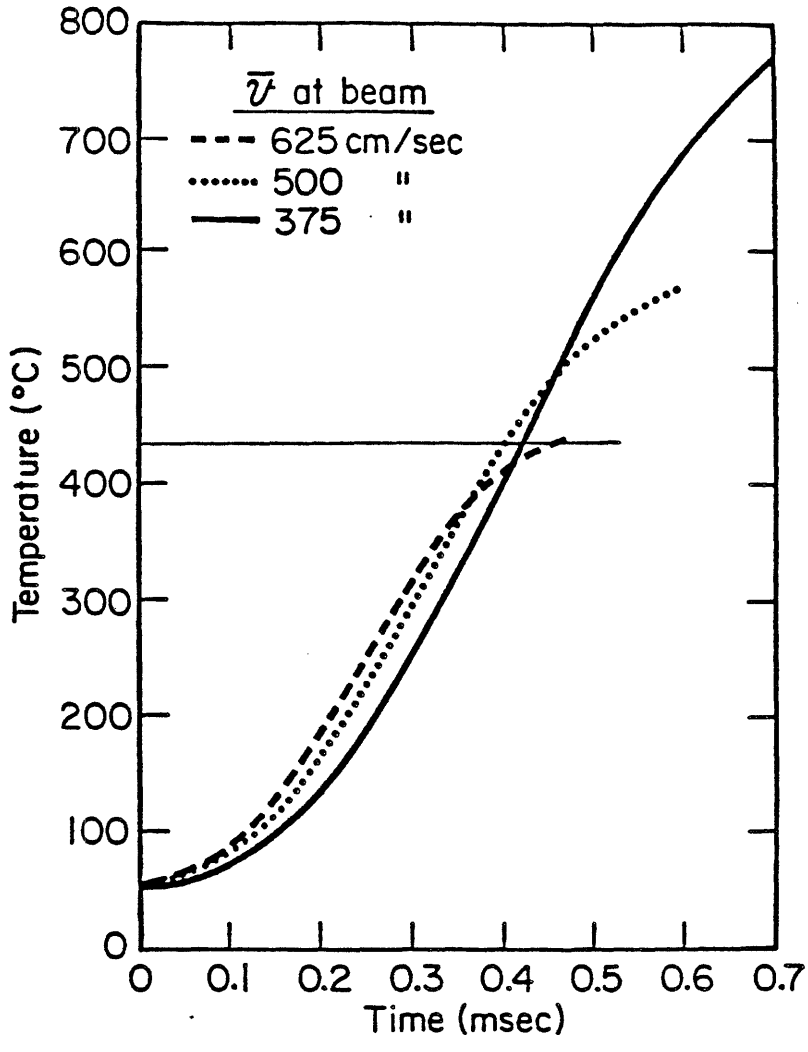

Figure 28. The calculated temperature of axial volume elements of reactant gas after entering the laser beam at time = 0. The velocities refer to average velocities of the reactant gas stream.

v. Effect of Latent Heats

The previous analyses have not included the effects of latent heats associated with the chemical reactions. They have, in fact, been thermal analyses of the process up to the point the reaction just begins. We have not considered the effects of exothermic latent heats in detail, but plan to in the future. The following simple calculations do permit conclusions to be made regarding the possibility of a self-sustaining reaction

without the input of energy from the laser and the anticipated maximum temperature rise in the reaction products.

To a first approximation, a reaction can be self-sustaining only if the latent heat released exothermically during the reaction exceeds the sensible heat required to raise the reactants to a temperature level where the reaction proceeds rapidly. For the Si_3N_4 synthesis reaction carried out under reference condition, the mass balance and heat balance equations are as follows. The overall reaction is:

$$3\,SiH_4 + 30\,NH_3 \rightarrow Si_3N_4 + 26\,NH_3 + 12\,H_2$$

assuming the excess ammonia does not crack. The heat of reaction is

$$\Delta H = -3\Delta H_{SiH_4,T} - 4\Delta H_{NH_3,T} + \Delta H_{Si_3N_4,T} \quad .$$

At 1100°K (JANAF, 1971)

$\Delta H_{SiH_4} = 2.14 \times 10^4$ joules/mole.

$\Delta H_{NH_3} = -5.56 \times 10^4$ joules/mole.

$\Delta H_{Si_3N_4} = 7.45 \times 10^5$ joules/mole.

Thus at 1100°K

$$\Delta H = -1.95 \times 10^5 \text{ joules/mole } SiH_4 \quad .$$

With 92% conversion (see Appendix IB), the actual heat released is approximately 1.80×10^5 joules/mole SiH_4. The sensible heat required to raise the 10/1 NH_3/SiH_4 reactant gas mixture at 1100°K is 4.4×10^5 joules/mole SiH_4. Thus, under reference conditions, the Si_3N_4 synthesis reaction cannot be self-sustaining because the sensible heat requirement far exceeds the latent heat released. This conclusion may not hold for all NH_3/SiH_4 ratios since the latent exceeds the sensible heat with stoichiometric gas mixture. For the SiH_4 pyrolysis reaction:

$$SiH_4 \rightarrow Si(s) + 2H_2 \quad ,$$

at 1100°K, the latent heat is:

$$\Delta H = 2.14 \times 10^4 \text{ joules/mole}$$

and the sensible heat required to raise the gas to this temperature is:

$$\Delta H_{sensible} = 5.76 \times 10^4 \text{ joules/mole}$$

With 65% conversion (see Appendix IB), the effective latent heat (1.60×10^4 joules/mole SiH_4) is less than the sensible heat requirement. This reaction cannot be self-sustaining unless the reaction is induced at a much lower temperature.

The temperatures we have measured have been at points within the reaction flame, so they correspond to a location where the reaction has proceeded to an unknown extent. The calculated temperatures at points where the reaction products were just observed are lower than measured temperatures by 400-600°C. These calculated temperatures must be lower than the actual temperatures, because they do not take the exothermic heat into account. With the same conversion efficiences used to compare sensible and latent heats, we estimate that the adiobatic temperature rise in the excess reactants and reaction products would be 260°C for Si_3N_4 and 181°C for Si syntheses processes. It is evident that this temperature rise can account for a part of the difference between observed and calculated temperatures.

Future analyses will take the exothermic reaction heat into account because it is evident from these calculations that their effect is large enough to be important. From an economic standpoint, it would also be desirable to minimize the amount of heat introduced by the laser. As our understanding of heat transfer processes improves, we will examine the use of other reactants to determine whether they will react under nearly thermoneutral conditions.

2. Powder Characterization

The characteristics of the covalent ceramic powders used to fabricate high performance ceramic parts ultimately determine the properties

of the fabricated bodies. We have attempted to fully characterize the physical, chemical, and crystalline characteristics of the laser synthesized Si, Si_3N_4, and SiC powders. The results of this analysis will allow us to develop a more accurate model of the powder synthesis process and indicate how close these powders are to the ideal characteristics described earlier. Our major synthesis efforts have been to produce Si powder for reaction bonding, and Si_3N_4 powder for sintering. We have undertaken initial synthesis experiments with SiC. Powder evaluation has employed a number of techniques to determine the various physical, chemical and crystalline properties of these powders.

Specifically, the particle size and distribution have been measured using SEM, TEM, BET (equivalent diameter), and x-ray line broadening. The particle shapes have been studied by TEM and SEM. The surface areas of the powders were measured by single point BET analysis and the powder density was measured by He pycnometry. Chemical analyses were performed using neutron activation analysis for O, wet chemical analysis for Si, H, N, O and C, and emission spectrographic procedures for other impurities. Infrared spectroscopy was also employed to determine the nature of the elemental bonding in selected powders. The crystalline characteristics of the powders were evaluated using Debye-Scherrer x-ray diffraction, electron diffraction, and dark field electron microscopy.

The results of the powder evaluation for Si, Si_3N_4, and SiC are presented below. A comprehensive tabular listing of the individual run conditions and the resultant powder characteristics appear in Appendixes IA and IB, respectively.

a. Si Powders

Several runs have been made with the goal of producing Si powders for characterization, to evaluate the reproducibility from run to run, and to supply powder for reaction bonding studies. The reaction to form Si powders is:

$$SiH_4(g) \xrightarrow{h\nu} Si(s) + 2H_2(g)$$

i. Physical Characteristics

The Si production runs 209S, 213S, and 214S were made at 0.2 atm with SiH_4 flow rates of 20, 20, and 11 cc/min and a laser intensity of 760, 1020, and 760 watts/cm^2 respectively. These powders, light to dark brown in color, were prepared in several gram lots. We will present the data for 209S in detail, and then compare 209S with 213S and 214S to evaluate the reproducibility from run to run.

The Si powders were spherical in shape and had a wider range of particle sizes than did the Si_3N_4 powders. Figure 29 shows the Si particles which range in size from 100-1000 Å. The average size of the Si particles was 490 Å with a standard deviation of 194 Å by TEM, and had equivalent spherical diameters of 436 Å as calculated from a BET surface area of 59 m^2/g. Figure 30a shows the particle size distribution for powder lot 209S as measured by TEM. It should be noted that the range in particle diameters is smaller for these laser synthesized powders than for powders prepared by conventional processing techniques.

The physical characteristics of the different lots of Si powders are compared in Table VI. These results indicate that the laser process is capable of yielding powders with similar physical characteristics from one synthesis run to the next.

TABLE VI

Physical Characteristics of Si Powders

Produced with Reference Conditions

Run Number	209S	213S	214S
SiH_4 Flow cc/min	20	20	11
Surface Area m^2/g BET	59	48	57
Size Å BET	436	543	458
Mean Size Å ± Standard Deviation TEM	490 ±194	630 ±275	470 ±270
Size Range TEM	100-1000	100-1500	100-500

Figure 29. TEM photograph of Si powders from lot 209S.

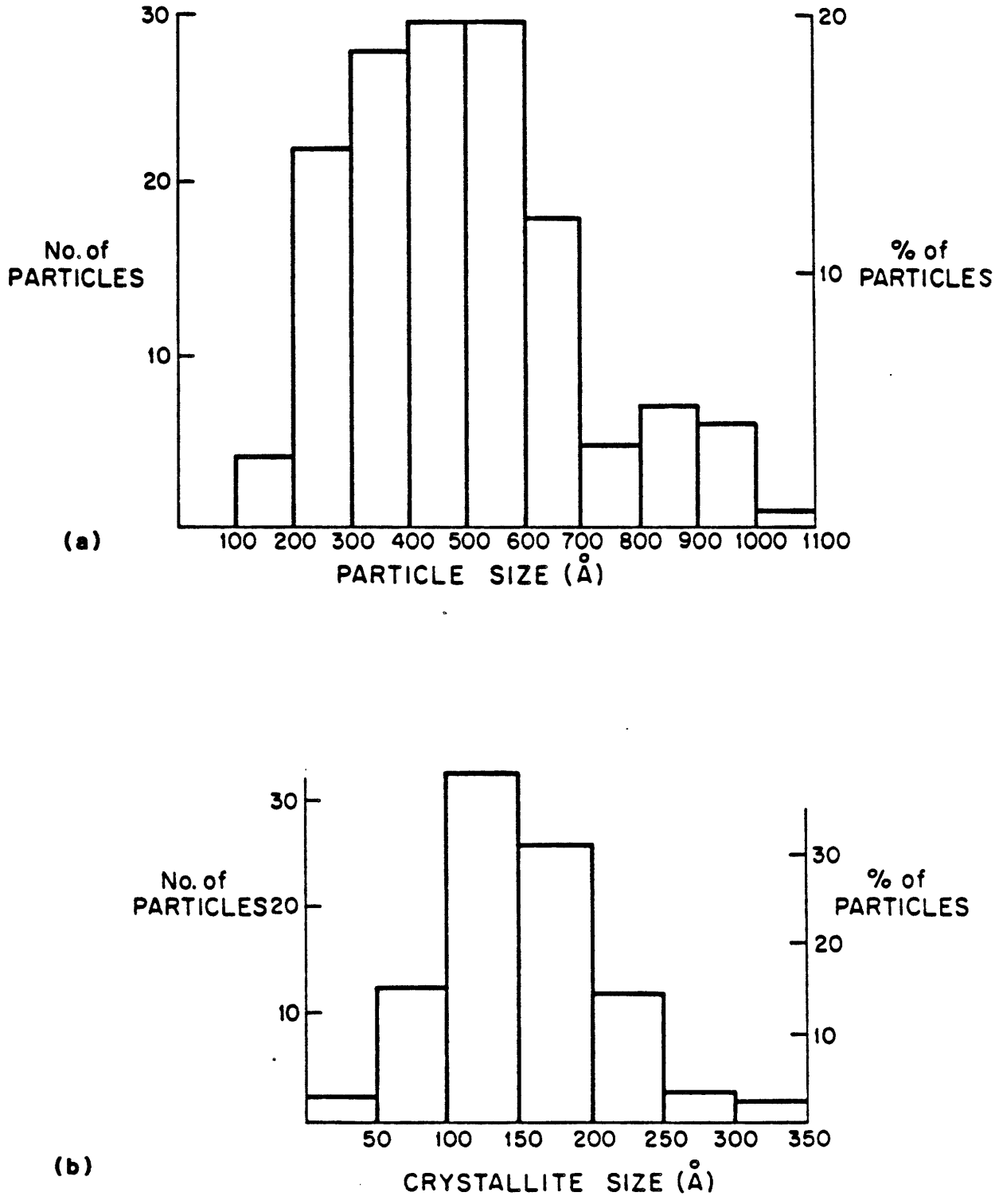

Figure 30. (a) Particle size distribution of silicon powders in lot 209S. (b) Crystallite size distribution within the same powders.

ii. Chemical Characteristics

The chemistry of these powders is as important as their physical properties. Table VII shows the chemical analysis of powder 209S. It is 99% Si with trace amounts of N and H, and larger amounts of O. (It should be noted that these Si powders do not oxidize pyrophorically with exposure to air.)

The 2.9 wt% O is comparable to Si powders produced by other techniques (Danforth, 1978). Table VII also shows the O contents of 213S and 214S. The wt% O_2 is not as uniform as the other powder characteristics.

TABLE VII

Chemical Characteristics of Si Powders
Produced with Reference Conditions

Run Number	209S	213S	214S
Si Wt%	99	-	-
N Wt%	0.02	-	-
H Wt%	0.15	-	-
O Wt%	2.92	1.0	3.4
Free Si Wt%	100	100	100
Conversion %	70	85	72

There are several possible sources of O_2: leaks in the synthesis or storage systems, O_2 in the reactant or inlet gases, and inadvertant exposure to the ambient atmosphere. While at times there may be very minor system leaks, calculated cell leak rates do not suggest sufficient O_2 to account for this level of contamination of the Si powders. We have measured 10-15 ppm O_2 in the argon buffer gases used in the system. If all of this O_2 (argon flow 1 liter/min) were to react with the hot Si powders, it would amount to 0.1 wt% O. The indications are that this is not the primary source of O in the synthesis process. The post production handling of these Si powder is done in an inert atmosphere

glove box with < 10 ppm O_2, which may account for some O, but it is doubtful that this is the major source.

We feel confident that we can both reduce the O content and make the level more reproducible based on experience with Si_3N_4. The contamination very likely occurs during processing and is not intrinsic. Oxygen contamination can be improved by further reducing the O_2 content of the argon, by improved monitoring and gettering, by reduced system leak rates, and by reducing the O_2 content of the glove box.

iii. Crystal Structure

All of the Si powders we have produced are crystalline to both x-ray and electron diffraction. Debye-Scherrer x-ray patterns revealed 11 peaks which indexed from Si(111) to Si(533). It remains to be seen whether they are fully crystalline or whether the powder is a mixture of crystalline and amorphous particles. Annealing experiments will be preformed to answer this question.

These x-ray patterns were also used to estimate the particle size from diffraction peak broadening using the expression(Cullity, 1956):

$$d = \frac{0.9\ \lambda}{B(p)\ \cos\ \theta_B}$$

where d is the crystallite diameter, λ is the wavelength, B(p) is the peak breadth at half intensity, and θ_B is the Bragg angle in radians. The particle size broadening B(p) can be separated from the machine broadening by B(g) by:

$$B^2(p) = B^2(h) - B^2(g)$$

where B(h) is the measured peak breadth at half height. A > 50 μm particle size Si standard was used to measure the machine broadening B(g). The peak breadths were taken as the difference between the two extreme angles at zero intensity (Warren, 1969).

The results of the x-ray analysis indicate a crystallite size of 154 Å for powder lot 209S, approximately 1/3 the TEM and BET particle sizes of 490 and 436 Å respectively. Most of the Si particles consisted of several smaller crystallites with random orientations in dark field TEM. Figure 31 shows a dark field image where the particles which have a (111) Bragg orientation appear white. Figure 30b shows the size distribution of these microcrystallites measured from dark field images. The average crystallite size is 156 Å ± 58 Å, which is in close agreement with the 159 Å value obtained from x-ray line broadening. The Si powders 213S, and 214S are crystalline to x-ray and electron diffraction, and they also exhibit microcrystalline grain sizes which range from about 1/4 to 1/2 the particle diameters.

The structure of these Si powders must be accounted for in any modeling of their formation process; e.g., the particles may crystallize on cooling from an amorphous solid, or might grow as clusters of crystalline solid particles, or crystallize on cooling or from a liquid droplet. Until such time as the reaction zone temperatures are known, it will be difficult to describe the formation mechanism. It is apparent from the agreement between the diameters measured by BET and direct observation techniques that there is no void space between the crystallites in the particles which are accessible to the absorbate gas. It is therefore unlikely that the particles were formed from the agglomeration of individual small particles.

The synthesis of Si from SiH_4 has a conversion efficiency from 65-85% based on the amount of SiH_4 passing through the laser beam. We are confident that the conversion efficiency can be improved to the 95% level observed with Si_3N_4 by increasing the optical path and/or preheating the SiH_4.

b. Si_3N_4 Powders

The laser synthesis of Si_3N_4 proceeds as:

$$3SiH_4(g) + 4NH_3(g) \xrightarrow{h\nu} Si_3N_4(s) + 12H_2(g)$$

Figure 31. Dark field TEM photomicrograph of Si powders from lot 209S.

The reaction between SiH_4 and NH_3 has been investigated to provide powders for sintering studies and to determine the effect of process variables on powder characteristics. Combined, they will enable accurate modeling of the synthesis process and provide a basis for manipulating variables to yield optimized powder characteristics.

i. Physical Characteristics

The Si_3N_4 powders all have the same general physical characteristics. Si_3N_4 powder lot 603SN, made under reference conditions, will be described in detail. The effects on powder characteristics of departures from reference conditions will then be presented.

The Si_3N_4 powder 603SN (Figure 32 and Table VIII) have spherical particles, are uniform in size and unlike the Si particles, lack any internal structure. They have a surface area of 117 m^2/g corresponding to an equivalent spherical diameter (corrected for composition) of 176 Å. The TEM measured average particle size is 168 $\pm$ 39 Å and the particles range in size from 100-250 Å. Figure 33 shows the particle size distribution of the Si_3N_4 powders. The Si_3N_4 powders have a much smaller average size and narrower particle size distribution than the Si powders described above. The powders from several runs were combined to yield sufficient powder for density measurement by He displacement pycnometry.* The measured particle density of a 3 g powder sample was 2.75 g/cm^3. The calculated density of these powders was 2.88 g/cm^3, based on a typical chemistry of 65% Si_3N_4 (3.18 g/cm^3) and 35% Si (2.33 g/cm^3). These results indicate that the individual particles have essentially theoretical density (within the accuracy of the test) and contain no pores which are not accessible to the surface. The close agreement between particle diameters measured by TEM and BET techniques is further confirmation that there is no porosity. If the powders contained internal porosity, which is open to the surface, the BET equivalent spherical diameter would be consistently smaller than measured by TEM. This has not been the case. In addition,

---

*Micrometrics, Norcross, Ga.

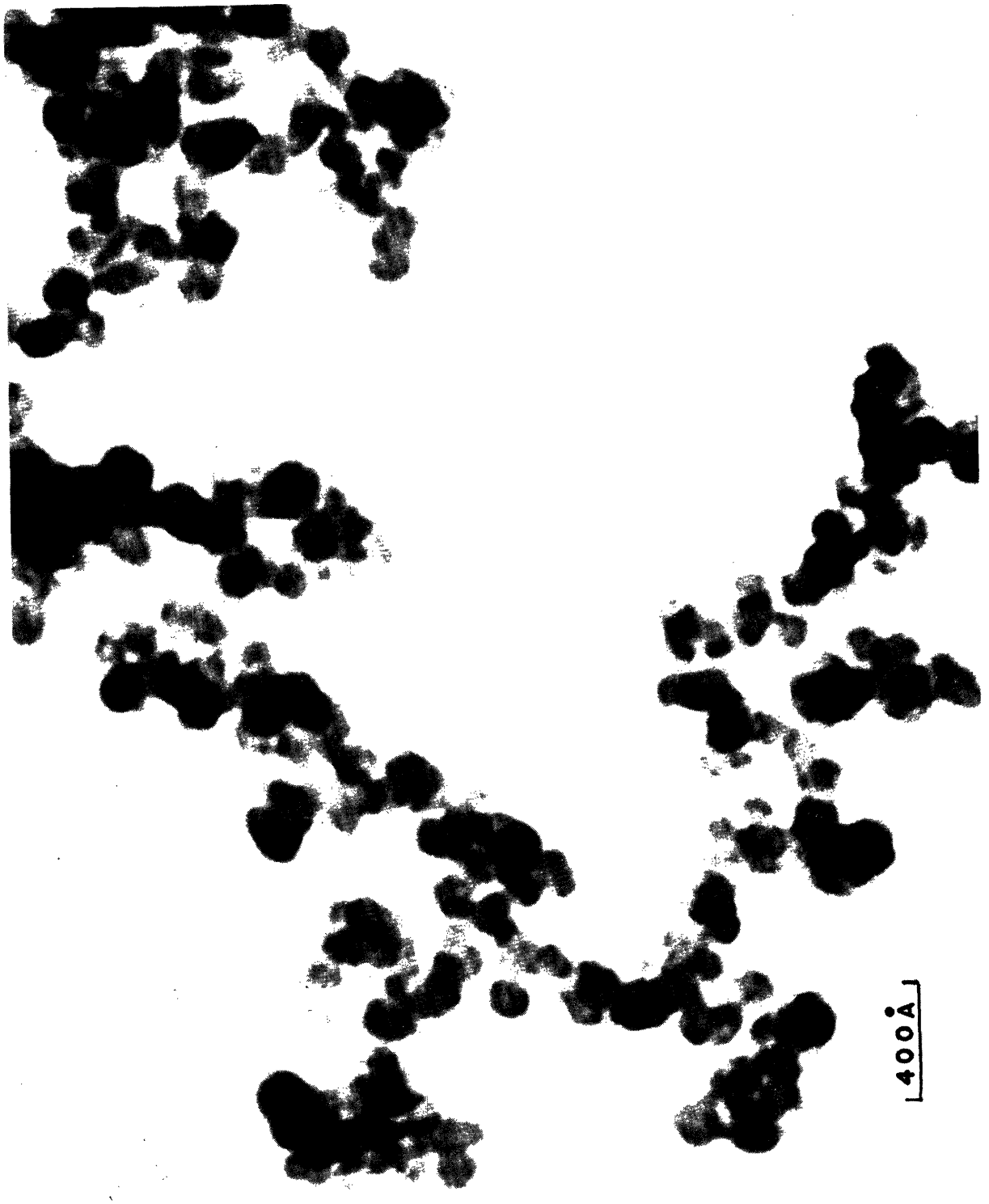

Figure 32. TEM photomicrograph of Si_3N_4 powders from lot 603SN.

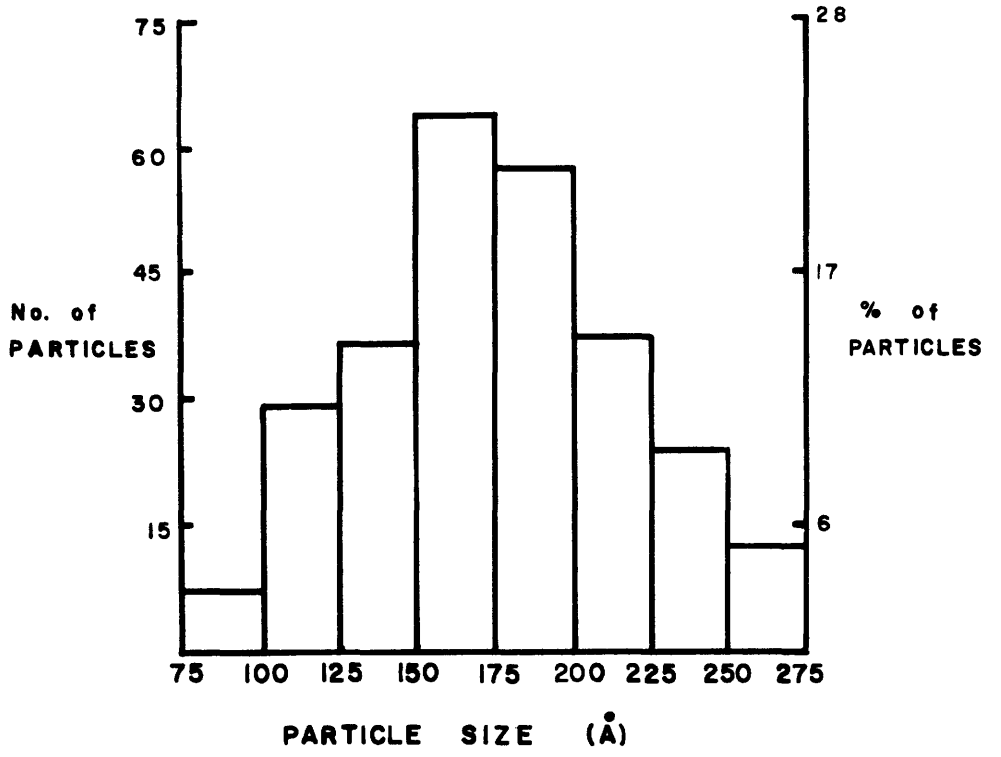

Figure 33. Particle Size Distribution Of 603SN Si_3N_4 Powder.

TABLE VIII

Physical Characteristics of Si_3N_4 Powder (603SN)
Produced with Reference Conditions

Surface Area m^2/g BET	117
Size Å BET	176
Mean Size Å ± Standard Deviation TEM	168 ± 39
Size Range Å TEM	100-250

TEM examination has not revealed any indication that these Si_3N_4 (or any other) powders contain any features which could be interpreted as porosity.

ii. Chemical Characteristics

Table IX summaries the chemical analyses of 603SN Si_3N_4 powder produced under reference conditions.

TABLE IX

Chemical Characteristics of Si_3N_4 Powder (603SN) Produced with Reference Conditions

Si Wt%	72
N Wt%	26
H Wt%	< 0.5
O Wt%	1.25
Free Si Wt%	35
Conversion %	92

The chemical analyses reveal that these powders contain 72 wt% Si and 26 wt% N. Stoichiometric Si_3N_4 contains 60 wt% Si and 40 wt% N, indicating 35 wt% free Si for Si_3N_4 powders produced under reference conditions. These powders contain very small amounts of H < 0.5 wt%, and an O content of 1.25 wt%. The small hydrogen content is due to the free H from the dissociation reactions of SiH_4 and NH_3.

It is estimated that with a surface area of 117 m^2/g, an adsorbed monolayer of SiO_2 would account for 4 wt% O. The O content of Si_3N_4 was observed to increase from 1.52 wt% to 2.48 wt% after exposure to air for 24 hours. Although the increase was substantial, again the indication is that the majority of the O content of the powders results during the synthesis process, not afterward. It was anticipated that minor changes in the synthesis apparatus and handling procedures would result in reduced O content of the Si_3N_4 powders to acceptable levels. These efforts have resulted in a decrease in the O content from typical values of 1-3 wt% for early runs to 0.3-0.5 wt% for more recent runs. The only other detected impurity was 20 ppm of Cu (emission spectrographic analysis), no doubt from the brass and Cu system employed.

iii. Crystallinity

The crystal structure of the as-synthesized Si_3N_4 powders was studied using Debye-Scherrer and electron diffraction techniques. The x-ray diffraction patterns reveal one very broad peak which corresponds to the most intense Si_3N_4 peaks [α(100), (210) and (102) and β(200) and (201)] as well as sharper peaks which correspond to Si. The broad Si_3N_4 peak could correspond to a crystallite size of approximately 20 Å, or could result from the overlapping of broadened peaks from larger crystallites. Alternatively, it could result from a highly distorted or amorphous structure. We observed no evidence of crystalline characteristics in Si_3N_4 powders using TEM techniques. So, we feel that the Si_3N_4 powders are amorphous. The x-ray line broadening analysis of the free Si peaks in the Si_3N_4 powder indicates a crystallite size of 95 Å. This size is close to that determined for Si powder produced from SiH_4 gas. Those results indicate that, under reference conditions, the Si_3N_4 powder consists of a mixture of amorphous Si_3N_4 particles and crystalline Si particles.

iv. Departures from Reference Conditions

To more fully understand the effects of processing variables on the synthesis of these powders, systematic departures were made from the reference conditions. These experiments were designed to empirically show how the departures affected the powder characteristics and also to yield a basis to test the accuracy of the synthesis modeling. It should be noted that, in some experiments, it was not possible to alter one variable independent of all others (refer to the specific process parameters in Appendix IA).

The process variables studied were the laser power intensity, the reaction zone pressure, the reactant gas velocity, and the effect of diluting the reactant gases with NH_3 and argon. The influence of these variables on powder size, chemistry, and reaction temperature was determined. The next section discusses these changes in relation to process models.

Laser Intensity Of the variables which were examined, variation in the laser power intensity had by far the greatest effect on the powder synthesis process and powder characteristics. This observation is largely true because the range examined, a factor of 10^2, was much larger than could be made with any other variables. Table X shows the variation of powder size, reaction temperature and stoichiometry, as the laser power density is increased from 760 to 2 x 10^4 and then 1 x 10^5 watts/cm^2 by focusing the beam with a 13 cm focal length lens.

The particle size decreases progressively as the power intensity increases. Earlier experiments revealed that for I = 10^9 watts/cm^2 (pulse length = 10^{-9} sec) the particle size was 25-50 Å. These results indicate a variation in particle size by a factor of 2-4 can be achieved by manipulation of the power intensity over many decades.

Laser power intensity has a major effect on the powder chemistry. Powders produced under reference conditions were brown to tan in color and contained 35 wt% free Si. Powders produced with 2 x 10^4 watts/cm^2 were a light tan-white in color, showed no evidence of Si by x-ray, and had 2 wt% free Si by wet chemical analyses. At 10^5 watts/cm^2, the powders were pure white and showed no Si by x-ray. There was insufficient powder to perform chemical analysis on the 10^5 watts/cm^2 powder; but, based on color, they appear to be stoichiometric.

Although the power intensity had a strong influence on the particle size and powder stoichiometry, there was no change in the crystal structure. All Si_3N_4 powders were amorphous to both x-ray and electron diffraction, despite an apparent higher reaction temperature. When free Si is present in these powders, it is crystalline.

Cell Pressure The effects of variations in the cell pressure are shown in Table XI.

As the pressure was raised, the particle size increased steadily. Despite the slightly higher power intensities of runs 021CN and 023 SN at

TABLE X

The Influence of Power Intensity on the Particle Size, Chemistry, and Reaction Temperature for Si_3N_4 Powder Synthesis

Run Number	603SN	609SN	621SM
Laser Power Density w/cm^2	760	2×10^4	1×10^5
Particle Size Å BET	176	114	98
Free Si Wt%	35	2	very low
Reaction Temperature °C	867	985-1020	> 1020
Crystallinity	amorphous	amorphous	amorphous

TABLE XI

The Influence of Pressure on the Particle Size, Chemistry, and Reaction Temperature for Si_3N_4 Powder Synthesis

Run Number	611SN	603SN	610SN	023SN	021SN
Pressure Atm.	0.08	0.2	0.5	0.75	0.75
Particle Size Å BET	167	176	211	220	221
Free Si Wt%	60	35	14	23	15.6
Reaction Temperature °C	-	867	1060-1080	1050-1125	-
Crystallinity	amorphous	amorphous	amorphous	amorphous	amorphous

0.75 atm, these had a larger particle size than powder lot 610SN, which was produced at 0.5 atm. Although the reaction temperature is not absolutely consistent, it shows a definite trend toward increased reaction zone temperature with increased pressure. It can also be seen in Table XI that the Si_3N_4 powders become more stoichiometric as the pressure is raised from 0.08 to 0.5 atm. There was no variation in the crystallinity of the Si_3N_4 powders with increased pressure.

Gas Velocity The third process variable studied was the reactant gas velocity. Table XII shows two pairs of comparable experiments where the velocity was altered. In powder lot 603 and 605SN, the NH_3/SiH_4 ratio was 10/1, while in lots 020 and 614SN it was 5/1. In both sets of experiments the particle size decreases, and the powders become less stoichiometric with increasing velocity. There was no detectable change in the crystal structure of these powders.

Reactant Gas Dilution The influence of diluting the reactant gas with either NH_3 or argon was also investigated.

Table XIII shows the particle size, wt% free Si, and reaction zone temperature for NH_3/SiH_4 ratios of 5/1, 10/1, and 20/1 under otherwise reference conditions. The results reveal that there is no apparent trend in particle size with reaction zone temperature or dilution. It is also not clear whether there is a significant change in stoichiometry for dilution with NH_3.

A similar experiment was performed by diluting the reactant gas stream with argon 607SN. Table XIII shows that diluting the gas stream with 45% argon had virtually no influence on the particle size (176-173 Å) or chemistry (35-36 wt% free Si) but caused an increase in the reaction temperature.

c. SiC Powders

Synthesis experiments have been carried out to determine the possibility of producing SiC powders from laser heated reactant gases.

TABLE XII

The Influence of Reactant Gas Velocity on the Particle Size, Chemistry and Reaction Temperature for Si_3N_4 Powder Synthesis

Run Number	603SN	605SN	020SN	614SN
NH_3/SiH_4 ratio	10/1	10/1	5/1	5/1
Reactant Gas Velocity ave./max in cm/sec at laser beam	474/948	825/1650	191/382	477/954
Particle Size Å BET	176	151	210	155
Free Si Wt%	35	-	18.5	35.6
Powder Color	lt. brown-tan	Dk. Brown	Lt. Brown	Brown
Reaction Temperature °C	867	-	-	1025
Crystallinity	amorphous	amorphous	amorphous	amorphous

TABLE XIII

The Influence of Dilution of Reactant Gases with NH_3 and Argon on the Si_3N_4 Powder Characteristics

Run Number	614SN	603SN	615SN	607SN
NH/SiH_4 Ratio	5/1	10/1	20/1	10/1
% Argon Dilution	0	0	0	45
Particle Size Å BET	155	176	155	173
Free Si Wt%	35.6	35	38.1	36
Powder Color	brown	lt. brown tan	brown	brown
Crystallinity	amorphous	amorphous	amorphous*	amorphous
Temperature °C	1025	867	800	990

* no crystalline Si present

Silane was used as the silicon source as in synthesis experiments with other powders. Methane (CH_4) and ethylene (C_2H_4) were used as carbon sources. The proposed reactions for these experiments were:

$$SiH_4(g) + CH_4(g) \xrightarrow{h\nu} SiC(s) + 4H_2(g)$$

and

$$2SiH_4(g) + C_2H_2(g) \xrightarrow{h\nu} 2SiC(2) + 6H_2(g) \quad .$$

Methane was expected to react more readily than ethylene because of its simple molecular structure even though it has no absorption bands in the vicinity of 10.6 μm. More complete information suggests that methane pyrolyzes via an ethylene intermediate (Powell, 1966) so the initial hypothesis may not, in fact, be valid. Ethylene was selected because it was reported (Patty, et al., 1974) to exhibit high absorptivity to the P(20) line of $00^{o}1 - 10^{o}0$ band in a CO_2 laser. They reported an absorptivity of 1.64 cm^{-1} atm^{-1} for dilute concentrations of ethylene in air. This absorptivity level is intermediate between measured levels of SiH_4 and NH_3 and is a very high absorptivity by any comparison with other gases.

The process conditions used in these synthesis experiments are summarized in Table XIV along with the characteristics of resulting powders. In general, the process conditions were nearly the same as the reference conditions used for Si and Si_3N_4 powders. The gas mixtures had nearly stoichiometric silicon to carbon ratios.

The physical characteristics of resulting powders are similar to those observed with Si and Si_3N_4 powders. TEM analysis (Figure 34) showed them to be small, uniform, loosely agglomerated spheres. The particles ranged from 180 Å to 260 Å with an average size of 210 Å. BET equivalent diameters and directly measured diameters were essentially equal to each other; again, indicating an absence of internal porosity which was open to the surface of the particles.

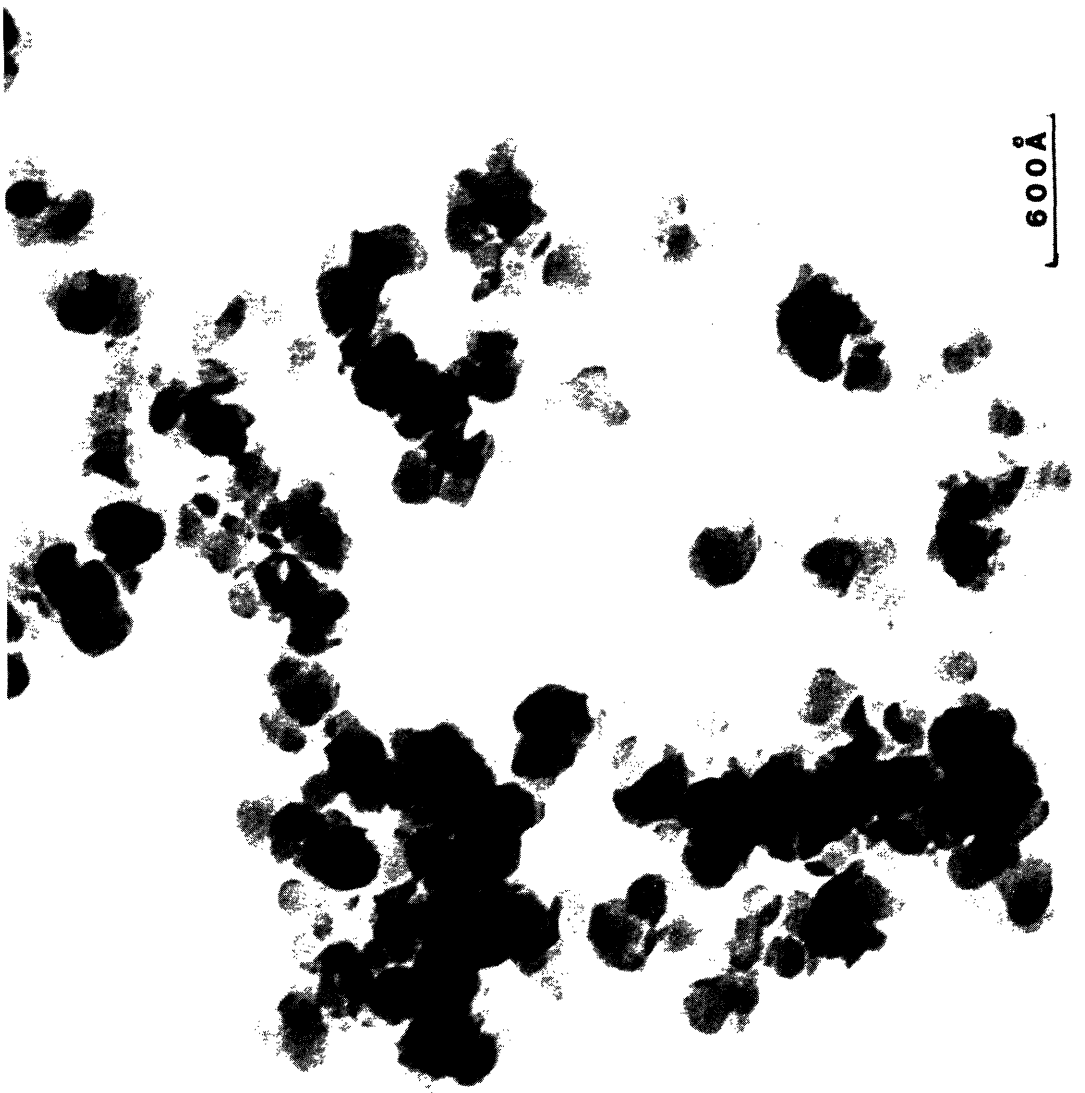

Figure 34. TEM Photomicrograph of SiC powders from lot 022SC.

TABLE XIV

Summary of SiC Process Conditions and Powder Characteristics

GASES	$SiH_4 + CH_4$	$SiH_4 + C_2H_4$
Cell Pressure (atm)	0.2	0.2
Laser Intensity (watts/cm^2)	760	860
Measured Reaction Temperature (°C)	710	865
Powder Chemistry (wt%)		
Si	99	80
C	0.2	14
O_2	0.3	1.4
Powder Size		
BET Equivalent (A)	305	274
TEM	-	230
Powder Crystallinity		
X-ray	crystalline Si	poorly crystalline
Electron Diffraction	crystalline Si	poorly crystalline

Chemical analysis showed that the powders formed with CH_4 contained virtually no carbon. The methane apparently did not react with exposure to the laser beam. Those formed with C_2H_4 did contain 14% by weight carbon compared with 33% for stoichiometric SiC. IR spectral analysis indicated that carbon combined as SiC in these powders, although we have not determined whether all of the carbon was combined in this manner.

The powders made from SiH_4 and CH_4 (613SC) were crystalline to both x-ray and electron diffraction. The diffraction patterns were identical to those for Si powder made from SiH_4. The particles ranged from 180 Å to 260 Å with an average size of 210 Å. The powders from run $O_{22}SC$ (SiH_4 and C_2H_4) showed some evidence of

crystallinity in both electron and x-ray diffraction. The peaks were broader than for 613SC indicating that these crystallite powders are either smaller or more poorly crystalline in nature. The patterns have not been indexed to date.

It is not known whether the higher reactivity of the C_2H_4 gas resulted primarily because of its higher optical absorptivity, an intrinsically high reactivity with silane, or some combination of factors. It is interesting to speculate whether resonance effects between the photons and the gas molecules enhanced the reaction. It is also apparent that its absorptivity improved the coupling efficiency relative to the CH_4/SiH_4 gas mixture in which the CH_4 acted as an optical dilutant. As shown in Table XIV, the measured reaction temperature was higher with C_2H_4 than with CH_4. Although the measured temperature levels probably are not accurate, the relative levels are likely correct. So the cause for the higher reactivity of C_2H_4 may simply result from a higher temperature at the point of reaction, attributable to the higher optical absorptivity. If this is so, higher laser intensities should cause CH_4 to react with SiH_4. Higher reactant gas pressures should also improve the stoichmetry of the powders.

The question of possible resonance effects on reactions is fundamentally important for our understanding, controlling, and exploiting this laser synthesis process. If they are important, unusual reaction paths and kinetics will be possible. It may also be possible to cause reactions in the presence of unwanted impurities which will not be incorporated proportionally if they do not couple to the laser light. If resonance effects do not occur, it will be correct to describe the reaction as a very fast "thermal domain" reaction as we are now approaching the problem.

d. Particle Agglomeration

The laser synthesized Si, Si_3N_4 and SiC powders exhibit most of the stated characteristics for an ideal powder. These powders appear to fall short of "ideal" in their apparent agglomeration. All of the TEM

analyses have revealed two dimensional networks of powders as shown in Figures 29, 30, and 32. The particles are usually in contact with one or more particles, yet there is no evidence of actual neck formation or other high strength bonding between the particles.

Possibly the observed loose agglomeration results from the sample preparation techniques which were employed. Typically, powders examined by TEM had been captured in a filter and were probably subjected to shear when removed.

To examine this question, a TEM grid was placed inside the reaction cell and powders were produced using reference gas flow and pressure conditions with 100 msec pulses of the CO_2 laser beam. These powders again revealed loose two dimensional agglomeration. This preliminary observation suggests that agglomeration occurs prior to capture in the filter assembly.

A simple calculation has been made to determine the frequency of collision and thus assess the likelihood of agglomeration before leaving the flame. Two possible solutions have been presented in the literature (Mason, 1977).

The perikinetic solution assumes particles of concentration, N in a fluid media of viscosity, η, move entirely by Brownian motion. For equisized non-interacting spheres, the frequency of collision of a single sphere with any other is:

$$\delta = \frac{3}{8} \frac{NkT}{\eta}$$

where N is the number per unit volume
k is the Boltzmann constant
T is the temperature in degrees Kelvin
η is the viscosity.

The second is the orthokinetic solution which assumes particles in

a flowing stream are brought together by the shearing action of flowing streams. For equisized noninteracting spheres the frequency of collision is

$$\beta = \frac{32}{3} b^3 N G$$

where b is the radius of the particles, and G is the gradient in the flow velocity. The following are values calculated for the reference conditions and for synthesizing silicon nitride.

$N = 8.2 \times 10^{11}$ cm^{-3} $\quad \eta = 3 \times 10^{-4}$ poise $\quad G_{ave} = 9.5 \times 10^{3} \frac{\text{cm}}{\text{sec cm}}$

$T = 1100°$ K $\quad b = 7.8 \times 10^{-7}$ cm

For the perikinetic case $\beta = 1.1 \times 10^{3}$ sec^{-1} and for the orthokinetic case $\beta = 5.5 \times 10^{-2}$ sec^{-1}. Clearly collisions due to Brownian (perikinetic) motion dominate. The collision frequency will be approximately 1000/sec. The collision frequency will be even higher if Van der Walls attractive forces are considered, but will be lower if all particles have identical charge, with the same sign and electrostatic forces considered. These calculations have not yet been made.

Under the reference conditions the average flow rate in the flame is estimated to be 200 cm/sec, and the dwell time of particles in the flame is 1.2×10^{-2} sec. On the average, a particle will undergo approximately 12 collisions while in the flame. On this basis, particles would be expected to undergo about 15 more collisions before reaching the filter.

Particles will not necessarily stick when they collide and may rebound. We have made no estimate as to the frequency of sticking, but assume that it will depend on the velocity of the particle, the Van der Walls attractive forces and possibly the electrostatic forces. Once the particles do stick, they may be held together by surface forces which reduce the total surface energy of the particle by forming the contact area between them (Easterling and Thölen, 1972). Sintering may even occur in the flame due to the same forces although we see no evidence of this

from TEM observations.

To avoid collisions between particles within the flame, this analysis dictates that the particle number density be decreased, the temperature be decreased, and/or the viscosity be increased. Parametric changes in run conditions will affect the number density of particles and local temperature and, to a limited extent, the viscosity. The effects of varied process parameters on powder characteristics show that conditions necessary to produce other desirable powder properties may not necessarily be compatible with those which inhibit agglomeration. This is a fundamentally important issue. We will continue to investigate this aspect of process modeling and powder characteristics.

3. Interaction between Process Variables and Powder Characteristics

We have discussed the laser heated gas phase reaction and the resulting powders separately. It is our ultimate objective to develop an understanding of the relationship between the two which is based on equilibrium thermodynamics and the kinetics of the gas phase process. With a somewhat improved description of the process, it should be possible to rationalize observations in terms of classical homogeneous nucleation and growth theory.

The variables which have a direct effect on the nucleation and growth kinetics include reaction temperature, heating rate, partial pressure of reactants, total pressure and dilution by inert gases. Most of these variables have been manipulated to demonstrate their empirical effect on Si_3N_4 powder characteristics. We have insufficient data to provide a basis for discussing Si and SiC synthesis processes.

We examined the following powder characteristics: size, size distribution, shape, stoichiometry, chemical impurities, and crystallinity. Process variables which were changed are laser intensity, cell pressures, gas velocities and to a lesser extent gas mixture. Of the characteristics and process variables examined, only particle size and stoichiometry were

influenced by laser intensity and gas pressure. No other variable had any significant effect on any other characteristics within the range of conditions examined.

- Increased laser intensity caused Si_3N_4 particle size to decrease and caused their Si/N_2 ratio to approach the stoichiometric composition.

We have shown that virtually all of the silane gas is consumed during particle growth and that particle size is limited by impingement of overlapping volumes of depleted reactant gas. The final particle size is therefore controlled by the number of embryos which reach supercritical dimensions and grow until depleted volumes impinge on one another. The homogeneous nucleation rate is very small until either the degree of supersaturation approaches a critical value or, if kinetically limited, a critical temperature is reached. The rate changes many orders of magnitude with small changes beyond either of these critical values. The narrow particle size distribution indicates that there was not appreciable nucleation during the time period between the appearance of the initial nuclei and cessation of growth with impingement. This can occur for two reasons. The growth process itself may effectively terminate the nucleation process by, for instance, reducing the supersaturation level below the critical level. Or, at the critical supersaturation level where nucleation rates first become appreciable, the growth rates may be extremely fast. In this case, the reaction effectively goes to completion and terminates with the appearance of the first nuclei.

The decreased particle size resulting with increased laser intensity results from forcing the spontaneous reaction temperature to higher levels, and correspondingly higher degrees of supersaturation, with the higher heating rates. Heating rates at the reaction temperature ranged from 10^6 to 10^8 °C/sec for laser intensities ranging from 760 to 10^5 watts/cm^2. The particle size is reduced because the nucleation rate is larger at higher temperatures, and it increases proportionally faster than the growth rate. This is the same conclusion reached for TiO_2 powders produced from $TiCl_4$ (Suyama and Kato, 1976).

The general defficiency of nitrogen in resulting particles could result either from slow reaction kinetics involving N_2-bearing species or from preferential vaporization of N_2 from hot particles. These results indicate that higher temperatures permit achievement of stoichiometric compositions for kinetic reasons. The effect of increased kinetic rates is self-assisting because the increasingly rapid exothermic reactions involved in the growth process drive the particle temperatures even higher.

- Increased reactant pressures caused Si_3N_4 particle sizes to increase and caused their compositions to be more nearly stoichiometric.

Previous analyses of the process showed that heating rate was independent of the pressure of optically absorbing species because the absorptivity and heat capacity both change proportionally with pressure. Pressure, itself, has less effect on nucleation rate than does temperature, so we would not anticipate that pressure would have any appreciable effect on how far the temperature could be driven beyond the level where nucleation rates become appreciable. This critical temperature level and the corresponding nucleation rates are expected to be essentially independent of relatively small pressure changes.

The results of our depletion volume analyses support this conclusion and explain the particle size dependence on pressure. For the range of pressures examined, the distance between growing nuclei was shown to be constant. The observed particle volumes are directly proportional to the mass of reactant gas within the depletion volumes and so are proportional to pressure.

The reason for increasing nitrogen content with increasing pressure has not been determined. It could be simply that the increased partial pressure of N_2-bearing species causes the increasing nitrogen content in the particles. It is also probable that the particle growth rates will increase with increasing reactant particle pressures. Consequently, the rate at which exothermic heat is liberated at the particles will increase with pressure, causing the particle temperatures to be proportionally higher.

As was already shown, higher reaction temperatures cause the particles to be more nearly stoichiometric. Pyrometric temperature measurements did indicate than the flame temperature rose with increasing pressure.

The gas velocity, the NH_3/SiH_4 ratio in the gas and dilution with argon had negligible effects on particle characteristics. The absence of an apparent gas velocity effect can be anticipated because the instantaneous heating rates at the reaction temperature change by only a factor of 2-3 with the range of gas velocities investigated. This variation would probably not influence nucleation rates. This same conclusion may apply to the gas composition and dilution effects although we do not have a sound basis for analyzing their effect at this point.

It is apparent that particle size is insensitive to process variables other than laser intensity and pressure for large ranges in conditions. Stoichiometry is manipulable in an orderly manner; powders can be made which range from mostly pure Si to stoichiometric compositions. All as-synthesized Si_3N_4 powders have been amorphous to date; but they crystallize rapidly at temperatures in excess of 1400°C. Silicon powders made from SiH_4 can be either amorphous or crystalline depending on laser intensity. It appears that we should be able to simultaneously achieve virtually all of the ideal powder characteristics which were sought while retaining some control over individual powder characteristics. We will continue to investigate means of extending the achievable range of particle sizes while retaining the narrow particle size distributions.

IV. Summary

This research program has investigated means of producing powders which will permit fabrication of ceramic bodies with superior characteristics. We have worked with Si_3N_4 and SiC because they are promising candidates for use in new generations of heat engines. Ideal powders will have particles which are small, uniform in size, equiaxed (tending toward spheres) in shape, composed of a specific phase(s), compositionally pure and free of agglomerations. In principle, gas phase synthesis processes can achieve these attributes; however, variations in time-temperature history throughout the conventionally heated reaction zones cause unacceptably large variations in particle characteristics. Also, the typically long exposure to elevated temperatures causes particles to bond to one another. We have elected to heat the reactant gases by absorbing IR light emitted from a laser. This unique means of transferring energy to the gas permits precise, uniform heating with unusually high heating rates and small reaction volumes. We anticipated that this laser heated synthesis process would overcome the deficiencies of conventional gas phase synthesis processes, while retaining their advantages.

In this process, optically absorbing gases are passed through a laser beam to cause a reaction in a definite volume within the region where the two interact. We have investigated process geometrics in which the gas stream and the laser beam intersect orthogonally and also where they intersect coaxially from opposite directions (counter flow). A CO_2 laser was used as the heat source to drive reactions in gases containing active components such as SiH_4, NH_3, CH_4 and C_2H_2 as well as various inert dilutants. The resulting Si, Si_3N_4 and SiC powders were collected and characterized as a function of process variables.

The results of this research program demonstrate that this laser heated synthesis process produces powders with virtually all of the desired characteristics. The resulting particles are small, uniform in size, round, and pure. The particles appear to be attached to one another in chain-like agglomerations; however, direct examination by

TEM revealed no neck formation between particles. We anticipate that they can be dispersed. Besides producing powders with ideal characteristics, this laser heated synthesis process is extremely efficient. Approximately 95% of SiH_4 is converted to Si_3N_4 powder in a single pass through the laser beam. Also, Si, Si_3N_4 and SiC powders can be produced from these reactants with as little as 2 kwhr of energy per kilo of powder. It is likely that this process can produce both a superior and lower cost powder than conventional gas phase or solid phase synthesis processes.

Much of our efforts have focused on developing an analytical description of the laser heated synthesis process. To develop a model, many fundamental property measurements were required, such as detailed absorptivity measurements for reactant gases as a function of pressure and emitted wavelength. Emissions from the reaction have been studied to identify reaction species and to estimate the reaction temperature. Computer analyses of the gas flow were used to predict gas stream dimensions and velocities. Combined with direct observations of both the reaction positions relative to the laser beam and the reaction temperatures, these analyses and characterizations have been used to describe the time-temperature history of the reactant gases throughout the course of the reaction.

With the process conditions used for the majority of these synthesis experiments (laser intensity = 765 watts/cm^2, pressure = 0.2 atm, gas velocity = 500 cm/sec), reaction products were evident within 3-5 mm penetration into the laser beam. Heating rates to the reaction temperature (approximately 800°C) were approximately 10^6°C/sec. The reaction was initiated in approximately 10^{-3} seconds and was completed in, at most, 7.5×10^{-3} seconds. The individual particles grew from and depleted a volume of gas equal to approximately 1×10^{-4} cm in diameter.

Most process variables were manipulated to determine their effect on particle characteristics. These interactions were interpreted in terms of changes in the process. Laser intensities up to 10^5 watts/cm^2 produced heating rates in excess of 10^8°C/sec. Variations in heating rates within different gas streamlines were analyzed in terms of the Gaussian

intensity in the laser beam and the parabolic velocity profile in the gas stream. The effects of nonabsorbing gases were also considered. Other than laser intensity, most process variables had very little effect on particle size. The gas depletion volume remained essentially constant. Increased laser intensity caused the particle size to decrease progressively and raised the reaction temperature. Qualitatively, the results follow expectations based on nucleation and growth theory. The general characteristics of the powders of the three materials are similar to one another, but they differ in detail. Silicon powders were crystalline under all but the lowest laser intensity conditions. Individual crystalline particles consisted of multiple grains which were approximately 150 Å in diameter. Mean Si particle diameters were in the range of 500-600 Å with a standard deviation of 35-50%. Silicon nitride powders were always amorphous. Mean particle sizes ranged from 25 to 220 Å, depending primarily on laser intensity. These powders were more uniform than the silicon powders. The standard deviations were approximately 25% and the ratio between the largest to the smallest observed particle was less than 2.5. Their stoichiometry varied with processing conditions. High laser intensities yielded stoichiometric powders; lower intensities produced powders which were rich in silicon. The silicon carbide powders are similar to the Si_3N_4 powders, amorphous and tending to be rich in silicon, with a mean particle size of approximately 230-250 Å. Powders of all three materials have spherical particles whose BET equivalent diameters equaled the directly observed mean diameters. This observation and direct density measurements indicate that individual particles contain no porosity. All of the materials were free of contaminants. The oxygen impurity level decreased progressively as handling procedures improved. In later powder batches, the O_2 content was less than 0.2% by weight. With the exception of Cu at a concentration of 20 ppm, no other impurities were detected.

This research program has easily achieved its primary objective. Powders which result from the laser heated, gas phase synthesis process have most of the characteristics presumed to be ideal for ceramic powders. The process also appears capable of reducing the cost of these powders because it requires very little energy per kg of powder and

utilizes feed materials very efficiently. The process should be developed further to eliminate the tendency of forming chain-like agglomerates and to increase the mean particle size. For many materials, it is desirable to have mean particle sizes of approximately 1000 Å rather than 250 Å typically produced by this process. Achieving a larger particle size will require an improved understanding of the nucleation and growth processes. It is also important to apply the process to other materials. Several electronic, magnetic, and optical ceramics processes would benefit from using powders with the characteristics demonstrated in this research program.

Appendix IA

Summary of Run Conditions for Powder Synthesis of Silicon, Silicon Nitride, and Silicon Carbide

Run Number	Power Density watts/cm^2	Pressure atm	SiH_4 cc/min	NH_3 cc/min	CH_4 cc/min	C_2H_4 cc/min	Argon cc/min	Gas Velocity at Nozzle Max cm/sec	Gas Velocity at Laser Beam Max cm/sec	Reaction Zone Temperature °C (pyrometer)
209S	760	0.2	20	0			1000	188	106	-*
213S	1020	0.2	20	0			1000	104	36.1	-
214S	760	0.2	11	0			1000	104	36.1	-
603SN	760	0.2	11	110			1000	1140	949	867 thermocouple 709
212SN	760	0.2	11	110			1000	1140	949	-
609SN	2×10^4	0.2	4.5	45			1000	468	287	985-1020
612SN	1×10^5	0.5	5	45			1000	424	355	-
021SN	1020	0.75	11	110			1000	304	231	-
023SN	891	0.75	11	110			1000	304	231	1050-1125
611SN	760	0.08	5	44			1000	1160	660	-
610SN	760	0.5	11	110			1000	456	337	1060-1080
605SN	760	0.2	17.8	178.2			1000	1850	1650	-
020SN	760	0.2	11	55			385	622	382	-
614SN	760	0.2	20.2	101.8			1000	1140	954	1025
615SN	760	0.2	5.8	115			1000	1140	949	675-700
607SN	760	0.2	6.1	60.5			1000 (dilution 54.4)	1502	934	990
022SC	865	0.2	11			9	1000	170	86	865
613SC	760	0.2	11		7		1000	188	-	710

* denotes measurement not made

Appendix IB

Summary of Results of Powder Characteristics

Run Number	Powder Color	Analysis Wt% Si	N	C	O	H	Free Si Wt%	BET Surface Area m^2/g	Equiv. Dia. Å	TEM Dia.	Crystal Structure	Conversion %	Infrared Spectroscopy
209S	brown	99	0.02		2.92	0.15	100	59	436	490	Cryst. Si	65-75	
213S	brown	-	-		1.0	-	100	48	543	630	Cryst. Si	80-90	
214S	brown	-	-		3.4	-	100	56.9	458	470	Cryst. Si	70-75	
603SN	light brown-tan	72	26		1.25	-	35	117	176	168	Amorph. Si_3N_4+ Cryst. Si	-	
212SN	light brown-tan	-	-		-	-	-	152	137	-	Amorph. Si_3N_4+ Cryst. Si	87	
609SN	tan-white	60.1	-		-	-	2	165	114	150	Amorph. Si_3N_4	-	
612SN	white	-	-		-	-	very low	190	98	120	Amorph. Si_3N_4	-	
021SN	light tan	64	33		0.96	-	15.6	88.5	221	-	-	87	
023SN	tan	66.6	29.7		0.3	-	23	91	220	-	-	-	
611SN	dark brown	82.6	-		1.8	-	60	134	167	-	-	-	
610SN	light tan	63.9	-		2.7	-	14	92	211	150	Amorph. Si_3N_4 with little Cryst. Si	-	
605SN	brown	-	-		-	-	-	124	151	-	Amorph. Si_3N_4+ Cryst. Si	-	
020SN	light brown	69	33		2.2	0.13	18.5	94	210	-	Amorph. Si_3N_4+ Cryst. Si	-	
614SN	brown	68	23.7		0.5	-	35.6	130	155	-	Amorph. Si_3N_4+ poorly Cryst. Si	78	
615SN	brown	70	23.5		-	-	38.1	119	155	-	Amorph. Si_3N_4 no Si peaks	108	
607SN	brown	71.4	-		3.5 5.6**	-	36	120	173	-	-	-	
022SC	brown to dark brown	80		14.1	1.37	-	49	97.5	247	230	Some Cryst. but not indexed	51	Si-C bonding
613SC	brown	96.9		0.2	0.33	-	99	84.3	305	-	Cryst. Si	58	No Si-C bonding

** second analysis

REFERENCES

1. Billy, M., Brossard, M., Desmaison, J., Girard, D., and Goursat, P., 1975, J. Amer. Ceram. Soc., 58: 254.

2. Braker, W., and Mossman, A.L., 1971, "Matheson Gas Data Book," 5th Edition, p. 506, Matheson Gas Products, E. Rutherford, NJ.

3. Coble, R.L., 1960, Proc. of the 4th Intl. Conf. on Reactivity of Solids, Amsterdam.

4. Cochet, G., Mellottee, H., and Delbougo, R., 1975, Proc. Conf. on Chem. Vapour Deposition, 5th Int., Editors: Bloucher, J.M. and Hintermann, T.E., pp. 43-55, Fulmer Res. Int.

5. Cullity, B.D., 1956, "Elements of X-Ray Diffraction," p. 261, Addison-Wesley Pub. Co., Inc., Reading, MA.

6. Danforth, S.C., June, 1978, "Effective Control of the Microstructure of Reaction Bonded Si_3N_4 as Related to Improved Mechanical Properties," Ph.D. Thesis, Brown University, Providence, RI.

7. Dressler, K. and Ramsay, D.A., 1959, Phil. Trans., A, 251: 553.

8. Dubois, I., 1968, Canadian J. Physics, 46: 2485.

9. Easterling, K.E., and Thölen, A.R., 1972, Acta. Met., 20: 1001-8.

10. Galasso, F.S., Veltri, R.D., and Croft, W.J., 1978, Bull. Am. Ceram. Soc., 57: 453.

11. Garing, J.S., Nielsen, H.H., and Narahorn, K., 1959, J. Molecular Spect., 3: 496-527.

12. Gaydon, A.G., and Wolfhard, H.G., 1970, "Flames: Their Structure, Radiation, and Temperature," Chapman and Hall, Ltd., London.

13. Greskovich, C.D., Prochazka, S., and Rosolowski, J.H., November, 1976, Basic Research on Technology Development for Sintered Ceramics, Report AFML-TR-76-179, G.E. Research and Development Laboratory under contract with the AF Materials Laboratory.

14. Haas, C.H., and Ring, M.A., 1975, Inorganic Chemistry, 14: 2253.

15. Haggerty, J.S., and Cannon, W.R., October 1978, Sinterable Powders from Laser Driven Reactions, under Contract N00014-77-C-0581, M.I.T., Cambridge, MA.

16. JANAF Thermochemical Tables, 1971, NSRDS-NBS37.

17. Jensen, C., Steinfeld, J.I., and Levine, R.D., 1978, J. Chem. Physics, 69: 1432.

18. Lin, Sin-Shong, 1977, J. Electrochem. Soc., 124: 1945.

19. Mason, S.C., 1977, J. Colloid and Interface Sci., 58: 275-285.

20. Patanker, S.V., and Spalding, D.B., "Heat and Mass Transfer in Boundary Layers," 2nd Edition, Intertext Books, London.

21. Patty, R.R., Russwarm, G.M., and Morgan, D.R., 1974, Applied Optics, 13: 2850-4.

22. Pease, R.W.B., and Gaydon, A.G., 1976, "The Identification of Molecular Spectra," 4th Ed., Chapman and Hall, London.

23. Powell, C.F., 1966, "Chemically Deposited Nonmetals in Vapor Deposition," p. 343, Editors: Powell, C.F., Oxley, J.H., and Blocher, J.M., John Wiley and Sons, Inc., New York.

24. Purnell, J.H., and Walsh, R., 1966, Proc. Royal Soc., Series A, p. 545, London.

25. Ronn, A.M., 1979, Scientific American, 240: 114.

26. Spalding, D.B., 1977, "Genmix: A General Computer Program for Two Dimensional Parabolic Phenomena," Pergamon Press, Oxford.

27. Suyama, Y., and Kato, A., 1976, J. Amer. Ceram. Soc., 59: 146-49.

28. Tindal, C.H., Straley, J.W., and Nielsen, H.H., 1942, Physical Review, 62: 151-59.

29. Vande Hulst, H.C., 1957, "Light Scattering of Small Particles," John Wiley and Sons, Inc., New York.

30. Warren, B.E., 1969, "X-Ray Diffraction," p. 258, Addison-Wesley Pub. Co., Inc., Reading, MA.